Politecnico di Torino

Corso di Laurea Magistrale in
Mechanical Engineering

A.a. 2024/2025
Sessione di Laurea dicembre 2025

Analysis of the effect of temperature on Vickers, Brinell, and Knoop hardness measurements

Relatore:
Prof. Genta Gianfranco

Candidato:
Panarese Luigi

Correlatori:
Dott. Germak Alessandro
Dott. Prato Andrea

TABLE OF CONTENTS

ABSTRACT

In 2023, the European Association of National Metrology Institutes (EURAMET) launched project 22RPT01 TracInd BVK-H. The main objective is to improve the traceability and reliability of hardness measurements using optical measurement methods, namely Brinell, Vickers, and Knoop (BVK) hardness (H) tests. In this framework, this thesis tries to determine the sensitivity coefficients and associated uncertainties for BVK tests that relate hardness to the temperature of the calibration block in a range $15\ °C\ \div\ 35\ °C$.

The analysis was performed on thirty-two different configurations of Brinell, Vickers, and Knoop hardness scales at different hardness levels and variable applied loads. The experimental data were collected using primary hardness standardizing machines (PHS DW & PRIMARY and MHSM hardness standardizing machines) and optical measuring instruments provided by the INRiM hardness laboratory.

Assuming a linear relationship between temperature and hardness, the data analysis was conducted using a Weighted Total Least Square (WTLS) method, which allowed the estimation of the coefficients. In general, the sensitivity coefficients are mostly negative, indicating a weak tendency for hardness to decrease with increasing temperature as expected from the constitutive theoretical model: in average, the sensitivity coefficients are below $1\ H\ °C^{-1}$. Anyway, the statistical significance varies between tests and hardness levels. The cases considered satisfactory in terms of fit goodness return a mean relative sensitivity coefficient $0{,}06\ \%\ °C^{-1}$, independently of the test and the hardness level of the block.

INTRODUCTION

Temperature plays a pivotal role in shaping the behavior of materials. From the depths of space to the production line of a metallurgical industry, materials are constantly subjected to temperature fluctuations that can significantly alter their properties. Understanding how temperature affects materials is crucial for engineers, scientists, and anyone working with materials in various applications.

A solid increases its energic content when it is supplied with heat. Materials store this energy in three ways. When heat is transformed into the kinetical energy of atoms, ions and molecules the temperature of the body increases. Then, heat can also be stored both as potential energy, one example is the thermic dilatation of railways in summer, and as phase transformation. In this project the interest is only related to the kinetic response of the steel. Dilatation or phase transition won't be considered.

The temperature of a solid is related to the amplitude of the thermic vibrations of particles around their equilibrium position in the crystalline lattice. The more atoms move, the higher the temperature will be. Oscillations are more frequent, the average length of the bond increases and the strength decreases, involving the reduction in the elastic properties. This mechanism also facilitates the dislocation movement responsible for the plastic behavior [1]. To describe these phenomena a huge number of tensile/compression tests have been carried on many materials and the results exploited in thermo–dynamic databases.

Since many mechanical properties of materials are strictly related to plastic and elastic deformation, it is foreseeable that a change in temperature will cause a change in behavior itself. In fact, heat significantly affects strength, ductility, hardness, and toughness on bodies. Typically, as temperature increases, most materials experience a reduction in strength and hardness, while their ductility and toughness generally increase. Changes in material behavior potentially make technical standards less reliable, directly influencing the outcome of industrial processes and scientific research.

For this reason, in both industry and metrological research, standards are fundamental to ensuring consistency, reliability, and comparability in measurements. International standards such as ISO and ASTM provide unified procedures, definitions, and calibration methods that allow laboratories and institutions to produce results that are traceable and reproducible. Adhering to these standards is essential not only for maintaining measurement quality, but also for enabling meaningful data exchange and collaboration across different research and industrial environments. The possibility of adapting procedures with suitable corrections contributes to improving the quality of products and services in everyday life.

It is in this context that the thesis work is developed. The experience is carried out at INRiM (*Istituto Nazionale di Ricerca Metrologica*) in Turin, Italy, within the framework of the European research project 22RPT01 TracInd – BVK–H. The project aims to improve the traceability and reliability of hardness measurements, with focus on the Brinell, Vickers, and Knoop (BVK) hardness (H) scales. The necessity of the project arises from the fact that in the hardness field, standards present very wide constraints in terms of temperature, application time and measuring condition. The aim of the research is to find a relation which can be useful to industries and National Metrology Institutes (NMIs). Providing guidelines and correction factors could be crucial to obtain the most coherent values for the same tests [2].

The research's objective is to investigate the relative influence of temperature on BVK hardness measurements. In this work, the focus is pointed out on relative variations in hardness with respect to temperature, rather than on absolute values. This approach allows for the identification of sensitivity coefficients that can improve the accuracy and comparability of hardness measurements under varying thermal conditions. The final aim of the work is to describe the behavior of sensitivity coefficients $c_{T,i}$ as

hardness levels vary, so that, given the test conditions and the measured hardness, it is possible to obtain a correct value that is almost unique among different measuring entities. A key aspect of this study is the assessment of measurement uncertainty related to corrective sensibility coefficients. Quantifying these uncertainties and propagate them is essential to ensure the metrological traceability of hardness measurements and to support the development of robust calibration procedures.

The tests conducted in the laboratories of INRiM have seen the employment of advanced measuring equipment, such as primary hardness machines and optical microscopes. Moreover, both active and passive temperature control are necessary to maintain the temperature in the desired range during experiments. The experience is an initial attempt to investigate the relative influence of temperature on hardness measurements. As methodologies continue to evolve, future studies will be able to refine the measurement process obtain more reliable measures and reduce associated uncertainties.

1. THEORETICAL BACKGROUND

1.1. INTRODUCTION TO HARDNESS

Hardness is an important material property determined by measuring an indentation size on material, whether metallic or non-metallic. This property is useful since it can be correlated to other mechanical properties of material such as yield strength, resilience and nominal stress at the break. Hardness test found its role in industries for its simplicity and for the possibility to execute a non–disrupted test on the final part.

Friedrich Mohs formulated the first definition of hardness in 1822. He defined a systematic scale based on the capability of a mineral to scratch another one. Over the years, various methods for determining the hardness of materials have been developed and employed at varying levels of success. From early forms of scratching, tests evolved into the generation of an indentation. The first measuring method for hardness was formulated by August Brinell in 1900, who proposed to generate the indentation by means of a steel sphere [3].

A. Marten formulated in 1912 the first equation of Hardness. The value would have been obtained by the equation (1).

$$H = \frac{F}{S} \tag{1}$$

$\mathrm{F} = \text{force / N}$
$\mathrm{S} = \text{surface deformation / mm}^2$

Subsequently to this formulation, hardness has been considered as the capability of material to not deform during the application of a force. In this sense, it can be confused with pressure or nominal stress. To avoid this mistake, it is necessary to remember that pressure is a mechanical quantity, while hardness is a material property. Despite both are calculated as the force exerted a surface, only pressure has $\mathrm{N/mm^2}$as unit of measurement, since the hardness value is based on the measurement of a deformed surface and it remains constant independently on the loads and stresses applied on the material in the time instant, as happen with pressure. Therefore, the unit of measurement of hardness is expressed in points of the hardness scale used for the measurements test (e.g. $HV\ 10$ or $HBW\ 2{,}5/187{,}5$).

Hardness testing is an empirical method and the measured value is strictly dependent on the specific test conditions. As a result, the same material may exhibit different hardness values depending on the test method employed, the applied force, and the scale of measurement. Hardness can in fact be assessed over a wide range of forces, spanning from the macro- to the nanoscale. ISO 14577 standard series define the procedures for determining hardness and related material parameters across three force–penetration regimes:

- Macro range: $2\ N \leq F \leq 30\ kN$
- Micro range: $F < 2\ N\ and\ h > 0.2\ \mu m$
- Nano range: $h \leq 0.2\ \mu m$

Micro- and nanoindentation fall within the domain of materials science, where they provide insight into fundamental deformation mechanisms. Nano-indentation is particularly valuable for investigating dislocation behaviour, enabling the study of grain-boundary effects and local malleability at the nanoscale. Micro-indentation, on the other hand, is well suited for analysing grain boundaries and thus supports the evaluation of local thermal and electrical conductivity as well as microstructural heterogeneity. At larger scales, macro-indentation (and to a certain extent micro-indentation) is primarily relevant for industrial

applications, where the focus lies on assessing ductility and plasticity. In figure 1.1. are reported the three different scales.

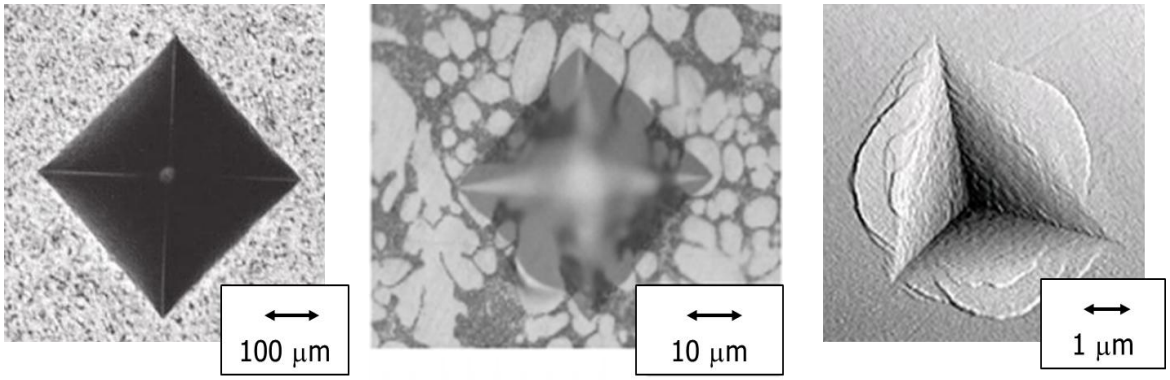

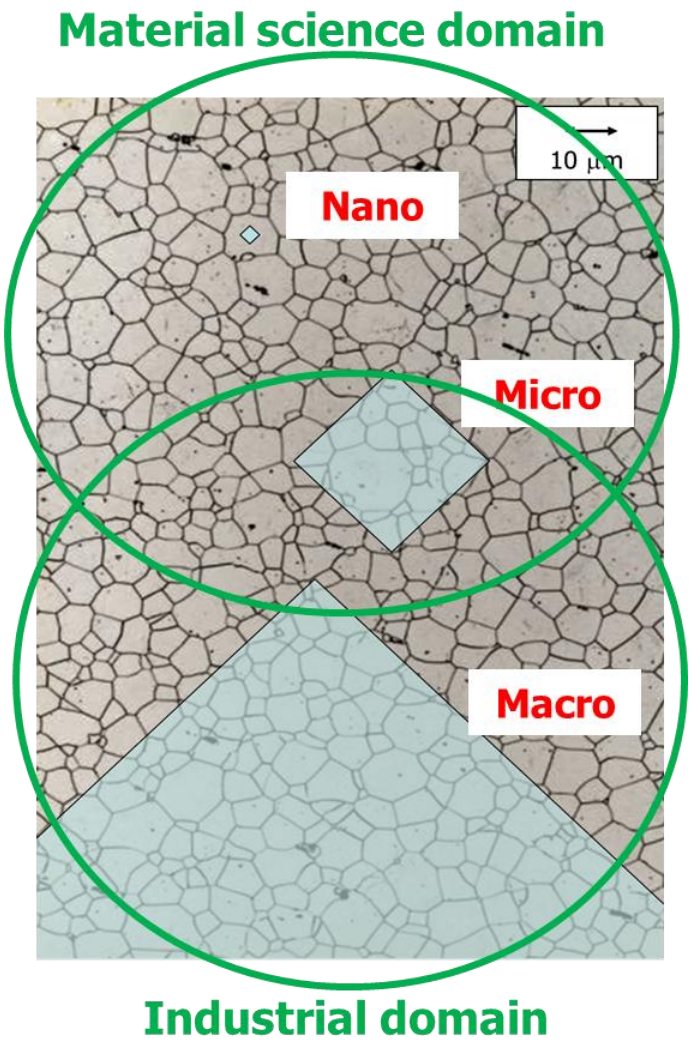

FIGURE 1.1. HARDNESS SCALES

1.1.1. BRINELL SCALE

Brinell Scales (indicated with "HB") were the first procedure that used an indenter to deform the material. The operation is done by means of a sphere made of tungsten carbide (WC). This procedure is described in UNI EN ISO 6506 [4] [5] [6] standard series, for the purpose of the project this thesis is based on UNI EN ISO 6506-3 which is the standard regulating the procedures for the calibration of hardness reference blocks at the calibration laboratory level. The application is limited to metallic materials up to a limit of $650\ HBW$.

Symbols and designations are reported in figure 1.2.

Symbol	Designation	Unit
D	Sphere diameter	mm
F	Test load	N
d	Mean diameter of indentation	mm

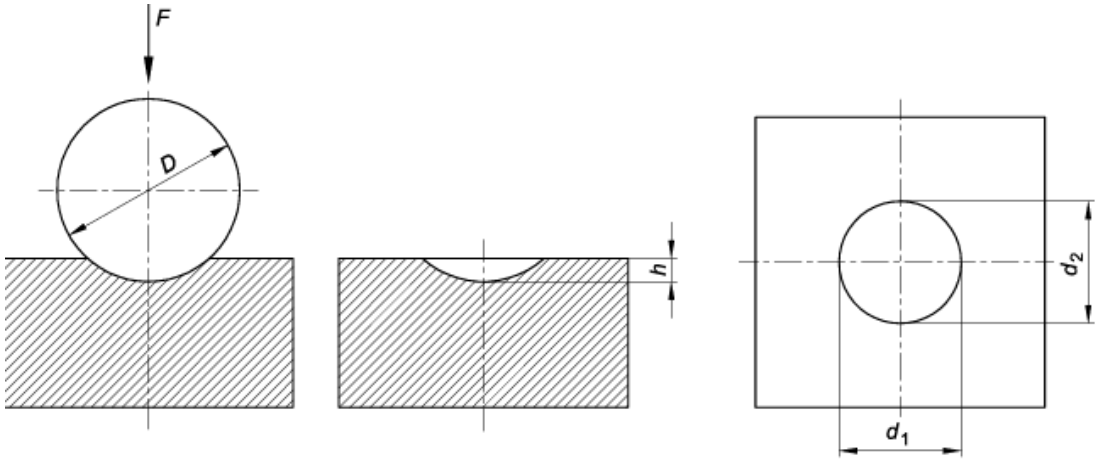

FIGURE 1.2. BRINELL DESIGNATION [4]

Once evaluated all these parameters the Brinell value is calculated with the equation (2).

$$HBW = 0.102\frac{2\,F}{\pi D - D - \sqrt{D^2 - d^2}} \tag{2}$$

Brinell tests are one of the mostly employed in industries due to their simplicity and rapidity to test the response to penetration of soft and mid–hard metallic materials. Surface finishing and non–uniformity don't influence the measurement since the size of indenter is big enough to overcome the imperfections.

Tests must be carried out with the following procedures:

- In the temperature interval $(23 \pm 5)\ °C$ for under control conditions, while in normal condition between $10°C \div 35°C$.
- The surfaces must be cleaned and rigidly supported.
- The time between the start and the attainment of the maximum load must not be less than $2\ s$ and larger than $8\ s$.
- The test load must be applied for a time interval of $10\ s\ \div\ 15\ s$.
- The distance between the centers of two adjacent indentation must be at least three times the diameter *d*
- The ratio load–diameter of the indenter must be chosen from the figure 1.3. depending on the material

Hardness symbol	Sphere diameter *D* / mm	Load–diameter ratio / N/mm^2	Load nominal value *F* / N
$HBW10/3000$	10	30	29420
$HBW\ 10/1500$	10	15	14710
$HBW\ 10/1\,000$	10	10	9807
$HBW\ 10/500$	10	5	4903
$HBW\ 10/250$	10	2,5	2452
$HBW\ 10/100$	10	1	980,7
$HBW\ 5/750$	5	30	7355
$HBW\ 5/250$	5	10	2452
$HBW\ 5/125$	5	5	1226
$HBW\ 5/62{,}5$	5	2,5	612,9
$HBW\ 5/25$	5	1	245,2
$HBW\ 2{,}5/187{,}5$	2,5	30	1839
$HBW\ 2{,}5/62{,}5$	2,5	10	612,9
$HBW\ 2{,}5/31{,}25$	2,5	5	306,5
$HBW\ 2{,}5/15{,}625$	2,5	2,5	153,2
$HBW\ 2{,}5/6{,}25$	2,5	1	61,29
$HBW\ 1/30$	1	30	294,2
$HBW\ 1/10$	1	10	98.07
$HBW\ 1/5$	1	5	49,03
$HBW\ 1/2{,}5$	1	2,5	24,52
$HBW\ 1/1$	1	1	9,807

FIGURE 1.3. BRINELL TESTS

The test is carried out in four phases:

- Application of the load. The indenter is approached to the point of the surface in the perpendicular direction, avoiding vibrations. Standards fix a time interval of $2\ s\ \div\ 8\ s$ for general test and a range $6\ s\ \div\ 8\ s$ for calibration tests.
- Maintaining of the load for the time suggested by standards.
- Measurement of the indentation along two mutually perpendicular directions.
- Calculation of Brinell hardness using the equation (2).

1.1.2. VICKERS SCALE

The Vickers scale is labelled with "HV". It was introduced to overcome the limitations of the Brinell test for what concerns hard materials. In fact, the indenter is a square base pyramid made of diamond and permits to reach harder levels. The angle on the vertex was selected of $136°$. Again, in this procedure the value of hardness is calculated as the ratio of the force applied and the total surface of the indentation. This procedure is described in UNI EN ISO 6507 [7] [8] [9] standard series. For the purpose of the project this thesis is based on UNI EN ISO 6507-3 which is the standard regulating the procedures for the calibration of hardness reference blocks at the calibration laboratory level.

Symbols and designations are reported in figure 1.4.

Symbol	Designation	Unit
α	Vertex angle between two opposite faces	$136°$
F	Test load	N
d	Mean value of the two diagonals	mm

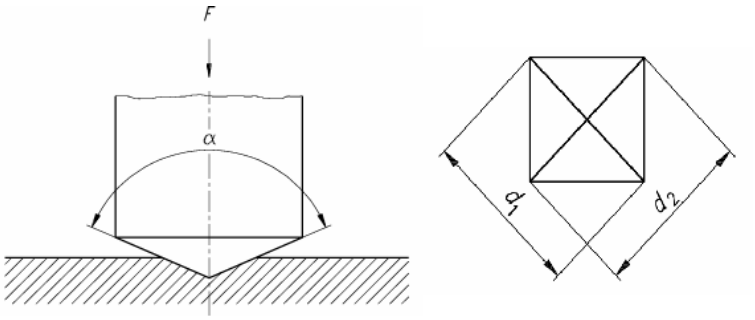

FIGURE 1.4. VICKERS DESIGNATION [7]

Once evaluated all these parameters the Brinell value is calculated with the equation (3).

$$HV = 0{,}102\frac{2\,F\sin\frac{\alpha}{2}}{d^2} \approx 0{,}189\frac{F}{d^2} \tag{3}$$

In according to the standard, Vickers hardness provides for three different test load ranges:

Test load ranges	**Hardness symbol**	**Previous designation (ISO 6507–1:1982)**
$F \geq 49{,}03$	$\geq\ HV\ 5$	Vickers hardness test
$1{,}961 \leq F < 49{,}03$	from $HV\ 0{,}2$ to $<\ HV\ 5$	Vickers hardness test with reduced load
$0{,}09807 \leq F < 1{,}961$	from $HV\ 0{,}01$ to $<\ HV\ 0{,}2$	Vickers microhardness test

FIGURE 1.5. VICKERS RANGES

Tests must be carried out with the following procedures:

- In the temperature interval $(23 \pm 5)\ °C$ for under control conditions and in normal condition a range $10°C \div 35°C$.
- The surfaces must be cleaned and rigidly supported.
- The time between the start and the attainment of the maximum load must be in a time interval of $2\ s\ \div\ 8\ s$ for general test and a range $6\ s\ \div\ 8\ s$ for calibration tests.
- The test load must be applied for a time interval of $10\ s\ \div\ 15\ s$ for macro–hardness and not more than 10 for microhardness.
- The distance between the centers of two adjacent indentation must be at least three times the mean diagonal *d*
- The load of the test must be chosen from the figure 1.6.

Hardness		**Hardness with reduced load**		**Microhardness**	
Hardness symbol	Load nominal value F / N	Hardness symbol	Load nominal value F / N	Hardness symbol	Load nominal value F / N
$HV\ 5$	49,03	$HV\ 0{,}2$	1,961	$HV\ 0{,}01$	0,09807
$HV\ 10$	98,07	$HV\ 0{,}3$	2,942	$HV\ 0{,}015$	0,1471
$HV\ 20$	196,1	$HV\ 0{,}5$	4,903	$HV\ 0{,}02$	0,1961
$HV\ 30$	294,2	$HV\ 1$	9,807	$HV\ 0{,}025$	0,2452
$HV\ 50$	490,3	$HV\ 2$	19,61	$HV\ 0{,}05$	0,4903
$HV\ 100$	980,7	$HV\ 3$	29,42	$HV\ 0{,}1$	0,9807

FIGURE 1.6. VICKERS TESTS

1.1.3. KNOOP SCALE

Knoop scale is labelled with "HK". It is like the Vickers test, but the indenter used is a pyramid with a rhomboidal base made of diamond. The angles on the vertex are selected of $172{,}5°$ and $130°$. Again, in this procedure the value of hardness is calculated as the ratio of the force applied and the total surface of the indentation. This procedure is described in UNI EN ISO 4545 standard series [10] [11] [12]. For the purpose of the project this thesis is based on UNI EN ISO 4545-3 which is the standard regulating the procedures for the calibration of hardness reference blocks at the calibration laboratory level.

Knoop tests are mostly employed dealing with extremely thin and brittle materials. All the Knoop tests regard microhardness, the load used are between $0{,}009807\ N$ and $19{,}613\ N$. For this reason and thanks to the elongated shape of the indenter, the procedure is mostly indicated for coatings and thin layers.

Symbols and designations are reported in figure 1.7.

Symbol	Designation	Unit
β	Vertex angle on z–y plane	$130°$
α	Vertex angle on z–x plane	$172{,}5°$
F	Test load	N
d	Length of long diagonal in z–x plane	mm
d_s	Length of short diagonal	mm

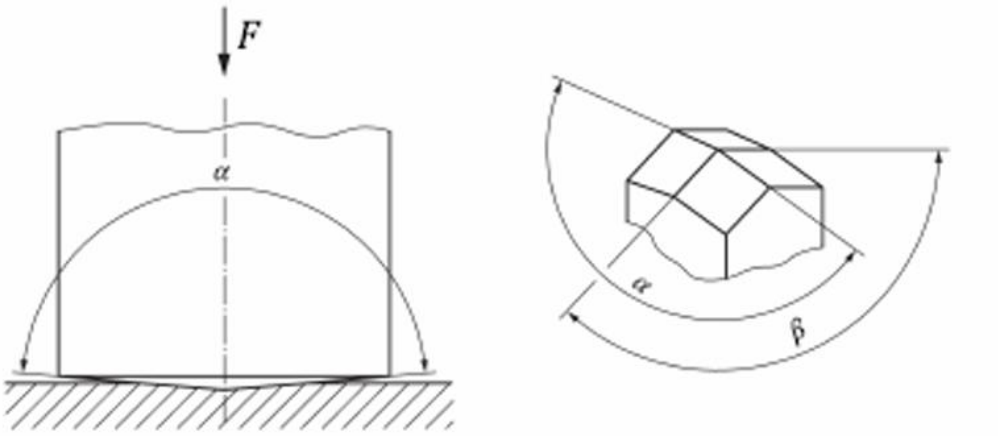

FIGURE 1.7. KNOOP DESIGNATION [10]

Once evaluated all these parameters the Brinell value is calculated with the equation (4)

$$HK = 1{,}45\ \frac{F}{d^2} \tag{4}$$

Tests must be carried out with the following procedures:

- In the temperature interval $(23 \pm 5)\ °C$ for under control conditions and in normal condition a range $10°C \div 35°C$.
- The surfaces must be cleaned and rigidly supported.
- The time between the start and the attainment of the maximum load must be in a time interval of $2\ s\ \div\ 8\ s$ for general test and a range $6\ s\ \div\ 8\ s$ for calibration tests.
- The test load must be applied for a time of $10\ s\ \div\ 15\ s$ for macro–hardness and not more than 10 for microhardness.
- The load of the test must be chosen from the figure 1.8.

Hardness Symbol	Nominal Value of test force F / N
HK 0,01	0,09807
HK 0,02	0,1961
HK 0,025	0,2452
HK 0,05	0,4903
HK 0,1	0,9807
HK 0,2	1,961
HK 0,3	2,942
HK 0,5	4,903
HK 1	9,807
HK 2	19,61

FIGURE 1.8. KNOOP TEST FORCES

The minimum distance between the centers of two adjacent indentations, oriented side–by–side, shall be at least 3,5 times the length of the short diagonal. For indentations oriented end–to–end, the minimum distance between the centers of two adjacent indents shall be at least twice the length of the long diagonal. If two indentations differ in size, the minimum spacing shall be based on the diagonal of the larger indentation. The constraints can be seen in figure 1.9.

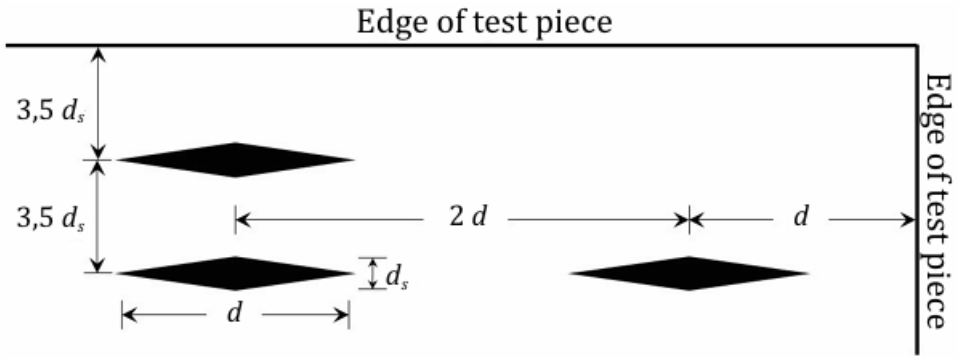

FIGURE 1.9. CORRECT DISTRIBUTION OF KNOOP TESTS [10]

1.2. INRiM– Istituto Nazionale di Ricerca Metrologica

Istituto Nazionale di Ricerca Metrologica (INRiM) is the Italian National Metrology Institute (NMI). It is a national public body supervised by the Ministry of University and Research, regulated and established by Legislative Decree No. 38 of 21 January 2004. It is born in 2006 as the merge between the *National Electrotechnical Institute "Galileo Ferraris"* and the *Institute of Metrology "Gustavo Colonnetti*" [13].

INRiM is member of *European Association of National Metrology Institutes* (EURAMET) which coordinates the collaboration between the European metrological institutes. EURAMET supports research programs with EU funding. Scientific research is the main mission of INRiM and involves the development of measurement science, materials research, the study of new standards for measurement units, and the innovative application or adaptation of measurement methods and techniques to sectors that pose new challenges to metrology and represent areas of strategic interest at national and international levels. This thesis is an example of a research project promoted by EURAMET.

Italy joins the International System of Units (SI) as one of the signatories of the meter convention in 1875. This common language includes seven *Base Quantity* (the length, the time, the mass, the electric current, the temperature, the amount of substance and the luminous intensity) each of these is described by a base unit. By combining them, it is possible to obtain all the *Derived Quantities* (velocity, acceleration, etc.)

As the Italian National Metrology Institute, INRiM has also the mission to realise, maintain and develop the national reference standards for all the unit of measurement. Since 2019, SI units have been defined through experiments that relate their values to fundamental physical constants, thus ensuring universal reproducibility. Each primary standard is the national reference with the lowest measurement uncertainty available.

INRiM is a signatory and has participated on behalf of Italy in the *Mutual Recognition Arrangement* (MRA) since its inception on 14 October 1999. This agreement was promoted by the *International Committee for Weights and Measures* (CIPM) and concerns the mutual recognition of national measurement standards and calibration and measurement certificates issued by the National Metrology Institutes of the countries that are signatories to the agreement.

In the international metrology, the concept of traceability chain (or pyramid) applies. Metrological traceability is the ability to link a measurement to a recognized standard through a chain of documented comparisons [14]. This concept is coordinated globally by *Bureau International des Poids et Mesures* (BIPM) and reinforced in countries by national laws (Weights and Measures Act in the UK and NIST Handbook 44 in the USA). In Italy, the *Sistema Nazionale di Taratura* (SNT) was established by Law 273/1991 [15]. This law stipulates that calibrations must guarantee metrological traceability to national or international standards.

In the Italian traceability hierarchy, INRiM is at the top as the guarantor of national primary standards. Below this structure are the *Accredited Calibration Laboratories* (LAT). These receive samples from INRiM and use them to calibrate their own measuring instruments with high accuracy. At the base are company laboratories that use work standards calibrated by LAT centers for internal checks. Finally, there are the instruments used in production, in test laboratories and by end users. These instruments are calibrated against company standards. The Pyramid of Traceability for hardness is illustrated in figure 1.10.

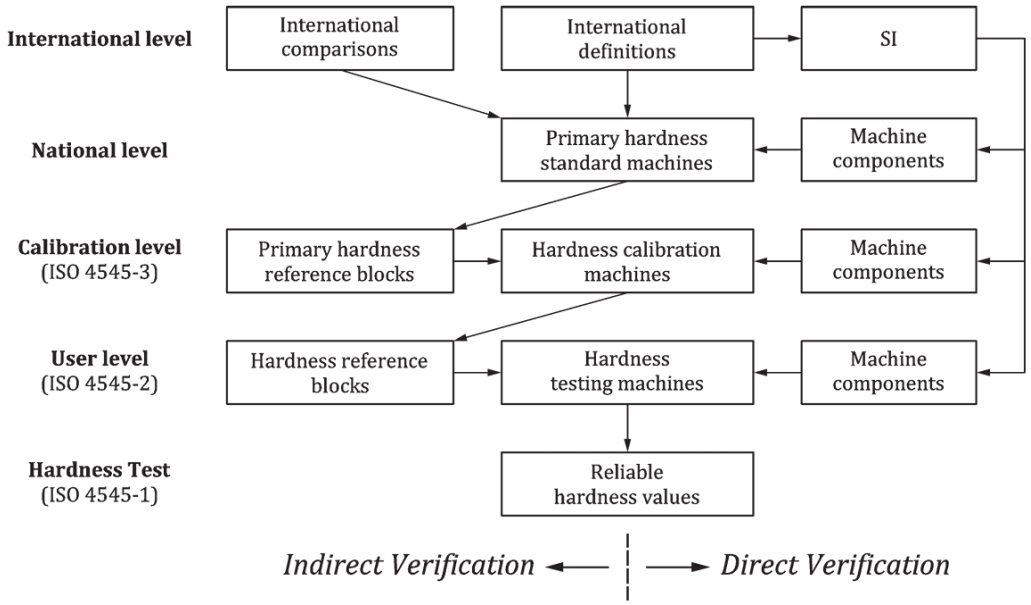

FIGURE 1.10. TRACEABILITY HIERARCHY FOR HARDNESS [10]

The calibration of a machine is the process of comparing the quantity values provided by a measuring instrument with a known reference sample. It does not involve any changes to the machine but is used to determine measurement error and the associated uncertainty. with such information it is possible to correct the measurement results, assess compliance and monitor the quality of the instrument in time [14]. Companies are required to periodically calibrate measuring instruments in accordance with Ministerial Decree 93/2017 [16]. To be considered as such, LATs must meet the requirements of technical competence,

quality management, and metrological traceability in accordance with the UNI EN ISO/IEC 17025:2017 standard [17].

Italian LATs are supervised by the single accreditation body ACCREDIA in accordance with European Regulation 765/2008. INRiM offers itself calibration services. INRiM and ACCREDIA have entered into a collaboration agreement whereby ACCREDIA recognizes and accepts the calibration certificates issued by INRiM in accordance with the metrological traceability criteria set out in ILAC P10: 07/2020, paragraph 2, points 1) and 3a).

The calibration and measurement capabilities of INRiM included in the CIPM MRA agreement are published in the BIPM database [18] and are identified in the calibration and measurement certificates issued by the presence of the CIPM MRA logo on the first page and the MRA note.

1.3. JRP – 22RPT01 TRACIND BVK–H

The thesis work carried out is part of the JRP – 22RPT01 TracInd BVK–H project promoted by EURAMET, and it is focused on the traceability of hardness measurements in the Brinell, Vickers and Knoop scales. The project lasts 36 months, starting on 1 September 2023 and coordinated by TUBITAK – UME. The overall objective of this project is to establish a traceable, consistent, and reliable indentation measurement methodology, considering the influence of measurement parameters [2].

The need for this project is also motivated by the results of previous studies. For example, an interlaboratory comparison of Brinell hardness measurements carried out in 2005 at NMI level revealed significant deviations between participants, mainly due to differences in the numerical aperture (NA) of the imaging systems used.

Similar inconsistencies are often observed in hardness block calibrations, where measured values diverge from the nominal values of the blocks despite full compliance with the relevant ISO standards. These results clearly demonstrate the lack of a fully standardised measurement methodology and instrumentation and further emphasise the need for this project.

The main participants of the project are:

- National metrology institutes including INRIM (Italy), PTB (Germany), TUBITAK – UME (Turkey), CMI (Czech Republic) and GUM (Poland).
- Universities and research institutions such as the Polytechnic University of Turin and the University of Zenica.
- Companies and industrial partners, namely EASYDUR SRL, LTF S.p.A., MPA NRW

The project is divided into six work packages (WP). Specifically, attention will be focused on WP3, which concerns the chain of traceability from NMIs to the user level. Currently, the available traceability chain is based on idealized conditions that do not accurately represent real–world operating environments of the users. It assumes static uniaxial force application through a perfectly known indenter, at a constant temperature, on specimens exhibiting purely elastic behavior. However, actual conditions introduce several additional influences, among which temperature plays a critical role.

The following factors on which such information is only partially known or not known will be studied and investigated:

- short term creep
- indenter’s geometry
- temperature
- alignment of applied load.

The expected results of the project can be seen in several areas. The primary beneficiary can be identified as the industrial community. More accurate and reliable traceability can lead to better recommendations for test equipment manufacturers. These are fundamental benefits for companies that want to produce high–quality products that are more durable and safer. Metrology and the scientific community can benefit from improvements to existing standards: ISO 6506–1, ISO 6506–2, and ISO 6506–3 for Brinell, ISO 6507–1, ISO 6507–2, and ISO 6507–3 for Vickers, and ISO 4545–1, ISO 4545–2, and ISO 4545–3 for Knoop hardness tests, which currently have deficiencies [2]. An ordered recap is shown in figure 1.11. translated from [19]:

General objective

Improving the reliability and traceability of hardness measurements in BVK scales	
Main objectives of the project	**Expected impact**
Universal definition of BVK hardness	**Industry and end users**
Establish clear criteria for hardness limits and identify the optimal measurement parameters.	Greater reliability in hardness measurements. Production of more accurate measuring instruments that comply with international standards.
Development of reference standards for hardness	**Metrology and scientific community**
Create stable and traceable hardness samples to ensure reliable measurements on an industrial scale.	New definitions and methodologies for measuring BVK indentations. Standardization of testing methods to improve consistency globally.
Creation of a chain of traceability from NMIs to end users	**International standards**
Define advanced uncertainty models and provide technical specifications for calibration and hardness testing instruments.	Revision and improvement of ISO and ASTM standards relating to hardness (e.g., ISO 6506, 6507, 4545)
Automation of hardness measurements	**Economic, environmental, and social impact**
Optimize existing software to improve accuracy and reduce operational errors in hardness measurements	Reduced production costs thanks to more precise measurements. Greater safety in industrial products. Lower environmental risk through more reliable materials for infrastructure and hazardous substance management.
Dissemination and implementation of results	
Collaborate with metrology institutes, industries, and regulatory bodies to ensure the adoption of new methodologies.	

FIGURE 1.11. OBJECTIVES AND OUTCOMES OF JRP – 22RPT01 TRACIND BVK–H PROJECT [2]

This thesis is focused on the influence of temperature and must be considered parallel to the master's thesis work *Analisi dell'effetto di creep nelle misure di durezza Brinell, Vickers e Knoop (2025)* of Chiara Merolli, former student at Politecnico di Torino, who studied the effects of the short term creep [19].

1.4. LITERATURE REVISION

Numerous scientific studies have investigated the influence of temperature on material hardness, both during production and testing phases. Although the literature is extensive, it is challenging to find sources that specifically address hardness variation within the temperature range relevant to this research $(15 \div 35)\ °C$.

In according with EURAMET, a hardness measure can be considerably influenced by the temperature of the environment, especially if small lengths have to be determined [20]. In 2014, Baron et al. introduced a predictive model for hardness in steels within the range of $(-196\ °C \div 20)\ °C$, also proposing a mathematical relationship linking temperature to properties such as toughness and yield strength [21].

However, the study focuses exclusively on low–hardness steels and a temperature range that only partially overlaps with the scope of this work.

In 2008, Pavlina and Van Tyne demonstrated a mathematical correlation between yield strength and hardness, emphasizing that this relationship is dependent on the crystal structure of the metal. This is particularly relevant for steels, which can exhibit a variety of microstructures (ferrite, pearlite, bainite, martensite, and austenite) each with distinct mechanical behavior [22].

In 2016, Torres et al. analyzed steel hardness by examining the behavior of various crystal structures at temperatures above $20\ °C$. Their research focuses on the softening mechanism, where hardness decreases significantly above $500\ °C$. Although the temperature range explored is broad (with intervals of $100\ °C$ between tests) the authors highlight that different crystal structures exhibit different slopes in the hardness–temperature relationship. At low and moderate temperatures, however, all structures show a gentle slope, indicating a relatively minor variation in hardness. The study also proposes an Arrhenius–like model to describe the trend, referencing the work of Ito (1923), which is applicable primarily at temperatures above $500\ °C$ [23].

Additionally, Guo et al. confirmed the decrease in Vickers hardness with increasing temperature in cemented carbides, demonstrating that this phenomenon is not limited to steels but also occurs in high–hardness non–ferrous materials [24].

In the second part of the twentieth century, metrology has introduced sensitivity coefficients and linear corrections of influence parameters to express a hardness value as the scale formula plus a sum of weighted corrective contributions [25]. Equation (5) is an example of metrological model of Rockwell hardness that considers N variables [26].

$$HR^{REF} = N - \frac{h}{S} + \sum_{i=1}^{N} \Delta HR_i = N - \frac{h}{S} + \sum_{i=1}^{N} c_i (X_i - X_{REF}) \tag{5}$$

c_i =sensitivity coefficient of the $i-$ th variable
X_i =value of the $i-$ th variable at the moment of the hardness test
X_{REF} =reference value of the $i-$ th variable

In his research for *International Organization of Legal Metrology* (OILM) Kersten, in 1983, reported the results of a series of Vickers and Rockwell A tests carried on a $100\ HV$ block. The author collected the values in a temperature range of $1 \div 40°C$ and measured a negative temperature coefficient for the Vickers test $c_{t,HV} = -0{,}0525\%\ °C^{-1}$ [27].

In order to be reliable in adjusting the results, Rizza, Prato, Machado and Germak propose a concrete procedure for deriving the sensitivity coefficients and the related uncertainties. The authors emphasize the importance of reporting, not only the corrected value, but also the contribution of uncertainty introduced by the correction process [28].

2. TESTS

After introducing the standards and background of the thesis, it is necessary to explain the experimental campaign that was conducted. It is recalled that the aim is to verify that there is a real correlation between hardness and temperature and to evaluate its effects so that the sensitivity coefficients and their uncertainties can be extrapolated in order to standardize the values obtained. In this sense, the question arises as to whether different hardness values may have different sensitivity coefficients. For this reason, four different hardness levels were examined:

- Soft → reference hardness block $55{,}2\ HRA$
- Medium Soft → reference hardness block $518\ HV$
- Medium High → reference hardness block $706\ HV$
- High → reference hardness block $915\ HV$

To ensure the reliability of the results, as already mentioned in the previous paragraph, specific areas were selected on each test piece in order to minimize the effects of any material inconsistencies. These areas were therefore chosen to ensure that the measured hardness was as little affected as possible by any inconsistencies.

Five indentations were made in each test area, which was marked out by an oval or rectangle. Each of these indentations within the contours corresponds to one of the aforementioned temperatures taken into consideration:

- $15°\ C$
- $20\ °C$
- $25°\ C$
- $30\ °C$
- $35°\ C$

To avoid systematic errors due to environmental conditions, an attempt was made to perform the tests at all temperatures on the same day and with as little time between them as possible. In all cases, the measurements of the indentations and the relative numerical calculation of hardness were performed at room temperature, assuming that on these scales the influence of thermal expansion is negligible on the result, given the low temperature changes and the already tiny sizes taken into consideration [24].

The experimental campaign involves performing eight different hardness tests:

- $HBW\ 2{,}5/187{,}5$
- $HBW\ 2{,}5/62{,}5$
- $HBW\ 2{,}5/31{,}25$
- $HV\ 30$
- $HV\ 1$
- $HV\ 0{,}2$
- $HK\ 2$
- $HK\ 0{,}2$

The tests were divided into two main stages. The first four, Brinell and macro-Vickers, are performed on the *PHS DW & PRIMARY* hardness standardizing machine. For this stage, the machine allowed the indentations to be performed at the desired temperature. Once the block had returned to room temperature, the indentation is measured using the *AVAMS 4.0* system. The second part of the tests, Micro Vickers and Knoop, is carried out on *The Primary Micro Hardness Standardizing Machine & GalVision*.

The figure 2.1. provides a graphical summary of the 160 hardness tests performed.

	Hardness Value / H							
	Hardness Level **Soft**							
Temperature / °C	HBW 2,5/187,5	HBW 2,5/62,5	HBW 2,5/31,25	HV 30	HV 1	HV 0,2	HK 2	HK 0,2
15	x	x	x	x	x	x	x	x
20	x	x	x	x	x	x	x	x
25	x	x	x	x	x	x	x	x
30	x	x	x	x	x	x	x	x
35	x	x	x	x	x	x	x	x
	Hardness Level **Medium Soft**							
Temperature / °C	HBW 2,5/187,5	HBW 2,5/62,5	HBW 2,5/31,25	HV 30	HV 1	HV 0,2	HK 2	HK 0,2
15	x	x	x	x	x	x	x	x
20	x	x	x	x	x	x	x	x
25	x	x	x	x	x	x	x	x
30	x	x	x	x	x	x	x	x
35	x	x	x	x	x	x	x	x
	Hardness Level **Medium Hard**							
Temperature / °C	HBW 2,5/187,5	HBW 2,5/62,5	HBW 2,5/31,25	HV 30	HV 1	HV 0,2	HK 2	HK 0,2
15	x	x	x	x	x	x	x	x
20	x	x	x	x	x	x	x	x
25	x	x	x	x	x	x	x	x
30	x	x	x	x	x	x	x	x
35	x	x	x	x	x	x	x	x
	Hardness Level **Hard**							
Temperature / °C	HBW 2,5/187,5	HBW 2,5/62,5	HBW 2,5/31,25	HV 30	HV 1	HV 0,2	HK 2	HK 0,2
15	x	x	x	x	x	x	x	x
20	x	x	x	x	x	x	x	x
25	x	x	x	x	x	x	x	x
30	x	x	x	x	x	x	x	x
35	x	x	x	x	x	x	x	x

FIGURE 2.1. EXPERIMENTAL PLAN

2.1. MATERIALS

For the experimental campaign in this work hardness blocks produced by the Japanese company *Yamamoto Scientific Tool Laboratory* (YSTL) are used. Yamamoto's blocks, thanks to their high uniformity, are worldly recognized as one of the best standard blocks for hardness in the market.

All the blocks employed in the research measure $\phi 64 \text{ x } 15\ mm$ and are made of JIS SK85 (equivalent to AISI 1085 for American standards). According to the producers, blocks are first cut from a plate material to avoid being affected by center segregation. Then a certain heat treatment is carefully applied to get a stable microstructure. After heat treatment is completed, blocks are ground, lapped and then undergo a thorough polishing process, followed by a wet buffing to improve measuring precision [29].

SK85 is a carbon tool steel in accordance with JIS G4401. It is classified as high–carbon steel, with approximately $0{,}86\ \%\ \mathrm{C}$, making it a hypereutectoid steel, very close to the eutectoid point, but with its own characteristics.

Its composition is declared by *Yamamoto Scientific Tool Lab* [30].

Composition	C	Si	Mn	P	S
$wt.\%$	0,86 %	0,17 %	0,22 %	0,011 %	0,004 %

The company uses a single chemical composition to reproduce a wide range of hardness levels by selecting the appropriate microstructure. By controlling the cooling rate during heat treatment, it is possible to modify the steel structure so to obtain the appropriate phases for the wanted hardness. Subsequent secondary heat treatments further refine the characteristics of the material by acting on precipitation of carbides, phase distribution, and morphology, with the aim of optimizing hardness and mechanical strength.

The figure 2.2. shows the CCT curves for high–carbon steels. It is possible to observe the main microstructures that form from austenite during continuous cooling, namely martensite, ferrite, retained austenite, bainite, and pearlite.

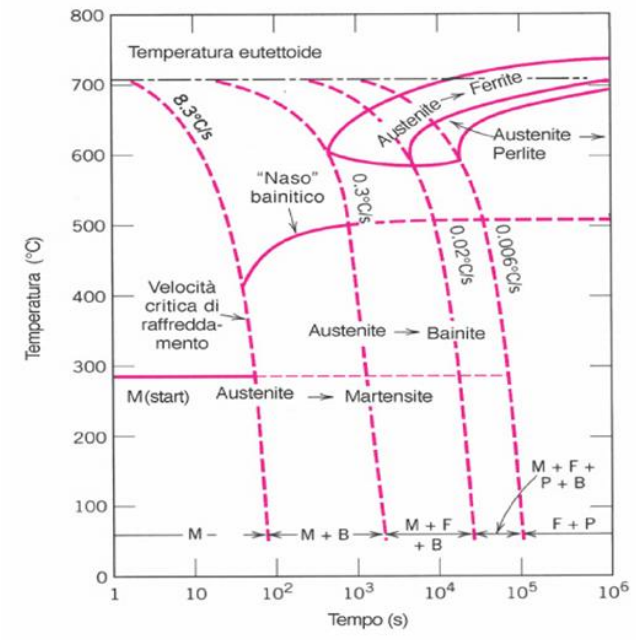

FIGURE 2.2. COOLING CURVES AND MICROSTRUCTURES FOR HYPEREUTECTIC STEEL

SOURCE: DISPENSE DEL CORSO DI TECNOLOGIA DEI MATERIALI METALLICI, POLITECNICO DI TORINO, A.A. 2020/2021. [31]

To obtain a hardness value of approximately $180\ HB$ in SK85 steel, an annealing treatment at 950 °C is required. The subsequent slow cooling promotes the formation of lamellar pearlite, a microstructure composed of alternating layers of ferrite α and cementite Fe_3C, as illustrated in the figures 2.3. and 2.4. [30].

In its maximum hardness configuration, SK85 steel can reach values close to $1000\ HV$. This microstructure consists of untempered martensite, retained austenite, and insoluble spheroidal carbides. The steel is quenched in oil held at $60\ °C$ and kept in the quenching medium until thermal stabilisation is achieved. The resulting martensitic phase exhibits a morphology known as plate martensite, characterized by its flat, elongated structure [32].

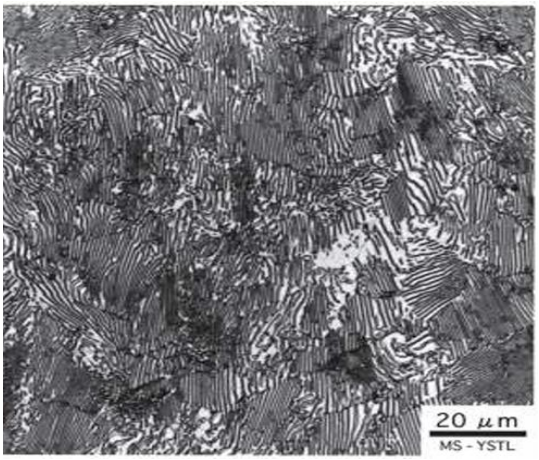

FIGURE 2.3. LAMELLAR PERLITE OF CARBON STEEL SK85.
SOURCE: YAMAMOTO SCIENTIFIC TOOL LABORATORY, STANDARD MICROSTRUCTURE CATALOG. © Y.S.T.L. [30]

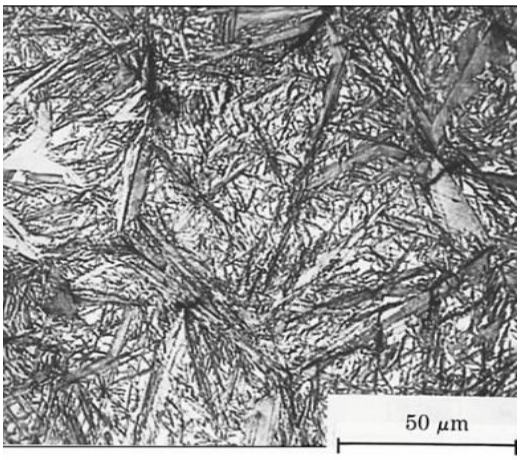

FIGURE 2.4. MARTENSITE IN A HIGH CARBON STEEL.
SOURCE: DISPENSE DEL CORSO DI TECNOLOGIA DEI MATERIALI METALLICI, POLITECNICO DI TORINO, A.A. 2020/2021.

Intermediate hardness values can be obtained by applying different cooling strategies, such as austempering or tempering at variable temperatures. Choosing the most suitable heat treatment allows distinct microstructures to be obtained, each characterized by specific mechanical properties and hardness levels.

Figure 2.5. shows the indicative hardness values associated with the main microstructures obtainable in high–carbon steels, with reference to the heat treatments used.

Treatment	Resultant Microstructure	Vickers Hardness (HV)
Oil Quenching	Martensite	≈ 1000 [32]
Quenching and Tempering ($120\ °C$, 1h)	Tempered Martensite + ε–Carbide	≈ 700 [31]
Austempering ($320\ °C$)	Lower Bainite	≈ 600 [32]
Austempering ($420\ °C$)	Upper Bainite	≈ 400 [32]
Air Cooling	Fine Perlite	≈ 250 [30]
Annealing	Coarse Perlite	≈ 180 [32]

FIGURE 2.5. HARDNESS VALUES OF HYPEREUTECTIC STEEL MICROSTRUCTURES AND HEAT TREATMENT [32] [31]

Following heat treatment, the blocks undergo surface finishing so that the surfaces where the tests will be performed are suitable for optical indentation detection. These treatments are essential to ensure that the blocks are suitable for indirect verification of hardness testers according to national or international standards (ISO, JIS, ASTM).

It is essential that roughness does not affect the generation of the indentation and its measurement. At the same time, to reduce costs and waste, it is not necessary to have the best possible tolerance for every type

of test. Consulting Yamamoto's hardness block catalogue, in figure 2.6., it can be seen that tests involving large spherical indenters, such as the Brinell $HBW\ 10$ and Rockwell $HRB\ W$ tests, do not require anything more than lapping (roughness $Ra \geq 0{,}02\ \mu m$). The blocks intended for micro and nano hardness testing undergo superfinishing processes. As regards standard macrohardness tests, such as Vicker and non–spherical Rockwell tests, the upper surface of the piece is polishing (estimated average roughness value of $Ra\ \approx 0.01 \div 0.4\ \mu m$) [29].

Assortment	Hardness value	Tolerance	Calibration number(n)	Variation (R=Max.-Min)	Materials (JIS notation)	Dimension (mm)	Finished surface	Standard based
HMV (1, 0.1)	1600	±10%	4 (2×2)	2% (HV1)	Si_3N_4	□10×5	□	JIS B 7735
HMV (1,0.1,0.01)	900, 800, **700**, 600, **500**, 400, 300	±15	6 (3×2)	5% (HV0.1)	SK85	ϕ25×6	□	JIS B 7735
〃	**200** (Be Copper)	±15	〃	〃	C1720P	ϕ25×6(2)	□	〃
〃	100 (C2600P), 40 (C1020P)	±10	〃	7 (100HV0.1), 4 (40HV0.1)	←	ϕ25×5※	□	〃
HMV (0.1,0.01,0.001)	30 (AU)	±10	〃	4 (HV0.1)	Au	ϕ25×5(0.8)	□	〃
UMV (0.01, 0.002)	900, 700, 500 (Berkovich 9.8mN tested)	±20%	6 (3×2)	10% (HV0.01)	SK85	ϕ25×6	■	JIS B 7735
〃 (0.01, 0.002)	200 (〃)	〃	〃	〃	C1720P	ϕ25×6(2)	■	〃
★HN-W for Nano indentation (HV0.01, 0.001 Berkovich 9.8mN tested)	Approx.400HV		6 (3×2 HV, Nano)		Single Crystal Tungsten	ϕ25×6 (W: ϕ9×6)	■	JIS B 7735
HV (30, 1)	1000 (SK120), 900, 800, **700**	±15	10 (5×2) /HV30,10	1.5%	SK85	ϕ64×15	○	JIS B 7735
HV (10,1)	600,**500**,400,300,**200**,150,100	〃	6 (3×2) /HV1	〃	SK85,etc.	〃	○	〃
〃	40	±10		(150HV and below 2.2%)	C1020P	ϕ64×10	○	〃
HS	100 (SK120), 95, **90**, 80, 70, **60**, 50, 40, **30**	±2	HV10 (5×2)	VHS≦1.5 (70HS and below1.2)	SK85	ϕ64×15	○	JIS B 7731
〃	20 (S20C), 7 (C1020P ϕ64×10)	〃	HS10 (5×2)	⊿HS (HS−VHS) ≦0.5	←	〃	○	〃
HL	HLE (Dia) 850, 800, 700, 600, 500	±15	(HV Calibration)		SK85	ϕ115×33	○	JIS B 7731
〃	HLD (WC) 880, 830, 730, 630, 520	〃			〃	〃	○	Related
HR C	70 (SK120), 67, 64, 62, **60**	±1	10 (5×2)	0.2	SKS3	ϕ64×15	○	JIS B 7730
〃	57, 55, **50**, 45, **40**, 35, **30**, 25, 20, 10	〃	〃	(40HRC and below 0.3)	SK85	〃	○	〃
HR A	87, 85, 83, **81**, 78, 75, 71, **65**, 56	〃	〃	0.3	Same as HRC	〃	○	〃
HR30N	83, **81**, 78, 73, **67**, 60, 55, 50, 41	〃	〃	0.6	〃	〃	○	〃
HR15N (45N)	92, **90**, 87, 85, **80**, 75 (43) (23)	〃	〃	〃	〃	〃	○	〃
HRB W	100, 95, **90**	±2	10 (5×2)	0.8	SK85	ϕ64×10	△	JIS B 7730
〃	**82**, 72	〃	〃	〃	Other steel	ϕ64×15	△	〃
〃	**62**, 52, **42**, 32	〃	〃	(50HRB and below 1.0)	C2600P	ϕ64×10	△	〃
HR30T W	78, 72	〃	〃	1.0	Other steel	ϕ64×15	○	〃
〃	62, **52**, 42, 38, 32	〃	〃	〃	C2600P	ϕ64×10	○	〃
HR15T W	87	〃	〃	〃	S35C	ϕ64×15	○	〃
〃	82, **78**	〃	〃	〃	C2600P	ϕ64×10	○	〃
HR(E·M·L·R·F·S) W	HRE**90** HRM107 HRL118 HRR123 HRF90	〃	〃	〃	(100HV)	〃	○	JIS K 7202
〃	HRM67 HRL92 HRR**105** HRS90	〃	〃	〃	(40HV)	〃	○	〃
HBW (10/3000)	600, 550, 500, 450, **400**, 350	±15	6 (3×2)	1.5%	SK85	ϕ115×18	●	JIS B 7736
〃	**300**, 250, 229 (d=4mm), **200**, 180	〃	〃	〃	〃	〃	●	〃
	HBW (10/3000) 150, HBW (10/500) 125	〃	〃	2.5%	S45C	〃	●	〃
	HBW (10/500) 100	〃	〃	3%	S10C	〃	●	〃

Finished test surface; ●Fine grinding, △plate lapping, ○Buffing, □Super finish, ■Super finish(fine), ※To be changed to ϕ25×6

FIGURE 2.6. EXTRACT FROM YAMAMOTO SCIENTIFIC TOOL LAB CATALOGUE

The experimental campaign was conducted on steel blocks characterized by four distinct hardness levels:

- Soft $55{,}2\ HRA$,
- Medium Soft $518\ HV$,
- Medium Hard $706\ HV$,
- Hard $915\ HV$.

For each block, specific zones were designated for testing under each hardness scale. These zones were carefully outlined to minimize the influence of surface anisotropy on the indentation results. Within each designated area, five indentations were performed, each at a different temperature ($15\ °C$, $20\ °C$, $25\ °C$, $30\ °C$, and $35\ °C$), while strictly maintaining the minimum spacing between indentations as prescribed by the relevant standards.

Figure 2.7. illustrates the tested samples along with their respective hardness levels and the layout of the measurement zones.

Reference Blocks	
	Soft: 55,2 HRA
	Medium Soft: 518 HV
	Medium Hard: 706 HV
	Hard: 915 HV

FIGURE 2.7. STANDARD BLOCKS USED IN TESTS

It is important to emphasise that the choice of blocks was mainly dictated by availability criteria. Reference hardness blocks differ each other in terms of structure, grain size, homogeneity and surface roughness depending on the type of hardness test they are intended to refer. For example, the block with a nominal hardness of 55,2 HRA is designed to ensure stability and repeatability of measurements specifically for the Rockwell test. This is because each hardness scale requires specific mechanical and microstructural properties, related to the load, the indenter geometry and the depth of penetration involved.

The same reasoning can be applied to the fact that all the blocks used refer to macro hardness tests. As will be discussed later, macrohardness blocks exhibit different homogeneity requirements compared to those for microhardness testing. For reduced loads tests smaller reference blocks are generally used, as they offer greater stability thanks to higher microstructural uniformity.

2.2. EQUIPMENT

As regards the equipment required for testing, the system consists of:

- Direct and indirect temperature control
- Primary Macro hardness standardizing machine
- Primary Micro hardness standardizing machine
- Optical measurement system

The temperature control system was designed and tested in collaboration with researcher Rugiada Cuccaro, C.T.E.R. Micheal Florio, and technologist Bertiglia Fabio from the AE 04 Physical Thermodynamics scientific sector.

Primary hardness standardizing machines were developed through the historical and technical collaboration between LTF S.p.A and INRiM. LTF S.p.A. is an Italian company specializing in the production, verification, and calibration of precision measurement and control instruments, particularly in the field of hardness metrology. In addition to being accredited as an ACCREDIA LAT calibration center (No. 067), it collaborates with international NMIs of Brazil, the USA, China, the UK, and others in the production of primary standardizing machines.

Both machines use dead weight system to apply the loads. Despite the advent of more sophisticated technologies, this type of machine offers high precision and repeatability thanks to calibrated masses and high reliability in time. The application of the load is monitored and plotted on the screen during the tests by means of a load cell while an interferometer measures the vertical displacement of the indenter.

LTF S.p.A. has developed the *Automatic Vickers Analysis Measurement Software* (AVAMS 4.0) used for the automatic optical measurement of the border of the indentation. This software is implemented in some primary micro-hardness standardizing machines produced by LTF S.p.A.

2.2.1. TEMPERATURE CONTROL

To perform temperature measurements, the test block must be heated or cooled to the desired temperature. The validity of the test strictly depends on the surface on which the indentation is made remaining at the desired temperature for the time necessary to position the block on the support, perform the set–up procedures, and finally perform the hardness test.

Preliminary tests are implemented to understand the mechanism of the system's heating exchange and consequently to be able to make the right decision about the temperature control system. These experiments are performed in the laboratories of Thermodynamics of INRiM.

Initially, the block is heated using a climatic chamber for enough time so that there is no temperature gradient between the surface and the internal volume. To ensure that the sample remained at the correct temperature for a sufficient period, it was left in the chamber overnight at $35°C$, then placed on an aluminium support block at room temperature, functioning as a heat dissipator, and monitored. The thermal inertia test is performed using a FLUKE model 1586A SUPER–DAQ multimeter in line with two Pt100 resistance thermometers and two TC–T thermocouples:

- Ch1 Pt100 s/n AFM01 located in climatic chamber (Tcamera)
- Ch1 Pt100 s/n AFM02 located on the support in the laboratory (Tlab)
- Ch3 TC–T s/n TCT– 03 located on the center of the block (T3)
- Ch4 TC–T s/n TCT – 04 located on the lateral position of the block (T4)

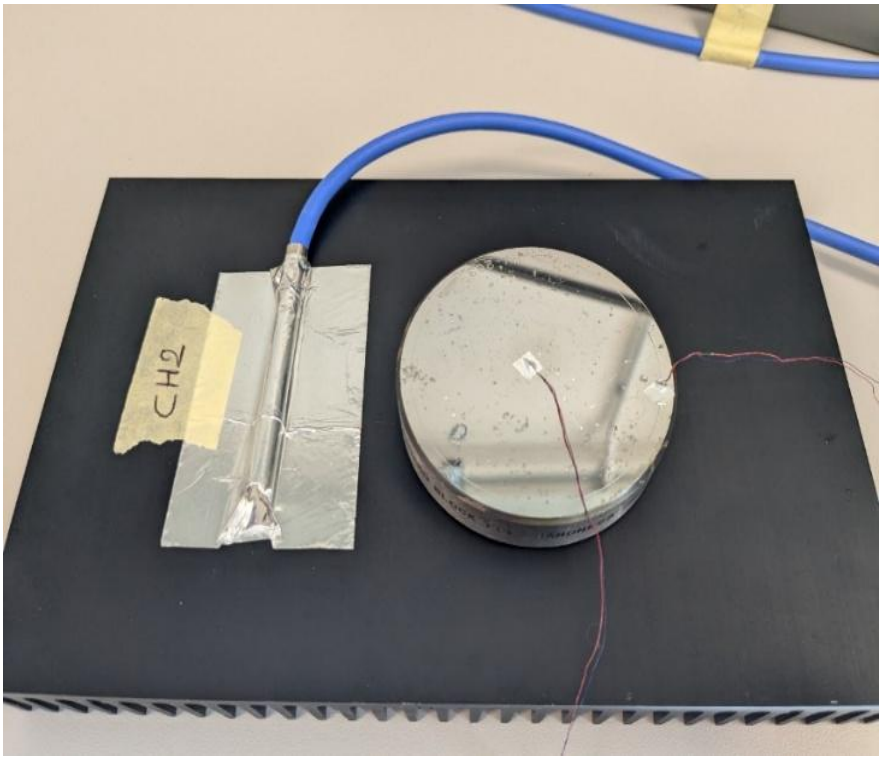

FIGURE 2.8. THERMAL INERTIA TEST SET-UP

The thermocouples are mounted on the surface of the sample using silver adhesive tape. One is inserted in the center of the sample TCT– 03, the other near the edge at $30\ mm$ from the first (TCT– 04). The Pt100 s/n AFM02 is mounted on an aluminium block that will house the sample after it has been thermostated. In figure 2.9. are reported the results of the experiment.

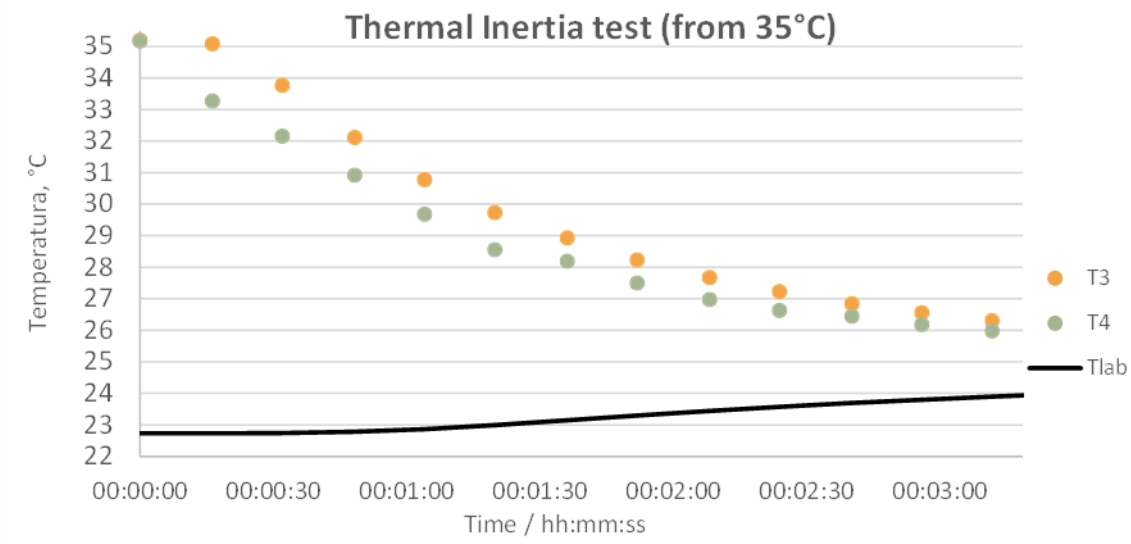

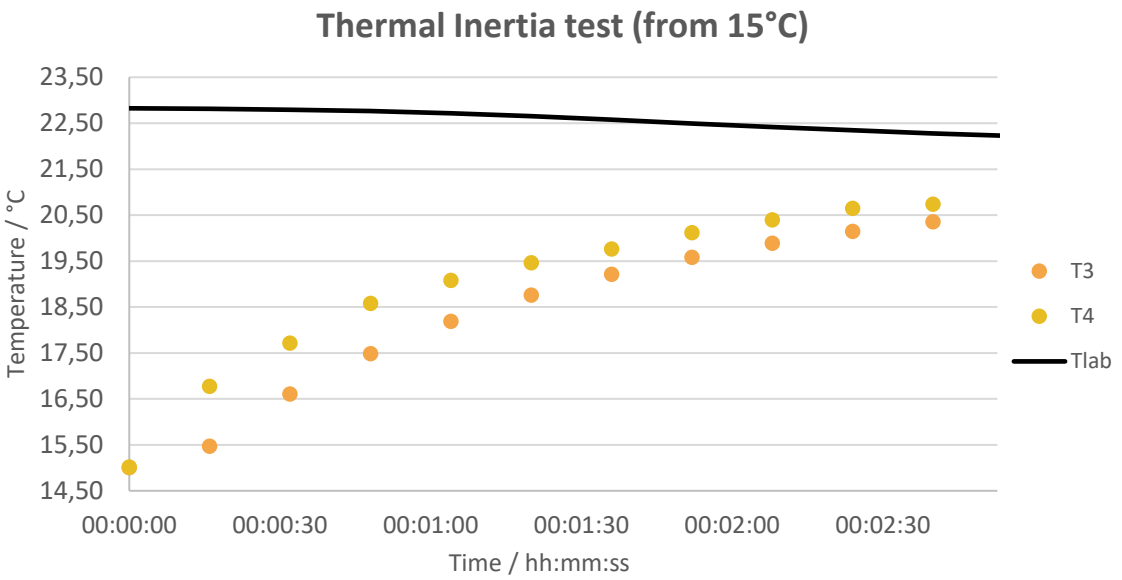

FIGURE 2.9. THERMAL INERTIA TESTS

The test result shows a cooling ramp of $5°C/min$, which invalidates the hardness tests at temperature of $35°C$. It is therefore necessary to consider a system capable of maintaining a constant surface temperature of the block. As for the process starting at $15°C$, a heating ramp of approximately $3°C/min$ is obtained in the first minute. In this case, it is decided not to invest time in active temperature control, but passive control is considered sufficient.

The proposed solution was to use a cooling system with water contained within a HAAKE C50P fluid thermostat. Temperature control is achieved by passing water at the desired temperature through a copper pipe welded to a hollow cylinder, which acts as a heat exchanger. The hollow cylinder acts as a seat for the metal block. With this technique, it is possible to both cool and heat the sample, but not to maintain its temperature easily. The choice was convincing for tests at temperatures of $15°C$ and $20\ °C$. In figure 2.10. are reported the photo of the whole system and the personal CAD model of the heat exchanger.

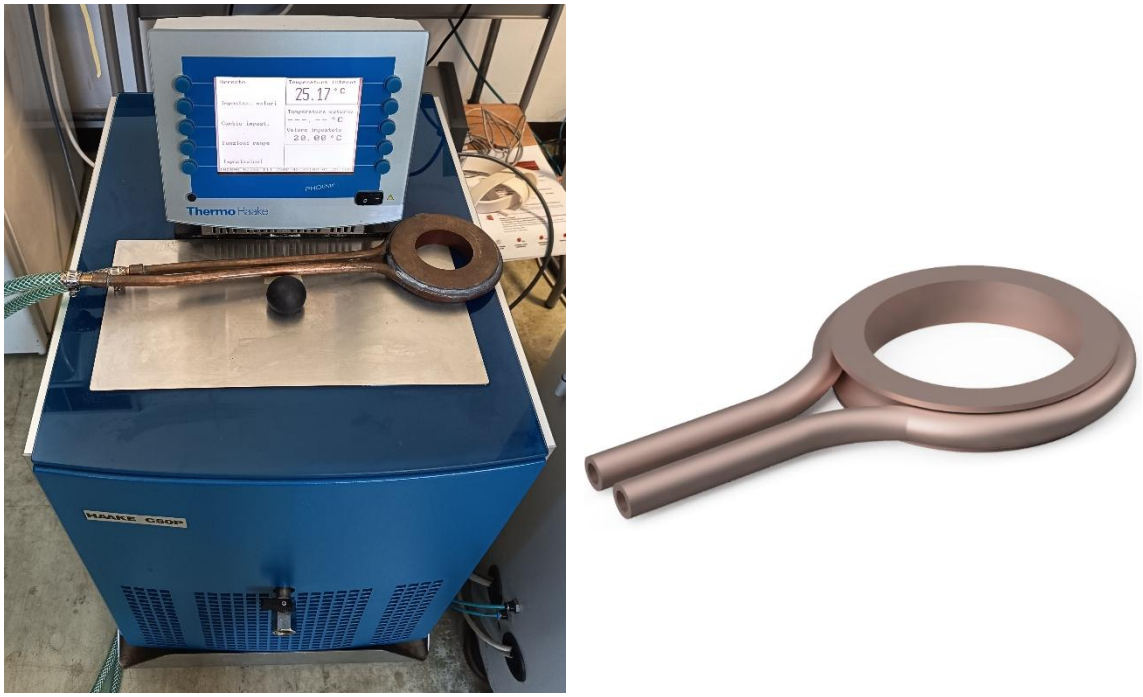

FIGURE 2.10. COOLING PASSIVE CONTROL SYSTEM SET-UP

In agreement with Rugiada Cuccaro, INRiM researcher in the AE04 Physical Thermodynamics sector, and implemented with the help of Micheal Florio, INRiM technical collaborator in the same sector, it was chosen an active temperature control. The set-up employs Watlow 17410–C6 heating bands powered up to $12\ W$ and a PID control system for test at $25\ °C$, $30\ °C$ and $35°C$.

This active control solution was selected for two main reasons. The first was to compensate the cooling ramp occurring in higher temperature cases, stronger than the test subjected to cooling. The second reason is that the active temperature control reduces the temporal uncertainties of the experiment, which is a good practice to follow when investigating such narrow temperature ranges as those under examination.

The system is composed of:

- DF1731SB linear bench power supply
- Watlow 17410–C6 heating band glued to the side surface of the block
- Eurotherm P116 PID controller
- 4–wire Pt100 thermoresistance applied between the heating band and the surface of the block
- Thermal insulation

The power supply is set to provide $60\ V$ and $50\ mA$ of direct current and is connected in line with the heater and the PID. The controller, powered at $220\ V$, acts as a relay. On the PID screen, it is possible to enter the desired set point (in red) and monitor the current temperature (in green) of the resistance thermometer applied to the side of the block. The entire system is shown in figure 2.11.

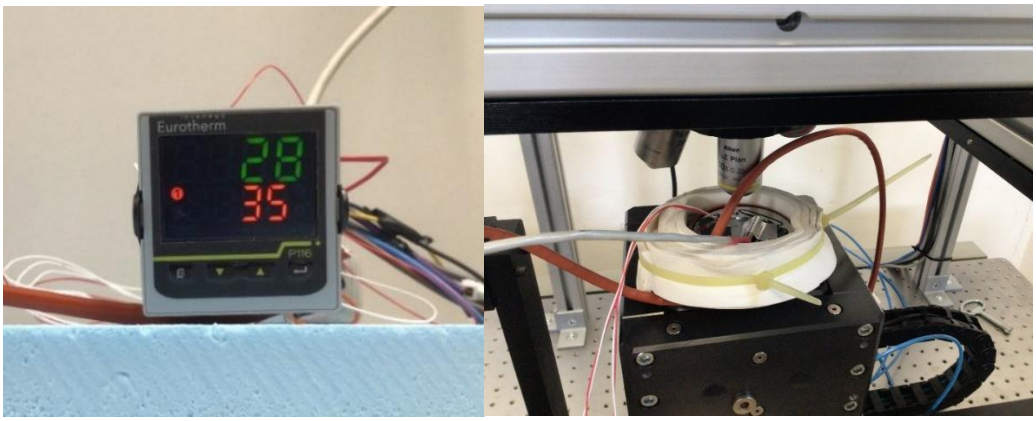

FIGURE 2.11. ACTIVE CONTROL SYSTEM SET-UP

In addition to the heater, two thermal insulators are also applied. When performing heating tests on the block without insulation, it is not possible to reach a temperature of $35°C$ due to excessive heat exchange with the anvil of the durometer and convective exchange with the air. After applying the insulating material, however, it is possible to reach and maintain the temperature in an estimated time of 35 min. The figures 2.12. and 2.13. show the importance of the application of the insulation during the heating tests.

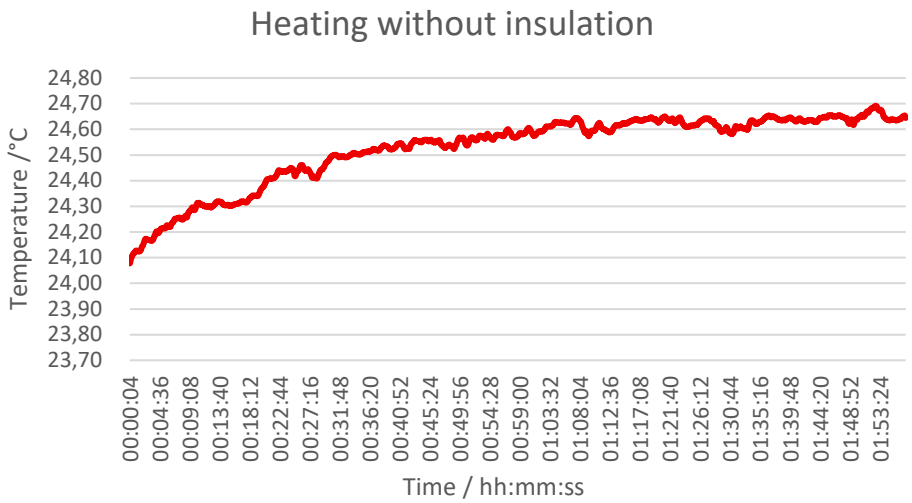

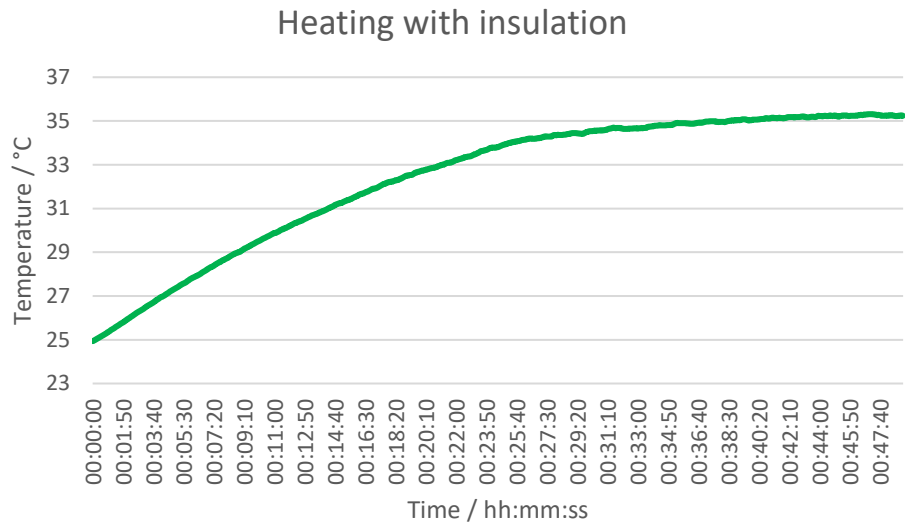

FIGURES 2.12. AND 2.13. COMPARISON BETWEEN THE SET UPS IN HEATING TESTS

2.2.2. BRINELL AND MACRO–VICKERS MACHINES

The primary hardness standardizing machine used in the Brinell and $HV\ 30$ tests is a PHS DW & PRIMARY machine [33], designed for primary hardness testing by INRiM and manufactured by LTF S.p.A. under license from CNR. It is composed of the elements that are indicated in figure 2.14:

1. Servomotor
2. External frame
3. Load Cell
4. Laser interferometer
5. Internal Frame
6. Aluminum basket
7. Calibrated masses
8. User interface
9. Joystick
10. Computer
11. Load selection ring–nut

FIGURE 2.14. PHS DW MACHINE

The external frame [2] supports the entire mobile structure and the anvil on which the hardness block rests. It is made of cast iron, a material selected for its high rigidity and damping capacity, which helps isolate the system from external vibrations. In addition to the anvil, the fixed structure houses the load selection mechanism [11], the laser interferometer [4], and the servomotor [1]. The servomotor supports the load cell [3], the internal frame [5], the aluminium basket [6], and the calibrated weights [7].

Relative motion between the mobile structure and the external frame is enabled by air bearings operating at a pressure of 4 bar, which ensure minimal friction and excellent repeatability. The servomotor is controlled from the user interface [8], which allows the operator to select either manual mode, using the joystick [9], or automatic mode, managed by the dedicated software [10].

The high precision of hardness measurements performed at the national primary institute is achieved through the use of a load-application system based on calibrated weights, which ensures excellent repeatability and traceability. This differs from common commercial hardness testers—lever-based, screw-driven, or hydraulic—which inherently exhibit greater variability.

During a measurement, the machine's kinematics are defined by the relative movement between the external frame, the internal frame, and the mass-carrying basket. The operating cycle consists of three main configurations, labelled A, B, and C, as illustrated in figure 2.17. The operator must ensure compliance with hardness testing standards by appropriately controlling the parameters governing these transitions, such as preload application, loading rate, dwell time, and unloading conditions.

The cycle begins at the upper working point. In this configuration (A), the inner frame and the basket, on which all the calibrated masses rest, are suspended by the load cell. In this state, two fundamental actions must be performed for the hardness test. The first is the choice of the indenter. The second is the choice of the load with which to carry out the test. For this machine, tests were performed with a 2.5 mm diameter tungsten Brinell indenter and a Vickers indenter.

Once the penetrator has been selected, insert it by screwing it through the locking washer on the side of the indentation and insert its tab into the centering bushing on the other side: pass the entire assembly through the ring nut and screw the ring nut to the loading basket.

FIGURE 2.15. INDENTER SYSTEM

In this position, it can also be chosen the load. In this configuration the internal frame supports the loading basket and all the sequential masses, freeing them from the base. The masses to be used during the test are selected using the load selection system ring–nut, shown in figure 2.16. This operation will position the rung that must support those of the masses that are not to be used. The load applied to the test piece will be the sum of all the masses applied. The weight of the masses must also be added to the suspended mass of the aluminium basket ($\sim 3\ kg$) and the total weight of 3 additional cylinders ($7\ kg$).

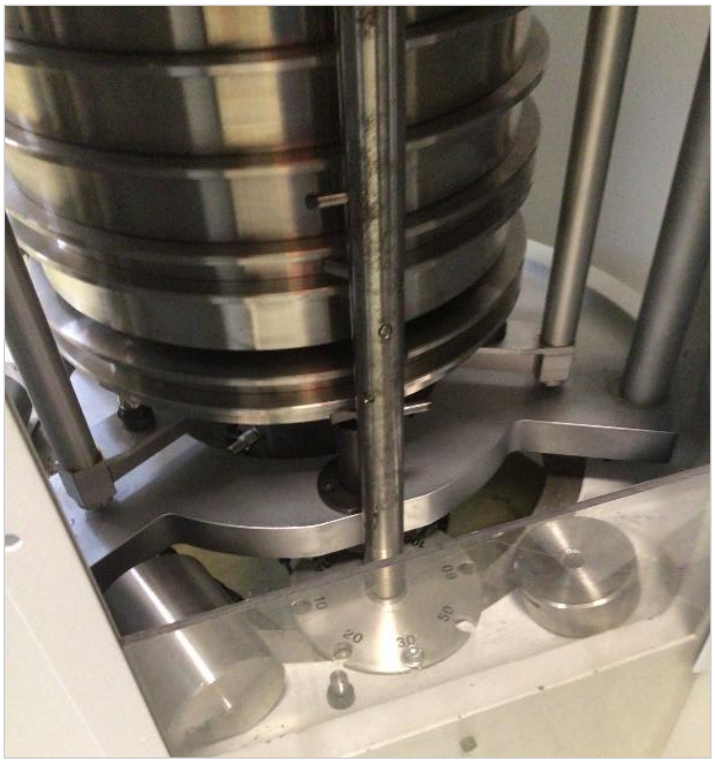

FIGURE 2.16. LOAD SECTION RING NUT

After these operations, the cycle can begin. The lasers are reset to zero, and the frame lowers at a speed of $0{,}2\ mm/s$ for a specified distance of $0{,}2\ mm$, in order to avoid noise caused by inertial forces on the load cell. After the travel, the load cell is reset and the indenter begins to approach the test piece, lowering the

frame at the set approach speed and supporting the masses with the lower supports. The standard defines the maximum approach speed, and the operator must satisfy it by adjusting the value on the computer software. In configuration B, the not used masses meet the rung of the load selection ring–nut and unload their weight to ground. In this moment the load cell measures the force of the test masses, the basket and the internal frame.

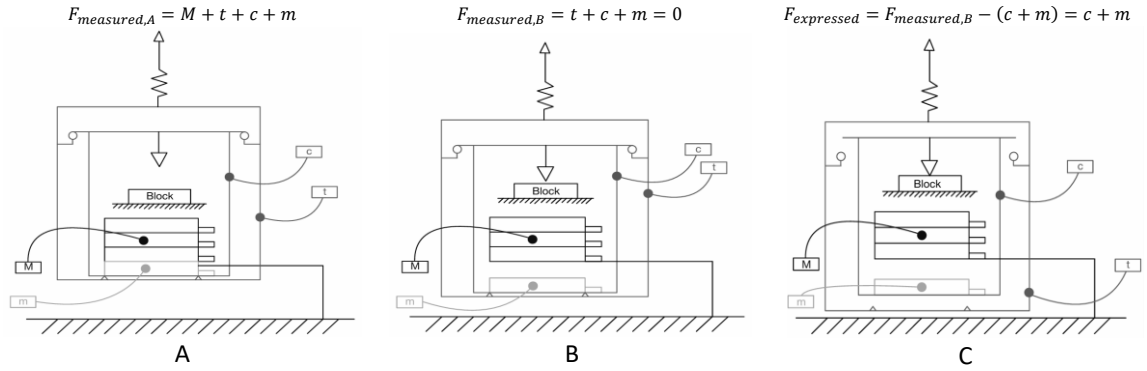

FIGURE 2.17. MOVING PARTS OF THE MACHINE
(c = basket, M = not chosen masses, m = chosen masses, t = inner frame)

The last configuration (C) starts when the indenter contacts the test piece and the suspended masses, and the basket gradually unload his weight on the block. In this moment the load cell detects a force variation equal to a given initial load value expressed in newtons. Figure 2.18 shows the measurements of the load cell and the laser interferometer during the configuration C. The approach stage finishes, and the load application stage starts (FIRST VIOLET LINE). In this stage the frame descends using the first set speed until the first set percentage is reached. The change from the first to the second set speed takes place gradually from the first to the second percentage and then continues at the second speed (these two steps are defined by a TWO DARK–BLUE LINES). When the loading cell detects that the load has been applied within the set tolerance, the application stage finishes, and the load maintenance stage starts (SECOND VIOLET LINE). This stage will last for the maintenance time and will be controlled by the internal PC clock. During this phase, the frame will continue its downward movement for the time set for further load advancement, continuing to use the second load application speed for the time set for further frame advancement and the frame advancement speed set for the remaining time (these two steps are defined as A PAIR OF SKY–BLUE LINES). The ascent starts will be determined each time when the exact additional load maintenance time (THIRD VIOLET LINE) on the indenter is reached, as set in the procedure.

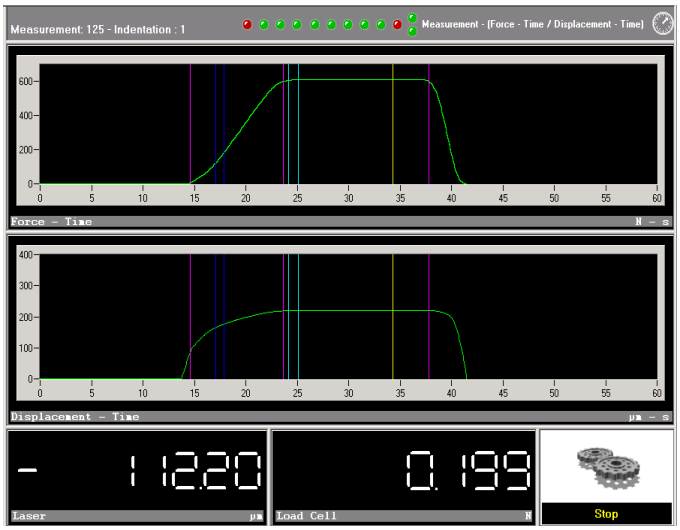

FIGURE 2.18. PRIMARY USER INTERFACE

2.2.3. MEASUREMENT WITH OPTICAL MICROSCOPE

An optical microscope is used to measure the indentation size. The entire system consists of:

1. Optical microscope
2. Light source
3. Interferometer
4. Mobile base
5. Laboratory power supply
6. Computer

FIGURE 2.19. MEASURING SYSTEM

To measure the indentation, select the appropriate lens and place the sample on the movable base, orienting it with the aid of the lens so that the length to be measured lies on the horizontal axis. The lens chosen is a lens with a numerical aperture $NA > 0{,}4$, as suggested in the article by Low, Hattori, Germak, and Knott [34]. In this configuration, ambient lighting has no effect on the optical detection of the indentation edge.

The edge of the indentation is measured using AVAMS 4.0 software. The *Automatic Vickers Analysis Measurement Software* is developed by LTF S.p.A. to:

- Acquire images of the indentation using a digital optical microscope.
- Automatically detect the diagonals of the indentation.
- Calculate hardness according to the Vickers or Knoop scales.
- Manage data measurement and generate reports.

The software follows a precise sequence of operations. The first step is to focus on the indentation to be measured and then adjust the black and white level of the image. The program, connected to the microscope camera, requires high contrast to recognize the outline of the indentation.

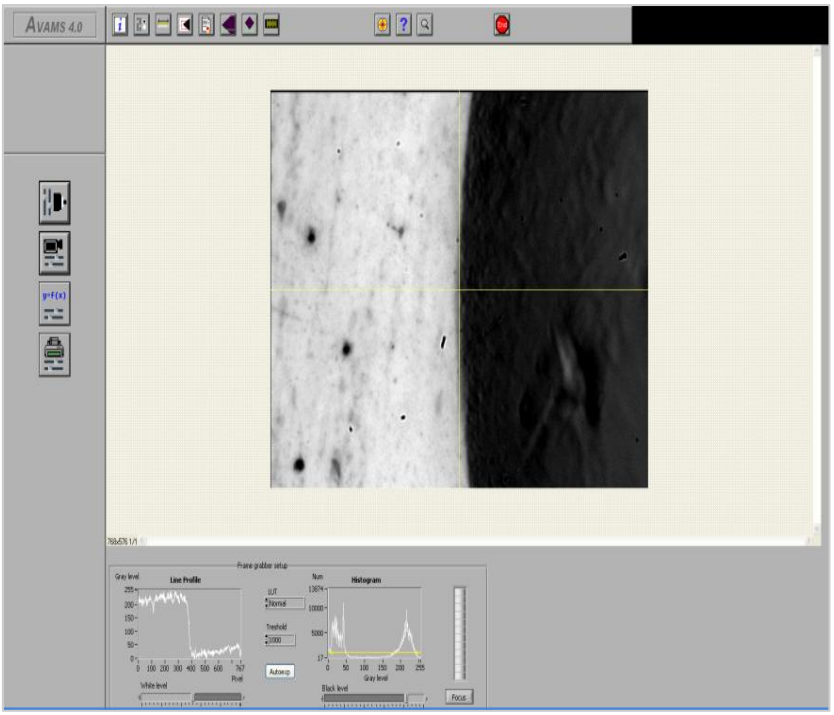

FIGURE 2.20. BRIGHTNESS AND CONTRAST ADJUSTING ON AVAMS 4.0

The next step is to decide on the parameters of the window with which AVAMS 4.0 searches for the corner of the indentation. The algorithm generates a rectangle of the chosen dimensions that recognizes the edge and iteratively calculates the corner of the indentation. Once the profile of the indentation has been selected, the software interpolates the edge through the computer pixels.

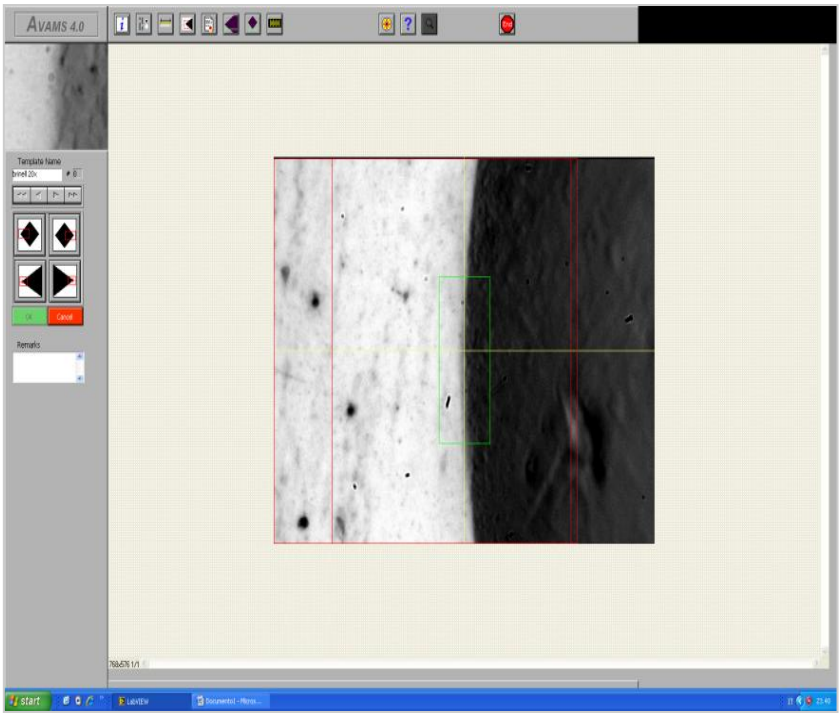

FIGURE 2.21. WINDOW SELECTION ON AVAMS 4.0

The measurement is then started. Starting from the interpolated profile, the software moves the mobile base to the right until it enters the area around the opposite part of the profile, measuring this distance x_i

with the interferometer and the uniaxial meter. The remaining displacements are calculated by the software by counting the pixels in the screen $x_{p,sx}$ and $x_{p,dx}$. The final measurement is obtained by summing the three components obtained

$$x = x_{p,sx} + x_i + x_{p,dx}$$

This provides repeatable measurements with adequate uncertainty.

The other direction to be evaluated is then measured by rotating the test piece by $90°$ and repeating the operation.

$$y = y_{p,sx} + y_i + y_{p,dx}$$

Once both measurements and their respective uncertainties have been obtained, the hardness is calculated in accordance with the standards.

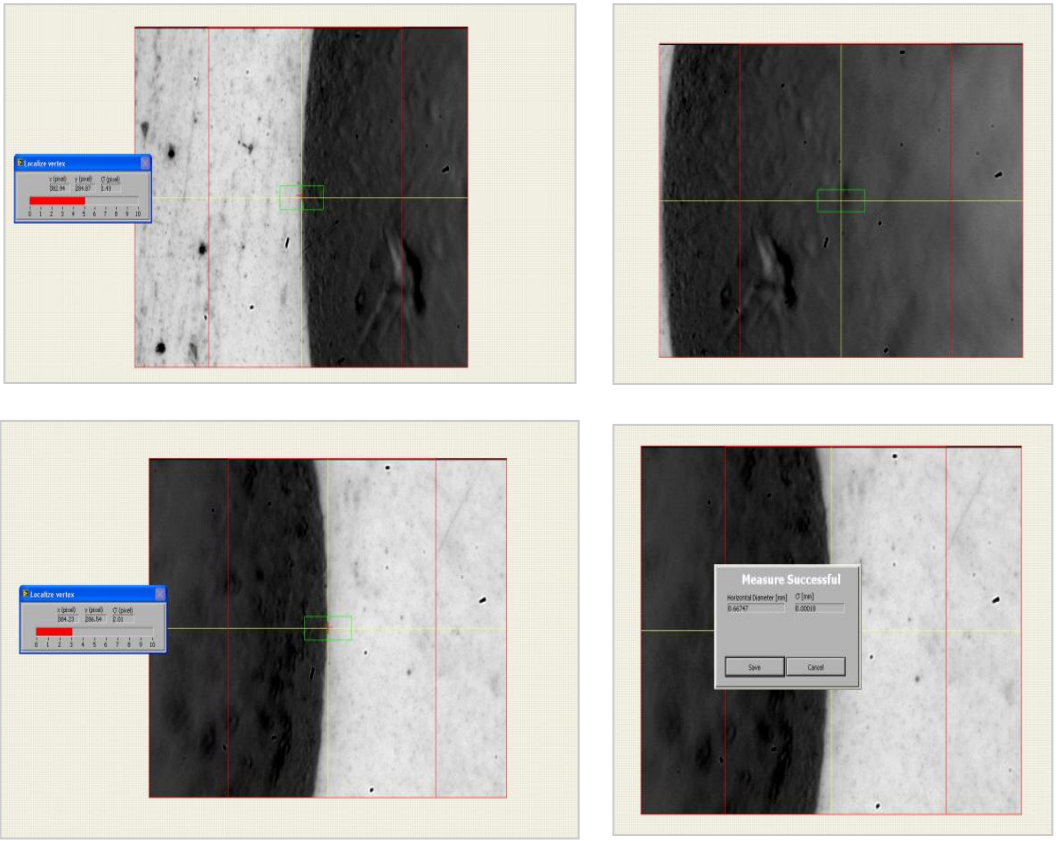

FIGURE 2.22. MEASUREMENT CYCLE ON AVAMS 4.0

2.2.4. MICRO–VICKERS AND KNOOP MACHINES

The *Primary Micro Hardness Standardizing Machine* (MHSM) is the system used to perform Vickers $HV\ 1, HV\ 0{,}2$ and Knoop $HK\ 2, HK\ 0{,}2$ microhardness tests. Like the PHS DW & PRIMARY, the system was designed through a collaboration between INRiM and the hardness testing department of LTF S.p.A. Galileo Durometria. Again, the use of direct weights ensures accurate and reliable testing. In addition, the MHSM offers the convenience of performing indentations and measuring indentations in a repeatable and automated manner in a single process, avoiding the need to move the block from one machine to another. The MHSM is illustrated in figure 2.23. and it's composed of:

1. Cabinet
2. Image acquisition microscope
3. Penetration station
4. Sample holder table
5. Anti–vibration table
6. Pneumatic handling system
7. GalVision software

FIGURE 2.23. PRIMARY MICRO HARDNESS STANDARDIZING MACHINE

The cabinet houses all the electronic components necessary for the complete control of the mechanical section of the MHSM. It also contains the computer equipped with the GalVision control and measurement software. The microscope includes a high–definition CCD camera for image display on the monitor and is fitted with a rotating turret carrying five different objectives.

The indentation station is composed of three main sections: an upper part, a central part, and the indenter extending below. The upper section includes a servomotor coupled with a micrometric screw shaft, whose movement is limited by inductive sensors and mechanical microswitches serving as emergency stops. The micrometric screw shaft drives the central section, which acts as a load application basket with a seat for calibrated masses. The lower section consists of the indenter itself, which protrudes from the air bearing.

The X–table is directly mounted on the anti–vibration table and enables the measurement of indentation lengths using an integrated laser positioned alongside it. It also allows the sample under calibration to be moved from the measurement position (under the microscope) to the indentation position (under the indentation station). The position of the X–table is continuously monitored by an internal encoder mounted on the slideway.

Above the X–table is the Z–table, which moves the specimen support vertically to focus the surface according to the selected objective. The Y–table, positioned above the Z–table, enables transverse translation of the specimen support, and its position is likewise tracked by an internal encoder. Finally, the R–table (rotating table), mounted above the Y–table, allows rotation of the indentation within the microscope's field of view to align the indentation axes with those of the measurement system.

To minimize the effects of residual vibrations, the entire mechanical structure is mounted on a Thorlabs anti–vibration table, model Nexus B75120B. The MHSM system operates with an air supply of $6\ bar$ and a flow rate of at least $(30 \div 50)\ L/min$. The air–feeding system for the pneumatic guides consists of two filters arranged in series and a pressure regulator, maintaining a working pressure of approximately $5\ bar$. The pneumatic system must provide air that is completely dry to ensure optimal performance and measurement stability.

The GalVision software acts as the user interface. The entire hardware system can be managed through the application. After loading the basket with the appropriate load, the operator must place the block on the movable table to perform the test. Focus. Record the X, Y, Z, R surface point and select the correct procedure. When the machine is started, the moving table takes the test piece to the indentation station, where a laser and a load cell monitor the test process and send the signal directly to the screen, as in figure 2.24. At the end of the indentation, the test piece is brought under the microscope where the software is

able to automatically focus on the surface, recognize the edge, and accurately measure the distance between one edge and another.

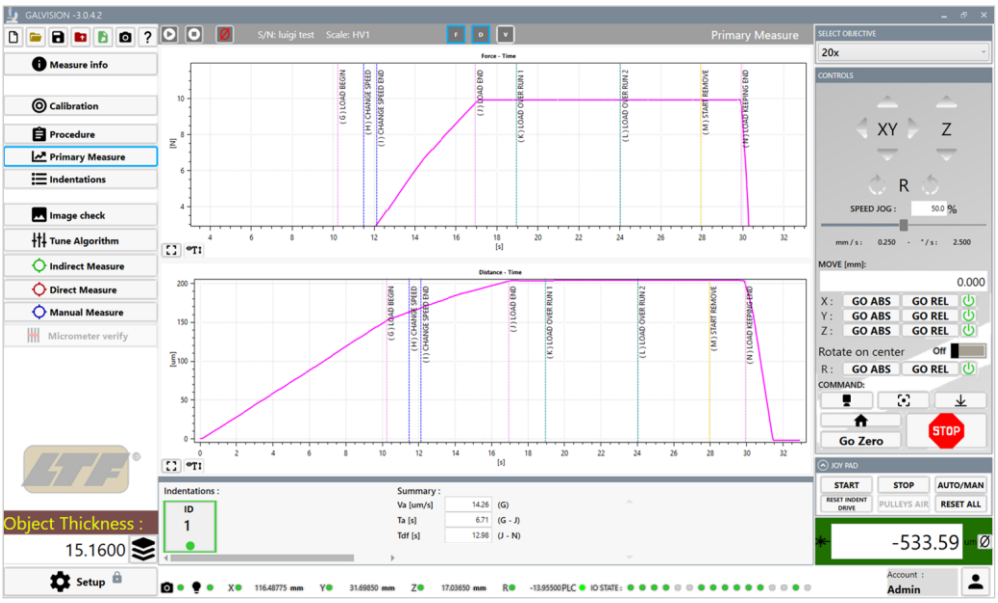

FIGURE 2.24. GALVISION USER INTERFACE

3. DATA ANALYSIS

The analysis of the data obtained from the tests forms the main body of the project. This step is mainly based on EURAMET's *Guidelines on the Estimation of Uncertainty in Hardness Measurements* (GUM) [20] and implements statistical procedures developed at INRIM. The primary objective of this analysis is to assess whether there is a dependency between hardness and temperature. Once this relationship has been demonstrated effective, the procedure involves calculating the temperature sensitivity coefficients c_T and the related uncertainties $u(c_T)$.

The procedure starts with the collection of the results coming from the experimental campaign. Each data x deriving from a measurement procedure can be represented by the measured value $\bar{x}$, the associated extended uncertainty $U\ (x)$ and the unit of measurement. In this case, during the experimental campaign, two measurements are associated with each test, the first relating to the calculated hardness $\overline{H}$ and its associated extended uncertainty $U(H)$, while the second to the temperature $\overline{T}$ and its associated expanded uncertainty $U(T)$.

$$H = \overline{H} \pm U(H) \quad (6)$$
$$T = \overline{T} \pm U(T) \quad (7)$$

A graphical representation of each data can be proposed in a Temperature – Hardness chart in figure 3.1. The red central circle coincides with the point $(\overline{T}, \overline{H})$. The red bars represent the interval in which the true value of the measurand has the $95\ \%$ of probability to exist, each of them has a total length equal to twice the expanded uncertainty $U(x)$, as indicated by the blue arrows for hardness.

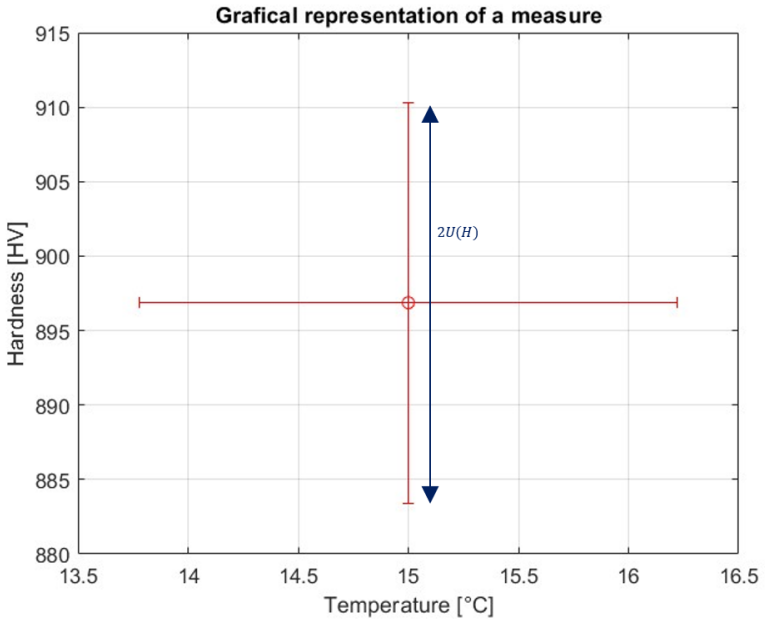

FIGURE 3.1. GENERIC EXPERIMENTAL POINT WITH EXPANDED UNCERTAINTIES

The procedure for evaluating the value of $\overline{H}$ is that contained in the hardness standards ISO 6506–3, ISO 6507–3, and ISO 4545–3 [6] [9] [12] and the results are reported in figure 3.2. In the same figure are reported the value of the nominal temperatures. At any test, the $\overline{T}$ value was obtained by recording the value returned by the PID connected to the 4–wire Pt100 thermoresistance, introduced in chapter 2.2.1 *Temperature Control*.

	Hardness Value / H							
	Soft Nominal Hardness Value (55,2 HRA)							
Temperature	HBW 2,5/187,5	HBW 2,5/62,5	HBW 2,5/31,25	HV 30	HV 1	HV 0,2	HK 2	HK 0,2
15	191	177	182	194	183	207	216	547
20	192	176	182	192	189	205	208	547
25	179	163	184	181	189	206	214	509
30	178	160	185	188	189	206	212	505
35	176	163	183	187	176	203	212	506

	Medium Soft Nominal Hardness Value (518 HV)							
Temperature	HBW 2,5/187,5	HBW 2,5/62,5	HBW 2,5/31,25	HV 30	HV 1	HV 0,2	HK 2	HK 0,2
15	547	496	451	513	520	490	535	570
20	547	490	449	510	517	545	531	569
25	509	460	420	518	524	508	525	576
30	505	465	423	516	518	528	537	509
35	506	456	436	508	510	458	519	561

	Medium Hard Nominal Hardness Value (706 HV)							
Temperature	HBW 2,5/187,5	HBW 2,5/62,5	HBW 2,5/31,25	HV 30	HV 1	HV 0,2	HK 2	HK 0,2
15	742	666	604	692	698	726	711	811
20	741	660	586	692	699	738	711	791
25	743	664	594	686	723	724	701	814
30	744	672	593	685	720	728	712	779
35	745	661	588	684	691	718	698	806

	Hard Nominal Hardness Value (915 HV)							
Temperature	HBW 2,5/187,5	HBW 2,5/62,5	HBW 2,5/31,25	HV 30	HV 1	HV 0,2	HK 2	HK 0,2
15	932	809	768	897	949	978	858	1080
20	933	805	705	896	948	990	946	1002
25	913	804	702	884	933	991	858	1001
30	925	805	721	888	947	980	902	978
35	931	798	697	887	994	985	853	995

FIGURE 3.2. EXPERIMENTAL RESULTS

The assessment of uncertainties related to hardness and temperature was not identical. For the former (i.e., those relating to hardness) the Calibration and Measurement Capabilities (CMCs) declared by INRiM were consulted [35]. CMC is a value, that expresses how well a laboratory can measure. In the hardness field the Italian NMI declares the following capabilities in the form of relative standard uncertainty w_H in function of the mean diameter d_m of the indentation.

$w_H = \frac{\left(1 + \frac{240}{d_m}\right)}{200}$	HBW 2,5/187,5 HBW 2,5/62,5 HBW 2,5/31,25
$w_H = \frac{\left(1 + \frac{43}{d_m}\right)}{200}$	HV 30
$w_H = \frac{\left(1 + \frac{20}{d_m}\right)}{200}$	HV 1 HV 0,2

However, the CMCs are the calibration measurement capabilities declared by the laboratory. In this case, to be more conservative, was chosen for all measurements a relative standard uncertainty

$$w_H = \frac{1{,}5}{200}$$

Once the value of the relative standard uncertainty has been determined, the following steps are taken to obtain the hardness coverage interval $H - U(H) \div H + U(H)$

$$u(H) = w_H * H \quad (8)$$

$$U(H) = 2 * u(H) \quad (9)$$

The uncertainty regarding the test temperatures was assessed by considering it as a category B uncertainty contribution. Together with Andrea Prato, it is decided to evaluate both the spatial and temporal uncertainty of the temperatures. The first assessment aims to measure the radial temperature variability on the upper surface of the block. To collect this distribution, tests are carried out in the most extreme cases, i.e., when the block is cooled to $15°C$ and when it is kept constant at $35°C$. In both cases, cooling by means of the heat exchanger and active heating control, the probe was passed when the entire system was in equilibrium with the environment. Figure 3.3. shows the values obtained from the test.

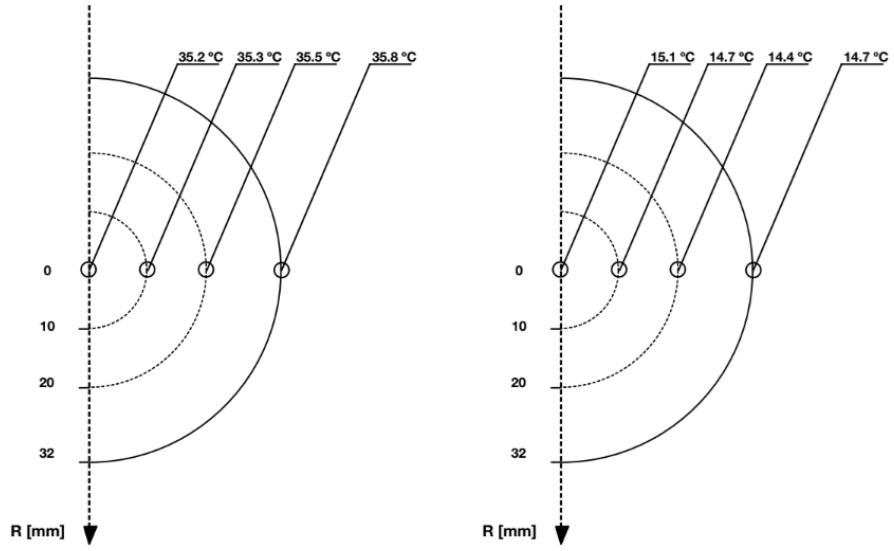

FIGURE 3.3. ASSESSMENT OF TEMPERATURE SPATIAL VARIATION

Due to the temporal uncertainty of the temperatures, two contributions are evaluated. Initially, the temperature variation during a test is measured at the center of the block. This experiment was performed for each of the temperatures in the program. However, it was found that with active control, the temperature variation is less than the PID resolution. Therefore, only the temporal variability is considered in cases where the block is cooled, i.e., in tests at 15 and 20 $°C$.

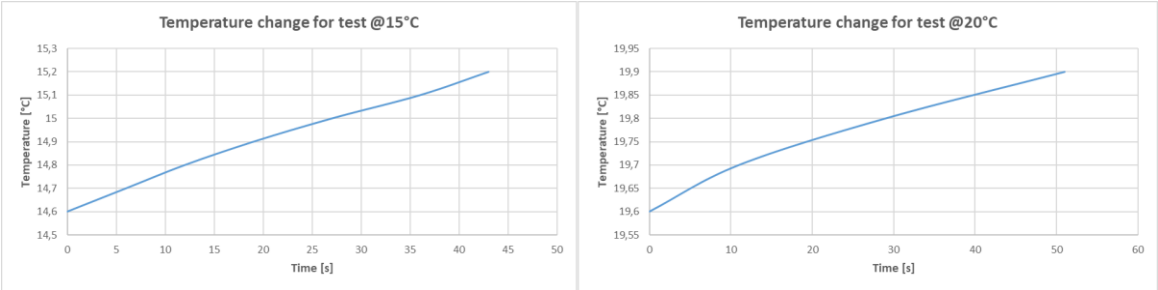

FIGURE 3.4. TEMPORAL VARIATION OF TEMPERATURE DURING AN COOLED HARDNESS TEST WITHOUT CONTACT WITH INDENTER

The second temporal contribution to the temperature uncertainty is evaluated by monitoring the temperature evolution caused by the heat exchange between the block and the indenter, which is at room temperature. To evaluate it, the temperature probe is applied on the center of the block. Once the metal is brought to 16,5 $°C$ or to 34 $°C$, the indenter is picked with the insulated and pressed on an area near to the probe. The temperature is monitored during the contact and the variability reported on a data file.

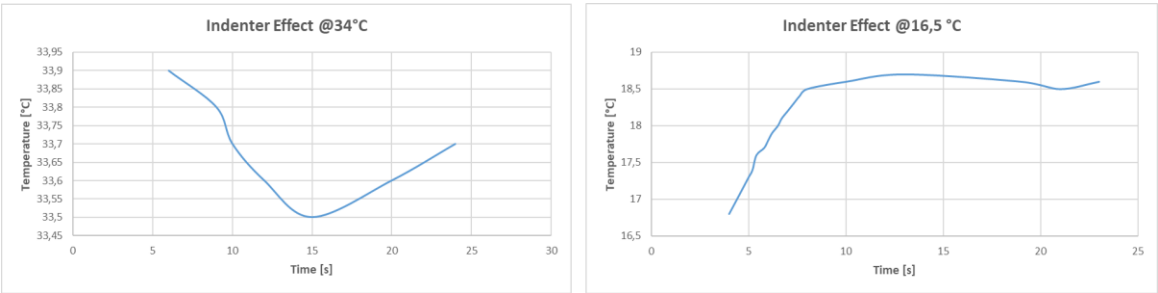

FIGURE 3.5. TEMPORAL VARIATION OF TEMPERATURE DURING AN COOLED HARDNESS TEST DUE TO CONTACT WITH THE INDENTER

According with GUM, the variance of each of the mentioned contributions is calculated with a uniform (or rectangular) distribution. For each contribution, the limits of the variability field $[T_{mean} - a; T_{mean} + a]$ have been taken. By considering all the values equiprobable, the variance is calculated as

$$u_i^2(T) = \frac{a_i^2}{3} \tag{10}$$

where i is the $i-$th contribution

The total variance is calculated as the sum of all the contributions as

$$u^2 = \sum u_i^2(T) = \sum \frac{a_i^2}{3} \tag{11}$$

In figure 3.6. the variance, the standard uncertainty and the expanded uncertainty calculated for each temperature are shown. It can be noted that when testing at low temperatures, the most relevant contribution is due to heat exchange with the indenter. Heat exchange due to contact with the diamond insert, a material known for its high thermal conductivity, has a significant impact compared to simple convection heating with air. On the other hand, when using active control for tests above room

temperature, the temporal contribution can be considered almost negligible. Although, as previously, there is an effect due to contact with the diamond insert, the most significant contribution is spatial. This variation is attributable to the heating method, which occurs from the outside inwards, creating a radial gradient.

	Temperature Variance				Uncertainty	Expanded uncertanainty
Temperature	Spatial	Temporal	Indenter	u^2	u	U
15	0,04	0,03	0,3	0,4	0,6	1,2
20	0,04	0,01	0,3	0,3	0,6	1,2
25	0,03	0	0,013	0,04	0,2	0,4
30	0,03	0	0,013	0,04	0,2	0,4
35	0,03	0	0,013	0,04	0,2	0,4

FIGURE 3.6. ASSESSMENT OF TEMPERATURE UNCERTAINTIES

3.1. STATISTICAL METHOD

The analysis starts by formulating a *Measuring model*, that is a function which relates the measurand Y (in this case the corrected hardness H_C) with a series of input X_i that have influence on it (in this case is temperature T). A linear measuring model has been adopted.

$$H_C = H_0 + c_T * T \tag{12}$$

This assumption is permitted by the fact that the phenomenon of decreasing hardness with increasing temperature follows an Arrhenius like law over a wide range of temperatures [23]. In a narrow range such as the one of interest, the trend can therefore be approximated as linear. In addition, linearity allows uncertainty to be propagated quickly and practically.

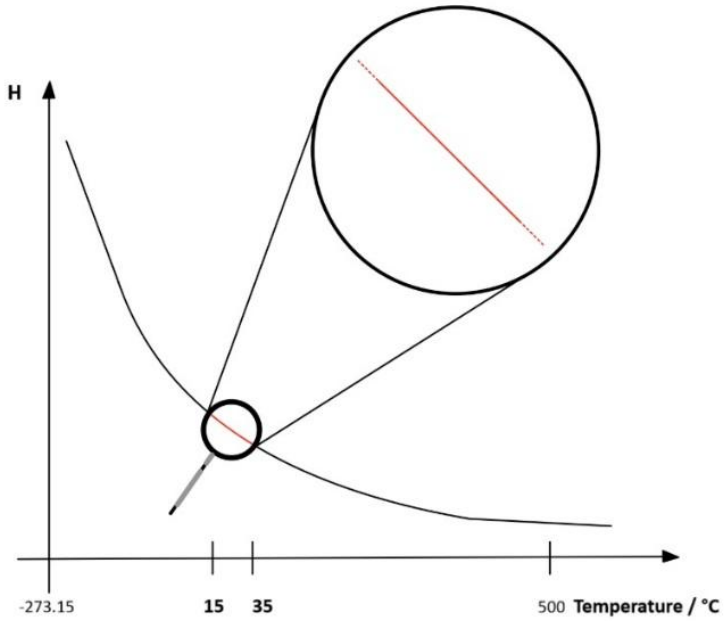

FIGURE 3.7. GENERIC TEMPERATURE-HARDNESS VARIATION

This measuring model is adapted to the new international definitions adopted by NMIs for the creation of hardness scales. For such cases Rizza et al. proposed a procedure to estimate the sensitivity coefficients and

their uncertainties by a Monte Carlo method applied to multiple linear regression [36]. A MATLAB script has been written and applied to the data from the tests. At each cycle, the algorithm generates a random point for each of the five pairs of measured points (T, H_{meas}) using a bivariate normal distribution, obtaining five new random points (a). Once per cycle, it applies Ordinary Least Squares (OLS) to the five points just generated (b). By repeating the process N times, N sensitivity coefficients $c_{T,i}$ and N standard uncertainties $u_{OLS}\ (c_{T,i})$ are collected (c).

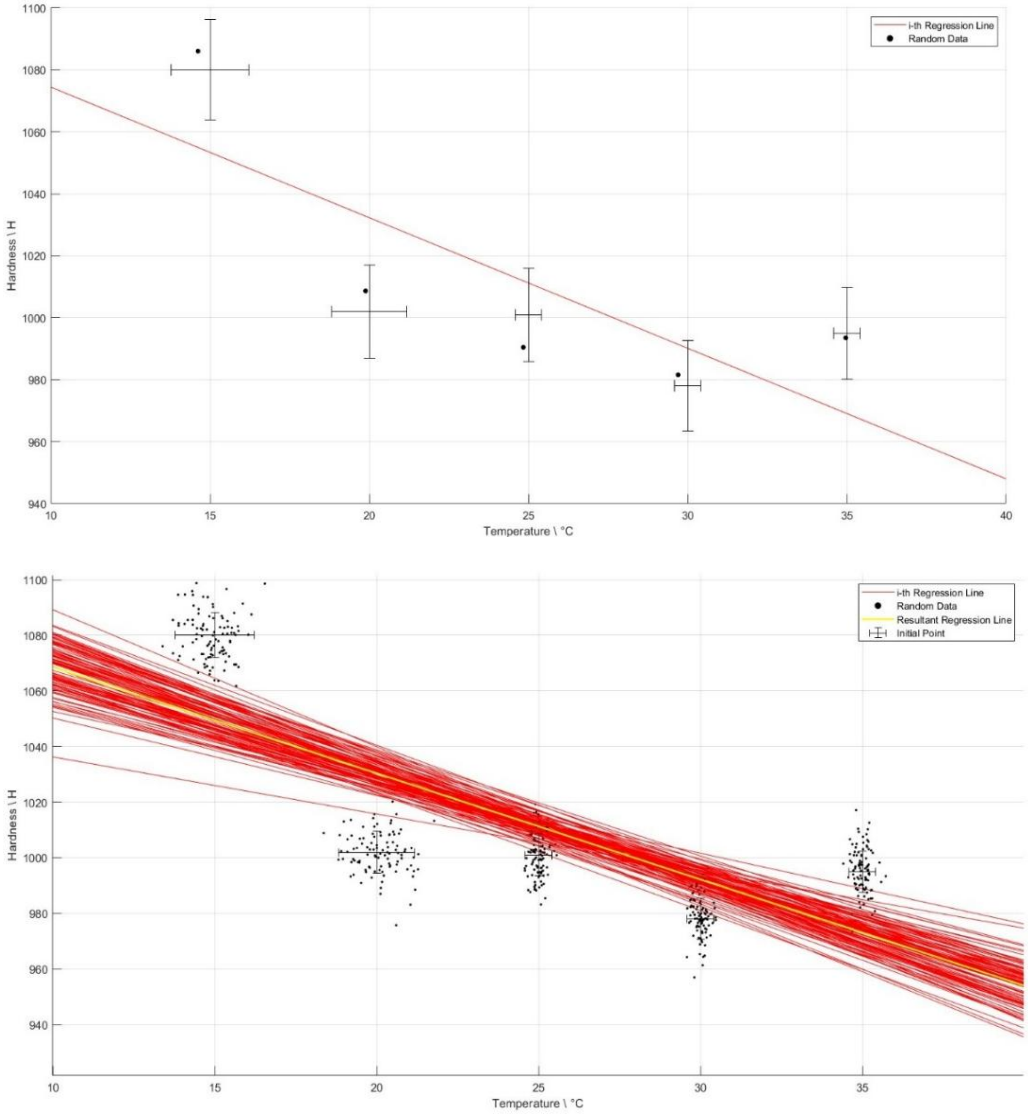

FIGURE 3.8. GRAPHICAL REPRESENTATION OF THE MONTE CARLO METHOD

From this set of data three values are estimated:

- The mean of the coefficients $\bar{c} = mean\ (c_{T,i})$
- The Monte Carlo standard uncertainty $u_{MC}(c) = \sqrt{\sum \frac{(c_i - \bar{c})^2}{N-1}}$
- The mean of the OLS uncertainties $\bar{u}_{OLS}(c) = mean\ \left(u_{OLS}(c_{T,i})\right)$

Finally, the total uncertainty of the sensibility coefficient is calculated as

$$u(c_T) = \sqrt{u_{MC}^2 + \bar{u}_{OLS}{}^2} \tag{13}$$

Being a probabilistic approach, as the number of cycles increases, this method converges towards an increasingly accurate estimate of the parameters. Although this method is elegant and easy to implement in the MATLAB environment, a deterministic instrument was also chosen for parameter estimation: *The Calibration Curves Computing Software* (CCC Software).

This statistical method was developed in a general form by NPL using XLGENLINE software and improved by Malengo Andrea and Pennecchi Francesca from INRiM. CCC is used to evaluate calibration curves for calibration services offered by the Italian NMI to industries [37]. The software takes the x_i and y_i data and the covariance matrices of both variables as input. It can perform the following kinds of regression:

- Ordinary least-squares regression, applicable when no uncertainties are related to variables;
- Weighted least-squares regression (WLS) chosen when only the y-axes are associated with an uncertainty;
- Weighted total least-squares regression (WTLS) used in the case of both variables are affected by uncertainties.

In this case it has been selected the algorithm based on the Weighted Total Least Squares tool, which solves an optimization problem by searching for the parameters that minimize a cost function. CCC uses an iterative procedure on an implicit equation to estimate the parameters c_T and H_0, while it linearizes the problem with regarding the uncertainties [38].

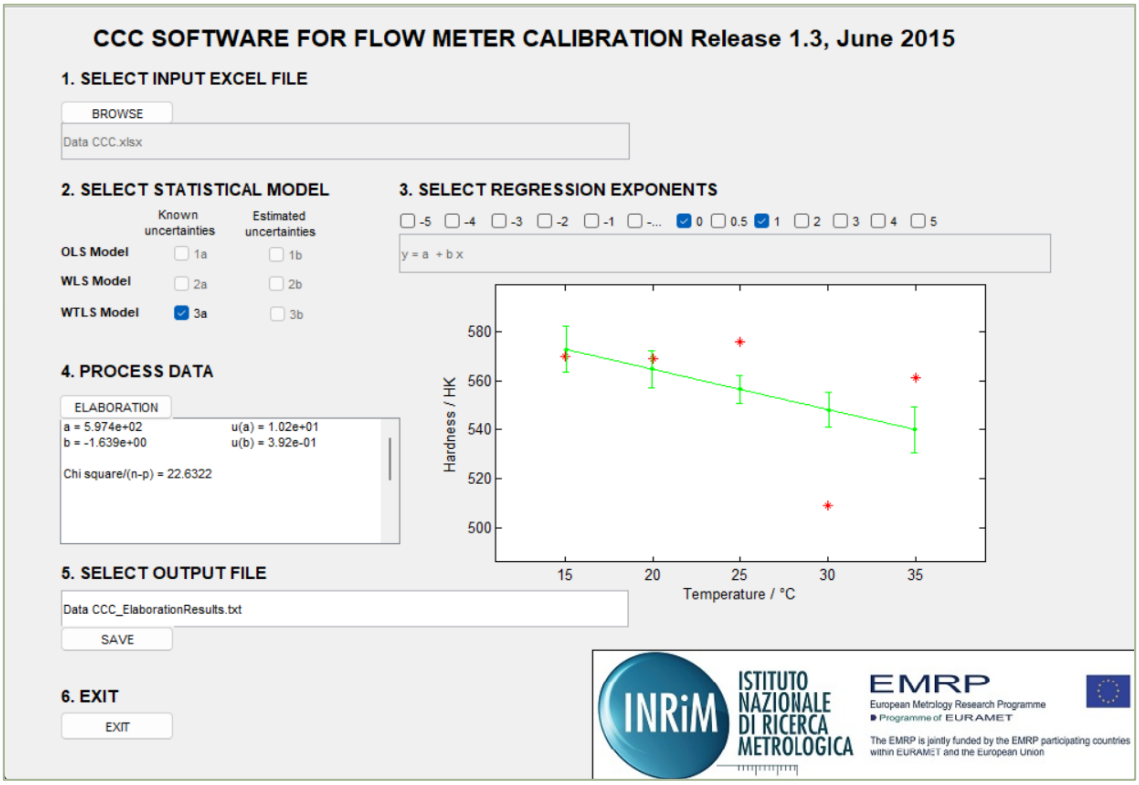

FIGURE 3.9. CCC SOFTWARE USER INTERFACE

As a result, it returns an estimate of the parameters and their uncertainty. The goodness of the fit is represented by the normalized chi square χ^2 value. This value compares the residual with the associated uncertainty for each individual point and indicates possible deficiencies in the model if the returned value is $\chi^2 \gg 1$. The figure 3.10. shows the application of the method to the experimental results of the HK 2 tests on the softer hardness block. In Appendix A are reported the results of each test.

$\boldsymbol{Soft}$						
Temperature / $°C$	Hardness / $HK\ 2$	c_T / $HK\ 2$ / $°C$	$u(c_T)$ / $HK\ 2$ / $°C$	H_0 / $HK\ 2$	$u(H_0)$ / $HK\ 2$	χ^2
15	207,2					
20	205,5					
25	205,9	-0,15	0,1	209,2	2,5	0,26
30	205,6					
35	203,4					

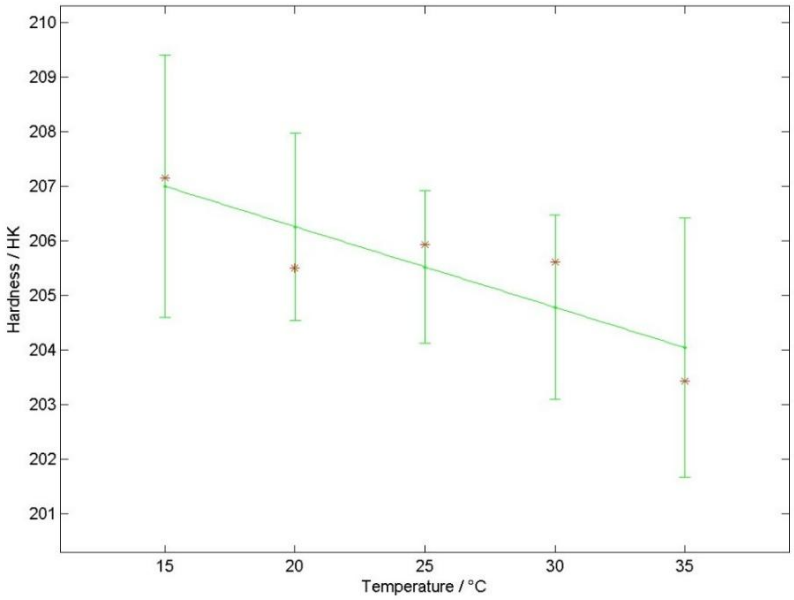

FIGURE 3.10. CCC OUTCOMES OF A HK 2 TEST ON A SOFT HARDNESS REFERENCE BLOCK

Having the possibility to apply both procedures to the same data, it was also interesting to compare the outcomes. As regards parameter estimation, the algorithms return values that are highly compatible. However, in terms of uncertainty, the values obtained using the Monte Carlo method tend to be around three times greater than those just obtained, as shown in the examples for $HV\ 1$ and $HK\ 0{,}2$ tests in figure 3.11. In the paper by Malengo and Pennacchi, this discrepancy is expected and attributed to the non-linearity of the parameters of the models [38].

Hardness			Comparison CCC-MC
Hardness Level	Hardness H	Test	u(a)_CCC / u(a)_MC
Soft	188	HV 1	29%
Medium Soft	518	HV 1	64%
Medium Hard	706	HV 1	30%
Hard	954	HV 1	33%
Soft	212	HK 0,2	44%
Medium Soft	557	HK 0,2	22%
Medium Hard	800	HK 0,2	35%
Hard	1011,257	HK 0,2	27%

FIGURE 3.11. UNCERTAINTIES RESULTS COMPARISON BETWEEN CCC SOFTWARE AND MONTE CARLO METHOD

3.2. RESULTS AND DISCUSSION

At this point in the discussion, the intercept, sensitivity coefficient, and their respective uncertainties have been found for each hardness level and each test method. The parameters are shown in the figure 3.12.

Hardness			Temperature Sensitivity					
Hardness Level	Hardness H	Test	Sensitivity b	St. uncertanty u(b)	Unit of Measurement	U(b)/b	Relative Sensitivity b/H	Unit of Measurement
Soft	197	HBW 2,5/187,5	-1,20	0,10	HBW 2,5/187,5 /°C	0,2	0,61	%/°C
Medium Soft	523	HBW 2,5/187,5	-2,45	0,25	HBW 2,5/187,5 /°C	0,2	0,47	%/°C
Medium Hard	743	HBW 2,5/187,5	0,17	0,35	HBW 2,5/187,5 /°C	4,1	0,02	%/°C
Hard	927	HBW 2,5/187,5	-0,22	0,44	HBW 2,5/187,5 /°C	4,0	0,02	%/°C
Soft	183	HBW 2,5/62,5	-0,86	0,09	HBW 2,5/62,5 /°C	0,2	0,47	%/°C
Medium Soft	473	HBW 2,5/62,5	-2,13	0,24	HBW 2,5/62,5 /°C	0,2	0,45	%/°C
Medium Hard	665	HBW 2,5/62,5	0,02	0,32	HBW 2,5/62,5 /°C	33,5	0,00	%/°C
Hard	804	HBW 2,5/62,5	-0,43	0,38	HBW 2,5/62,5 /°C	1,8	0,05	%/°C
Soft	168	HBW 2,5/31,25	-0,91	0,09	HBW 2,5/31,25 /°C	0,2	0,54	%/°C
Medium Soft	436	HBW 2,5/31,25	-1,09	0,04	HBW 2,5/31,25 /°C	0,1	0,25	%/°C
Medium Hard	593	HBW 2,5/31,25	-0,46	0,28	HBW 2,5/31,25 /°C	1,2	0,08	%/°C
Hard	719	HBW 2,5/31,25	-2,46	0,37	HBW 2,5/31,25 /°C	0,3	0,34	%/°C
Soft	183	HV 30	0,09	0,09	HV 30 /°C	2,0	0,05	%/°C
Medium Soft	513	HV 30	-0,13	0,24	HV 30 /°C	3,7	0,03	%/°C
Medium Hard	688	HV 30	-0,45	0,33	HV 30 /°C	1,5	0,07	%/°C
Hard	890	HV 30	-0,56	0,42	HV 30 /°C	1,5	0,06	%/°C
Soft	188	HV 1	-0,34	0,09	HV 1 /°C	0,5	0,18	%/°C
Medium Soft	518	HV 1	-0,38	0,25	HV 1 /°C	1,3	0,07	%/°C
Medium Hard	706	HV 1	0,13	0,33	HV 1 /°C	5,1	0,02	%/°C
Hard	954	HV 1	1,72	0,48	HV 1 /°C	0,6	0,18	%/°C
Soft	185	HV 0,2	-0,30	0,09	HV 0,2 /°C	0,6	0,16	%/°C
Medium Soft	506	HV 0,2	-2,35	0,38	HV 0,2 /°C	0,3	0,46	%/°C
Medium Hard	727	HV 0,2	-0,51	0,35	HV 0,2 /°C	1,4	0,07	%/°C
Hard	985	HV 0,2	0,09	0,47	HV 0,2 /°C	10,7	0,01	%/°C
Soft	206	HK 2	-0,15	0,10	HK 2 /°C	1,3	0,07	%/°C
Medium Soft	529	HK 2	-0,55	0,23	HK 2 /°C	0,8	0,10	%/°C
Medium Hard	706	HK 2	-0,52	0,33	HK 2 /°C	1,3	0,07	%/°C
Hard	883	HK 2	-1,08	0,51	HK 2 /°C	0,9	0,12	%/°C
Soft	212	HK 0,2	-0,10	0,10	HK 0,2 /°C	2,1	0,05	%/°C
Medium Soft	557	HK 0,2	-1,60	0,39	HK 0,2 /°C	0,5	0,29	%/°C
Medium Hard	800	HK 0,2	-0,44	0,39	HK 0,2 /°C	1,8	0,05	%/°C
Hard	1011,257	HK 0,2	-3,76	0,50	HK 0,2 /°C	0,3	0,37	%/°C

FIGURE 3.12. EXPERIMENTAL SENSITIVITY COEFFICIENTS

As a preliminary analysis, it can certainly be noted that there is a tendency for hardness to decrease as temperature increases. Just six of thirty-three combinations have a positive sensitivity coefficient $b > 0$ (highlighted in red).

Analysing the magnitudes of the sensitivity coefficients obtained, it can be seen that most of them fall within a range of $(0 \div 1)\ H/°C$. This result suggests that, although there appears to be a relationship whereby steel reduces its hardness as the temperature increases, the phenomenon is weak.

Furthermore, when examining how the sensitivity coefficient varies for each level as the test performed varies, no characteristic patterns or trends can be observed (figure 3.13.). The same conclusion can be applied when analysing the variation with respect to the hardness level for the specific test (figure 3.14.). Some examples are shown.

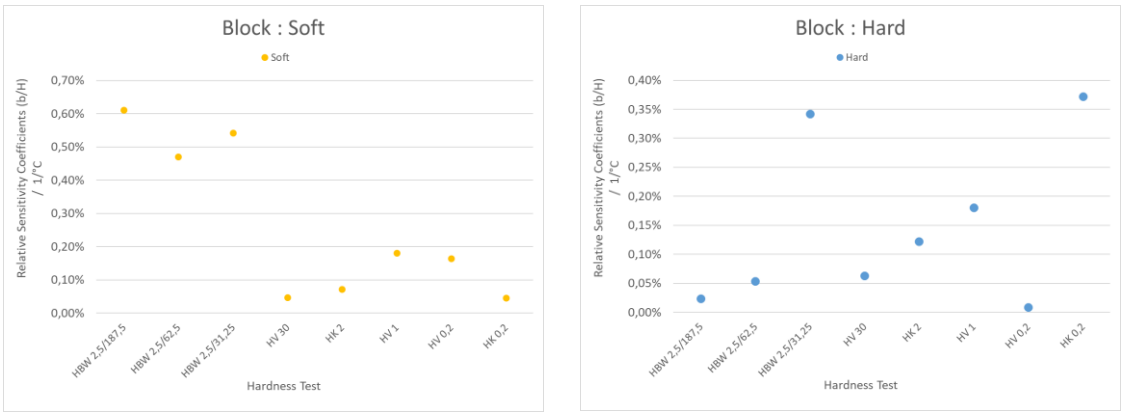

FIGURE 3.13 COMPARISON OF SENSITIVITY COEFFICIENTS BETWEEN TWO DIFFERENT BLOCKS

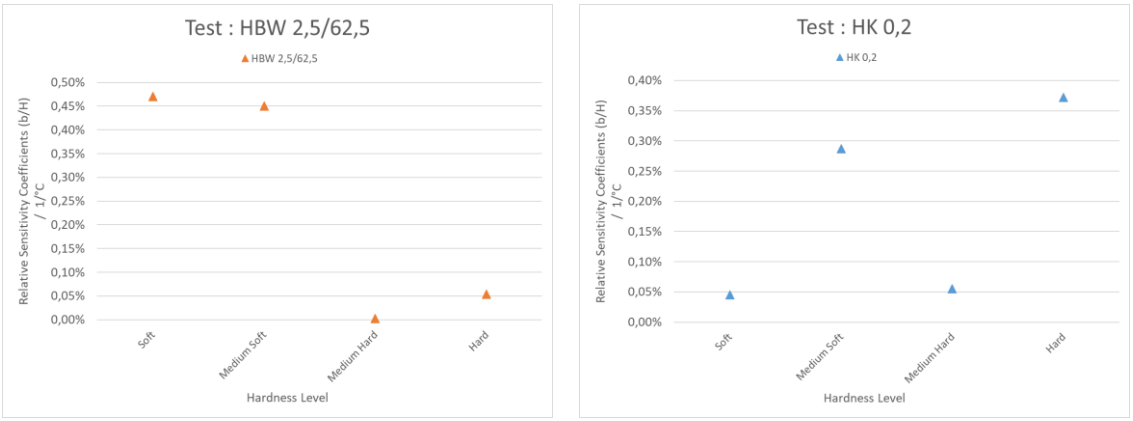

FIGURE 3.14 COMPARISON OF SENSITIVITY COEFFICIENTS BETWEEN TESTS

After a preliminary interpretation of the data, one might question whether some data are more reliable than others. In this direction, it is advisable to carry out an additional assessment about the natural phenomenon of non-uniformity in a hardness block through a significance test.

The inhomogeneity, combined with the intrinsic impossibility of performing two tests at the same point without the second being influenced by the first, makes it impossible to measure the same hardness value for the same hardness reference block. Therefore, the non-uniformity of the hardness block can hidden the effect of influencing variables, such as temperature in this specific situation.

ISO standards regulate hardness reference block by imposing maximum values for the calibration tests. For each hardness block, a minimum of five indentations must be made, uniformly distributed across the surface. Once the diameters have been measured, the non-uniformity is expressed as standard deviation of these 5 measurements

Most NMIs consider YAMAMOTO hardness blocks to be the best on the market for having the highest uniformity. These blocks are used in international comparisons between primary laboratories. NMIs as INRiM contribute to the BIPM database which contains reports on comparisons. In these documents, the standard deviations of the non-uniformity of the blocks are evaluated [39, 40]. Internal tests and comparative reports carried out by INRiM show the following relative standard deviations $u_{\%}$:

- 5 % for HV 0,2, HK 0,2 tests
- 1,5 % for HV 1, HK 2 tests
- 0,76 % for HV 30 tests
- 0,65 % for Brinell tests

The reported non-uniformity values reveal an important characteristic regarding the different methodologies. In fact, for hardness tests where the loads are lower and the indenters are sharper, the surface area affected by deformation is smaller and more subject to fluctuations [41]. On the other hand, cases with higher loads and a spherical indenter, such as in HBW 2,5/187,5 tests, average the different point variations.

The significance test is performed with the mentioned standard deviations to assess whether we are actually measuring a dependence on temperature or a random variation of the surface. The test consists of comparing the variance of the non-homogeneity var_{N-H} with the variance of the residuals obtained var_{RES}. Their ratio r provides an excellent measure of comparison: if the non-homogeneity has a greater variance than the residuals, then it means that the result obtained from the regression is weakly influenced by surface variation, but what we are measuring the effect of temperature.

$$var_{N-H} = u_{\%} * mean\left(H_{meas,i}\right) \tag{15}$$

$$var_{RES} = \frac{1}{M-2}\sum_{i=1}^{M}\left(H_{C,i} - H_{Meas,i}\right)^2 \tag{16}$$

where $M = 5$ number of experimental temperatures

$$r = \frac{var_{N-H}}{var_{RES}} \tag{17}$$

The ratio r is compared with Fisher's cumulative distribution F with $6-1$ and $5-1$ degrees of freedom, respectively for numerator and denominator. For the analysis, a confidence level of 80% was considered, accepting a maximum error risk of 20 %. Under the null hypothesis that "the data trend measures non-homogeneity and not dependence on temperature", we conclude that values with a p-value $> 20\%$ are not considered significant and the relative tests are considered invalid. Such a risk was chosen in order to have the same probability risk of false positive and false negative. In figure 3.15. are highlighted (in red) the measures that are not considered significant.

Hardness			Significativity with non-homogenity
Hardness Level	Hardness H	Test	p-value
Soft	197	HBW 2,5/187,5	98,50%
Medium Soft	523	HBW 2,5/187,5	98,49%
Medium Hard	743	HBW 2,5/187,5	0,04%
Hard	927	HBW 2,5/187,5	73%
Soft	183	HBW 2,5/62,5	97,42%
Medium Soft	473	HBW 2,5/62,5	96,60%
Medium Hard	665	HBW 2,5/62,5	56,86%
Hard	804	HBW 2,5/62,5	5,60%
Soft	168	HBW 2,5/31,25	99,48%
Medium Soft	436	HBW 2,5/31,25	99,55%
Medium Hard	593	HBW 2,5/31,25	80,61%
Hard	719	HBW 2,5/31,25	99,75%
Soft	183	HV 30	50,13%
Medium Soft	513	HV 30	53,18%
Medium Hard	688	HV 30	1,12%
Hard	890	HV 30	11,29%
Soft	188	HV 1	82,15%
Medium Soft	518	HV 1	12,33%
Medium Hard	706	HV 1	73,70%
Hard	954	HV 1	71,03%
Soft	185	HV 0,2	17,75%
Medium Soft	506	HV 0,2	99,63%
Medium Hard	727	HV 0,2	13,72%
Hard	985	HV 0,2	3,82%
Soft	206	HK 2	0,58%
Medium Soft	529	HK 2	32,47%
Medium Hard	706	HK 2	10,87%
Hard	883	HK 2	98,29%
Soft	212	HK 0,2	1,26%
Medium Soft	557	HK 0,2	41,36%
Medium Hard	800	HK 0,2	3,25%
Hard	1011	HK 0,2	9,95%

FIGURE 3.15 RESULTS OF THE SIGNIFICANCE TEST OF NON-HOMOGENEITY

The Knoop and Vickers methods show greater sensitivity than Brinell, especially at medium-high hardness. This result could suggest that microhardness is more influenced by temperature variations rather than by the non-homogeneity of the block.

Discarded cases can also be analysed. What is clear is the rejection of almost all Brinell tests. Besides the occurrence of errors during the generation and measurement of indentations, it can be hypothesized that the linear model is not the most suitable to describe the test, especially for $HBW\ 2{,}5/31{,}25$ series.

However, by looking at measurement results and the trends in rejected tests, there is a likely systematic difference between tests carried out with heating bands, $(25 \div 35)\ °C$, and tests carried out with a bath $15\ °C$ and $20\ °C$. In particular, a sort of systematic step between $20\ °C$ and $25\ °C$ is visible from the graphs. This phenomenon is evident in Brinell measurements and is less evident in microhardness measurements. The significance test carried out was therefore able to identify a methodological problem in the temperature control of the block. Future studies should investigate this trend. Figure 3.16. shows some of the rejected examples.

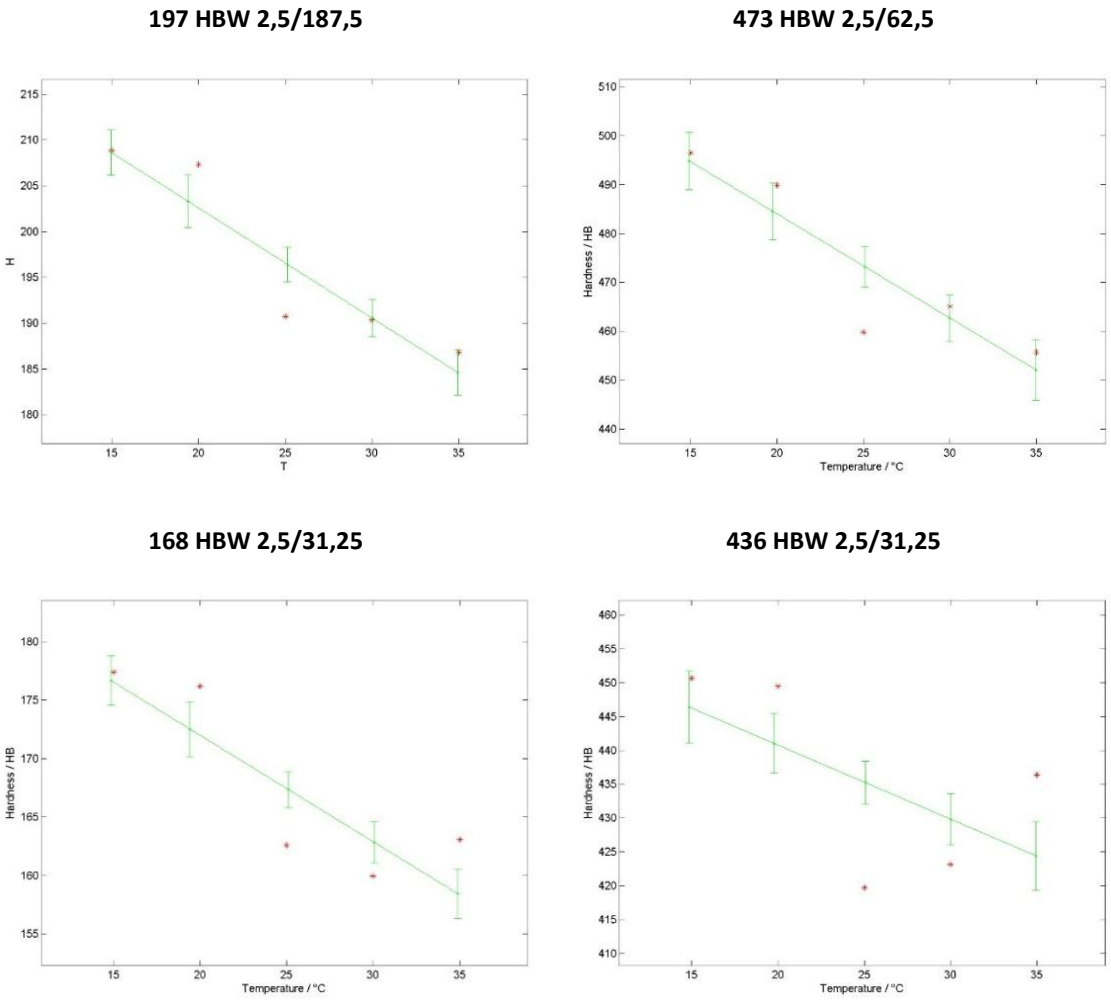

FIGURE 3.16. STEP OF HARDNESS DUE TO THE METHODOLOGY

Another useful tool for identifying data that appear to conform to the linear model but actually deviate from it is to analyse the normalised χ^2 values provided by the CCC software. Recalling that this parameter is a statistical indicator of how well the model fits the experimental data, the Chi-Square Test allows to highlight any significant discrepancies.

In this second significance test, the residuals are compared with the uncertainties associated with linear regression (green vertical lines in the temperature-hardness graphs of the experimental tests, see Appendix A) and no further with the inhomogeneity of the blocks. As before, the confidence level adopted is $80\ \%$ (with 3 degrees of freedom), but in this case the null hypothesis is formulated as "the data trend follows a linear type of regression". This means that data with a normalised chi-square value $\chi^2 > 4{,}46$ are not considered valid and can be excluded. The χ^2 procedure eliminates the false positives whose lack of fit to the linear model have been masked by the high non-homogeneity associated with microhardness tests. Figure 3.17 shows the tests accepted as valid, reported with the relative chi-square value and sensitivity coefficient.

Hardness			Temperature Sensitivity				Goodness of fit
Hardness Level	Hardness H	Test	Sensitivity b	Unit of Measurement	Relative Sensitivity b/H	Unit of Measurement	Chi Square
Hard	804	HBW 2,5/62,5	-0,43	HBW 2,5/62,5 /°C	0,05	%/°C	0,17
Medium Hard	688	HV 30	-0,45	HV 30 /°C	0,07	%/°C	0,093
Hard	890	HV 30	-0,56	HV 30 /°C	0,06	%/°C	0,36
Medium Soft	518	HV 1	-0,38	HV 1 /°C	0,07	%/°C	1,5
Medium Hard	727	HV 0,2	-0,51	HV 0,2 /°C	0,07	%/°C	1,6
Soft	206	HK 2	-0,15	HK 2 /°C	0,07	%/°C	0,26
Medium Hard	706	HK 2	-0,52	HK 2 /°C	0,07	%/°C	1,4
Soft	212	HK 0,2	-0,10	HK 0,2 /°C	0,05	%/°C	4,4

FIGURE 3.17. RESULTS OF THE ACCEPTED TESTS

Only eight of the thirty-two tests carried out are found to be reliable and significant. The low percentage of accepted cases is probably also affected by factors including the non-optimal choice of reference hardness blocks (especially for low loads scales), the repeatability of the machines and temperature control system, the operator inexperience and the inevitable presence of random factors. These elements influenced the final quantity of results.

These data suggest that the higher hardness level tested with relatively higher loads are the most susceptible to temperature variations:

- sensitivity coefficient $c_T = -0{,}56\ HV\ 30/°C$.
- sensitivity coefficient $c_T = -0{,}43\ \mathrm{HBW}\ 2{,}5/62{,}5\ /°C$.

On the other hand, Knoop tests, especially those performed at lower hardness levels, are the least affected by temperature fluctuations:

- sensitivity coefficient $c_T = -0{,}096\ \mathrm{HK}\ 0{,}2\ /°C$.
- sensitivity coefficient $c_T = -0{,}147\ \mathrm{HK}\ 2/°C$.

However, the sensitivity coefficients normalised with respect to hardness are particularly interesting. All values are within the range $(0{,}05\ \div\ 0{,}07)\ \%/°C$, regardless of the hardness level and the test. This implies that there is a general but weak variation in hardness reference blocks as the temperature changes.

4. CONCLUSIONS

The influence of the temperature effect in Brinell, Vickers, and Knoop hardness measurements is a crucial issue in industries. During the analysis, sensitivity coefficients and relative uncertainties were determined, describing the variation in hardness as a function of temperature in the range $(15 \div 35)\ °C$. The analysis was performed on thirty-two different configurations of Brinell, Vickers, and Knoop scales with different hardness levels and variable applied loads. The 160 experimental data (5 temperatures, 4 hardness blocks, 8 hardness scales) were collected using primary sampling machines (PHS DW & PRIMARY and MHSM primary hardness standardizing machines) and optical measuring instruments provided by the INRiM hardness laboratory.

To calculate the sensitivity coefficients and uncertainties, the Weighted total least-squares regression was implemented using MATLAB software. This approach made it possible to directly estimate parameters and their uncertainty, propagating the contributions deriving from the variability of the experimental data and the probability distributions associated with the variables.

Although carried out using top-level equipment, inhomogeneity has been identified as one of the critical factors that can significantly influence results. The quality and homogeneity of hardness reference block are therefore critical aspects for ensuring reliable and repeatable measurements. As can be expected, the hardness of steel decreases as the temperature increases, but the phenomenon cannot always be accurately described using linear regression. In majority of these experiments the fit between the measured values and the linear regression is not respected.

At the end of the data analysis process, the data suggest a general but weak relation between hardness and temperature. This trend can be seen in term of absolute sensibility coefficients in cases as $HBW\ 2{,}5/31{,}25$ and $HV\ 30$ tests, where the higher hardness level is reflected on higher hardness drop. Anyway, the relative variation of hardness due to thermal changes are found to be similar and independent on the methodology and level. The cases considered satisfactory in terms of fit goodness return a mean relative sensitivity coefficient $0{,}06\ \%\ °C^{-1}$, independently of the test and the hardness level of the block.

This thesis project suggests that a correlation can be appreciated even in narrow temperature ranges, which are fundamental when aiming to improve the accuracy and precision of primary samples. Practical implications can find space in the calibration process through comparison. For example, in industries is not always maintain reference temperature imposed by standard $(23 \pm 5)\ °C$. If a comparison is carried out at a temperature other than the one of the LAT, it is possible to calculate the “true” hardness value of the refence block. Moreover, performance in hot environments can be predicted. It is possible to estimate how hardness, and therefore resistance to wear or deformation, decreases as the operating temperature varies.

It is certain that this research should be continued and improved over time. In this sense, it is clear that the active temperature control system should be studied and improved to avoid the hardness step found during the experiments. The suggestion is simply using a bath with water and glycol equipped with a heat exchanger with a specifically designed seat that can be adjusted on the size of the calibration block.

This thesis aims to guide research for the first time, so that researchers with better equipment (e.g. adapted blocks) and more time available can refine the study method and expand the materials to be investigated. In conclusion, future developments in this research must focus on optimizing test conditions to reduce associated uncertainties.

BIBLIOGRAPHY

[1] W. D. Callister jr and D. G. Rethwisch, Scienza ed Ingegneria dei Materiali, EdiSES, 2020.

[2] EURAMET, *Traceability for indentation measurements in Brinell-Vickers-Knoop hardness,* EURAMET, 2023.

[3] B. O'Neill, *50 Years of Quality: History of Hardness Testing,* Quality Magazine, 2011.

[4] International Organization for Standardization., *Brinell hardness test - Part 1: Test method (ISO 6506-1:2014).,* ISO, 2014.

[5] International Organization for Standardization., *Brinell hardness test - Part 2: Verification and calibration of testing machines (ISO 6506-2:2014).,* ISO, 2014.

[6] International Organization for Standardization., *Brinell hardness test - Part 3: Calibration of reference blocks (ISO 6506-3:2014),* ISO, 2014.

[7] International Organization for Standardization., *Vickers hardness test - Part 1: Test method (ISO 6507-1:2018),* ISO, 2018.

[8] International Organization for Standardization., *Vickers hardness test - Part 2: Verification and calibration of testing machines (ISO 6507-2:2018),* ISO, 2018.

[9] International Organization for Standardization., *Vickers hardness test - Part 3: Calibration of reference blocks (ISO 6507-3:2018),* ISO, 2018.

[10] International Organization for Standardization., *Knoop hardness test - Part 1: Test method (ISO 4545-1:2017),* ISO, 2017.

[11] International Organization for Standardization., *Knoop hardness test - Part 2: Verification and calibration of testing machines (ISO 4545-2:2017),* ISO, 2017.

[12] International Organization for Standardization., *Knoop hardness test - Part 3: Calibration of reference blocks (ISO 4545-3:2017),* ISO, 2017.

[13] Istituto Nazionale di Ricerca Metrologica, "Sito ufficiale dell'INRiM," [Online]. Available: https://www.inrim.it/it.

[14] International Organization for Standardization , *ISO/IEC Guide 99,* ISO, 1984.

[15] ITALIA, *Legge 11 agosto 1991, n. 273. Istituzione del sistema nazionale per la metrologia legale.,* 1991.

[16] ITALIA MINISTERO DELLO SVILUPPO ECONOMICO., *Decreto 21 aprile 2017, n. 93. Regolamento sui controlli degli strumenti di misura in servizio e sulla vigilanza sugli strumenti conformi alla normativa nazionale ed europea,* Gazzetta Ufficiale della Repubblica Italiana, 2017.

[17] Ente Nazionale Italiano di Unificazione, *Requisiti generali per la competenza dei laboratori di prova e di taratura (UNI EN ISO/IEC 17025:2018),* Milano: UNI, 2017.

[18] Bureau International des Poids et Mesures, "Key Comparison Database," [Online]. Available: https://www.bipm.org/kcdb/.

[19] C. Merolli, Analisi dell'effetto di creep nelle misure di durezza Brinell, Vickers e Knoop, Torino: Politecnico di Torino, 2025.

[20] EURAMET, *GUIDELINES ON THE ESTIMATION OF UNCERTAINTY IN HARDNESS MEASUREMENTS,* EURAMET, 03/2011.

[21] A. A. Baron, *Method for Predicting the Fracture Toughness of Pipeline Steels within a Wide Temperature Range,* vol. 3, L. Pleiades Publishing, Ed., Volgograd: Russian Metallurgy, 2015, pp. 216-221.

[22] E. Pavlina and C. Van Tyne, *Correlation of Yield Strength and Tensile Strength with Hardness for Steels,* December 2008 ed., vol. Journal of Materials Engineering and Performance VOL 17(6), ASM International, 2008, pp. 888-893.

[23] H. Torres, M. Varga and M. Rodriguez Ripoll, *High temperature hardness of steels and iron-based alloys,* vol. Materials Science & Engineering A 671, Wiener Neustadt: Elsevier, 2016, pp. 170-181.

[24] B. Guo, L. Zhang, L. Cao, T. Zhang, F. Jiang and L. Yan, *The correction of temperature-dependent Vickers hardness of cemented carbide base on the developed high-temperature hardness tester,* Journal of Materials Processing Tech. ed., vol. 255, China: Journal of Materials Processing Tech, 2018, pp. 426-433.

[25] EA-4/02 M: 2022 , *Expression of the Uncertainty of Measurement in Calibration, December 1999,* European Accreditation.

[26] L. Brice, F. Davis and A. Crawshaw, *Uncertainty in hardness measurement,* vol. Report CMAM 87, Teddington: NPL, 2003.

[27] Kersten, *Factor influencing hardness measurement,* International Organization of Legal Metrology, 1983.

[28] P. Rizza, A. Prato, R. R. Machado and A. Germak, *The role of influence coefficients in hardness measurements: A case study in,* vol. Measurement 213, ELSEVIER, 2023.

[29] Yamamoto Scientific Tool Lab., *Standard Blocks for Hardness Catalogue,* 2008.

[30] YAMAMOTO Scientific Tool Lab., *Standard Microstructure Catalogue,* Chiba: YAMAMOTO Scientific Tool Lab., Ltd, 2014.

[31] W. D. j. Callister, Materials Science and Engineering, Wiley, 2018.

[32] T. Narongsak, T. Nipon, P. Tanabodee, J. Patiphan and H. Wanna, *Correlation of microstructure, mechanical properties, and strain hardening response via kocks-mecking analysis in heat-treated JIS*

SK85 high-carbon steel, vol. 139, The International Journal of Advanced Manufacturing Technology (2025), 2025, pp. 4613-4630.

[33] L. S.p.a., *PHS DW & PRIMARY User's Guide,* Antegnate: LTF, 2009.

[34] S. Low, K. Hattori, A. Alessandro Germak and A. Knott, *Proposed definition for the Brinell hardness indentation edge,* vol. 3, ACTA IMEKO, September 2014.

[35] Bureau International des Poids et Mesures, "BIPM key comparison database (KCDB)," BIPM, [Online]. Available: https://www.bipm.org/kcdb/.

[36] P. Rizza, M. Murgia, A. Prato, C. Origlia and A. Germak, *Determination of sensitivity coefficients and their uncertainties in Rockwell hardness measurements: a Monte Carlo method for multiple linear regression,* vol. 60, Metrologia-BIPM, 2022.

[37] EURAMET, *Calibration Curves Computing – CCC Software,* EURAMET.

[38] A. Malengo and F. Pennecchi, *A weighted total least-squares algorithm for any fitting model,* vol. Metrologia 50, B. &. I. P. Ltd, Ed., 2013, p. 654.

[39] EURAMET, "EURAMET SUPPLEMENTARY COMPARISON BETWEEN INRiM, UME AND PTB IN BRINELL HARDNESS SCALES (HBW1/30 – HBW2.5/187.5)," EURAMET.

[40] EURAMET, "EURAMET KEY COMPARISON BETWEEN INRiM AND UME IN VICKERS HARDNESS SCALES (HV1 - HV30)," 2018.

[41] K. Herrmann, "CCM Vickers key comparison," Physikalisch-Technische Bundesanstalt Braunschweig, Braunschweig, 2005.

APPENDIXES

APPENDIX A

HBW 2,5/187,5

$Soft$						
Temperature / $°C$	Hardness / HWB 2,5/ 187,5	c_T / HWB 2,5 /187,5$°C^{-1}$	$u(c_T)$ / HWB 2,5 /187,5 $°C^{-1}$	H_0 / HWB 2,5 /187,5	$u(H_0)$ / HWB 2,5 /187,5	p-value
15	209	-1,2034	0,0976	226,65	2,61	99,28%
20	207					
25	191					
30	190					
35	187					

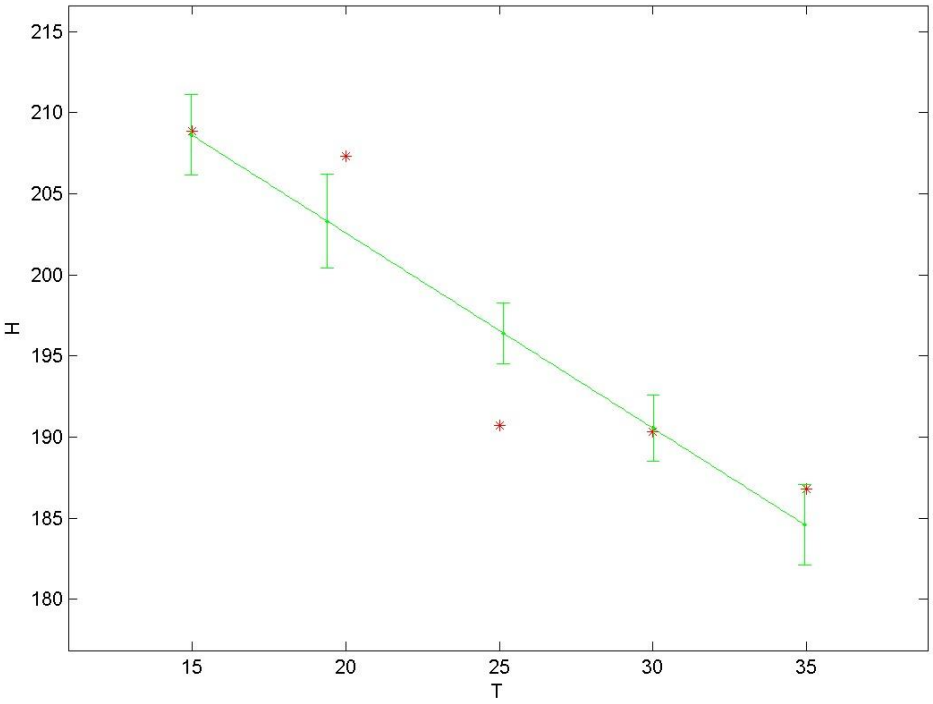

$Medium\ Soft$						
Temperature / $°C$	Hardness / HWB 2,5/ 187,5	c_T / HWB 2,5 /187,5$°C^{-1}$	$u(c_T)$ / HWB 2,5 /187,5 $°C^{-1}$	H_0 / HWB 2,5 /187,5	$u(H_0)$ / HWB 2,5 /187,5	p-value
15	547	-2,45	0,25	583,6	6,8	99,94%
20	547					
25	509					
30	505					
35	506					

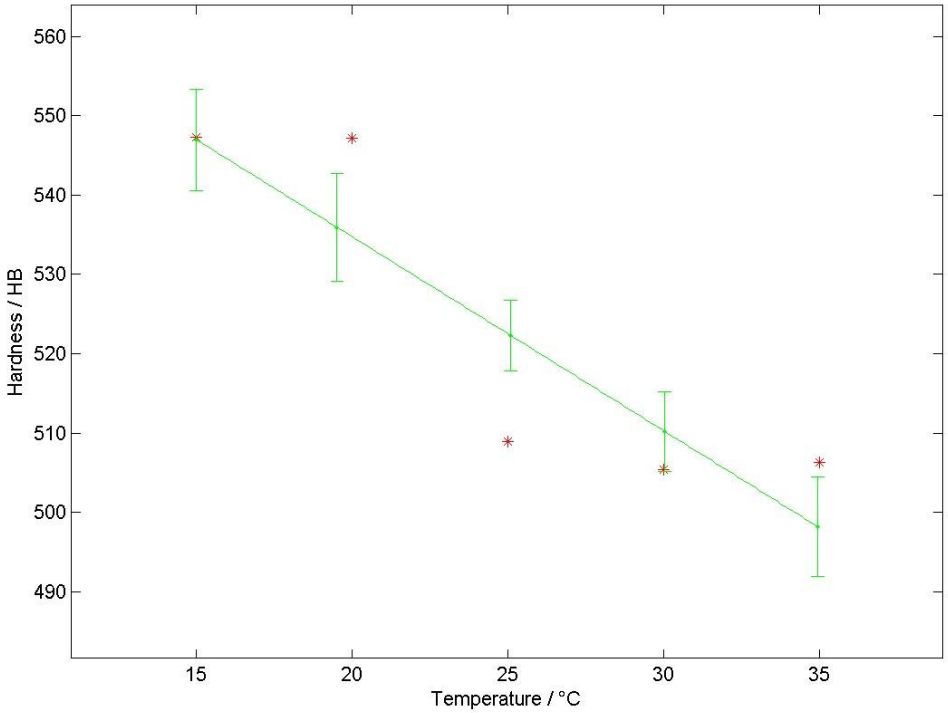

Medium Hard						
Temperature / $°C$	Hardness / HWB 2,5/ 187,5	c_T / HWB 2,5 /187,5$°C^{-1}$	$u(c_T)$ / HWB 2,5 /187,5 $°C^{-1}$	H_0 / HWB 2,5 /187,5	$u(H_0)$ / HWB 2,5 /187,5	p-value
15	742	0,17	0,35	738,5	9,15	5,36%
20	741					
25	743					
30	744					
35	745					

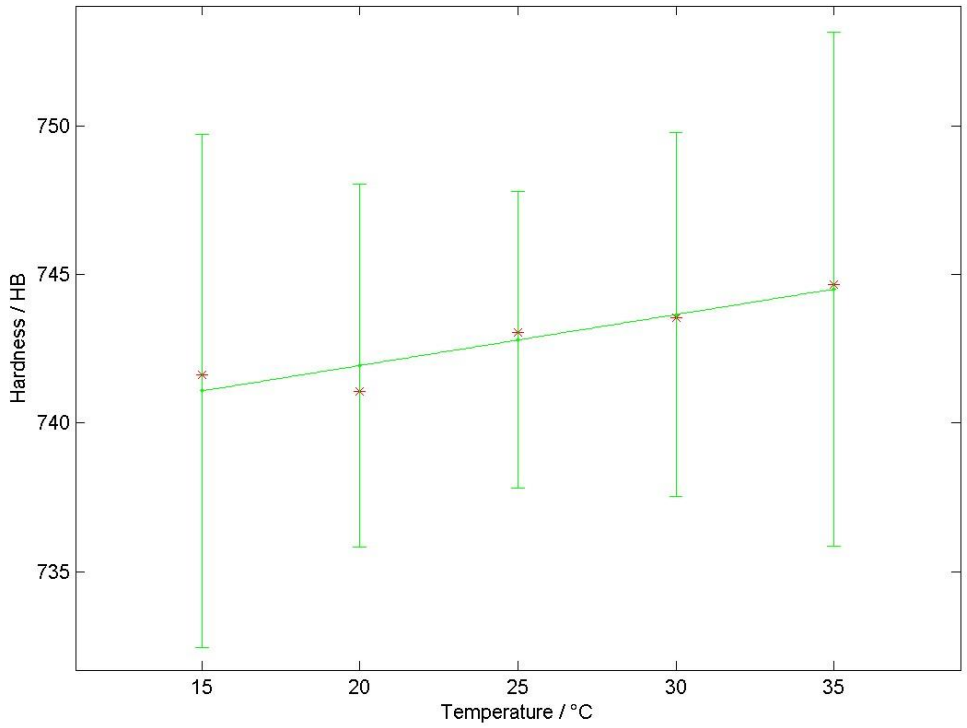

$Hard$						
Temperature / $°C$	Hardness / HWB 2,5/ 187,5	c_T / HWB 2,5 /187,5$°C^{-1}$	$u(c_T)$ / HWB 2,5 /187,5 $°C^{-1}$	H_0 / HWB 2,5 /187,5	$u(H_0)$ / HWB 2,5 /187,5	p-value
15	932	-0,22	0,44	932,2	11,5	100%
20	933					
25	913					
30	925					
35	931					

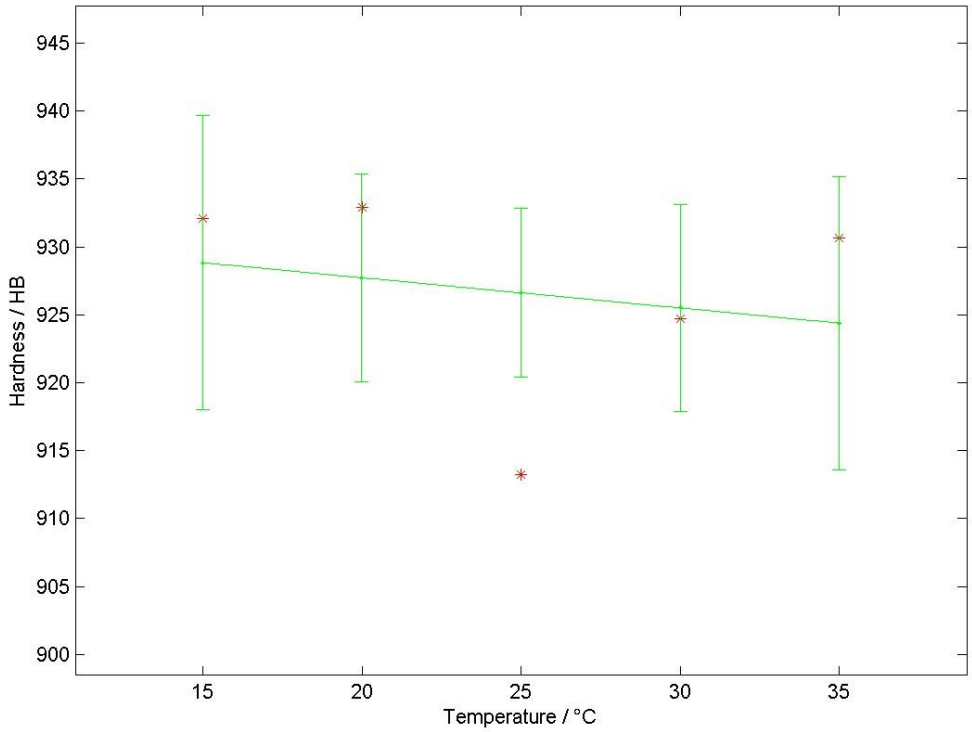

HBW 2,5/62,5

$Soft$						
Temperature / $°C$	Hardness / HWB 2,5/ 62,5	c_T / $HHWB$ 2,5 /62,5 $°C^{-1}$	$u(c_T)$ / $HHWB$ 2,5 /62,5 $°C^{-1}$	H_0 / $HHWB$ 2,5 /62,5	$u(H_0)$ / HWB 2,5 /62,5	p-value
15	191	-0,86	2,39	204,2	0,09	97,42%
20	192					
25	179					
30	178					
35	176					

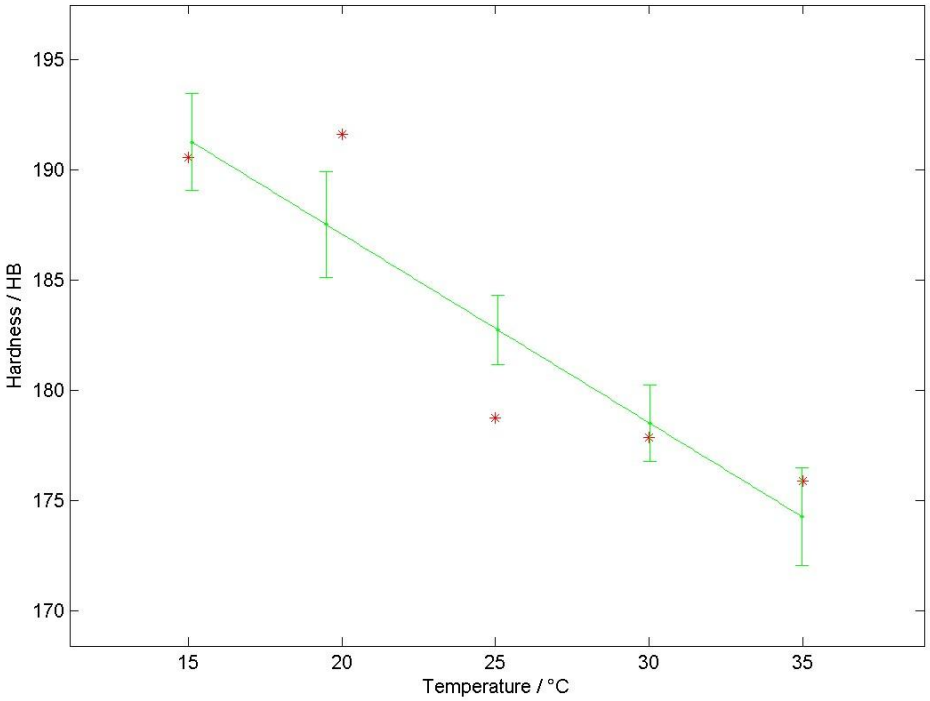

Medium Soft						
Temperature / °C	Hardness / HWB 2,5/ 62,5	c_T / HHWB 2,5 /62,5 °C^{-1}	$u(c_T)$ / HHWB 2,5 /62,5 °C^{-1}	H_0 / HHWB 2,5 /62,5	$u(H_0)$ / HWB 2,5 /62,5	p-value
15	496	-2,13	0,24	526,6	6,26	96,60%
20	490					
25	460					
30	465					
35	456					

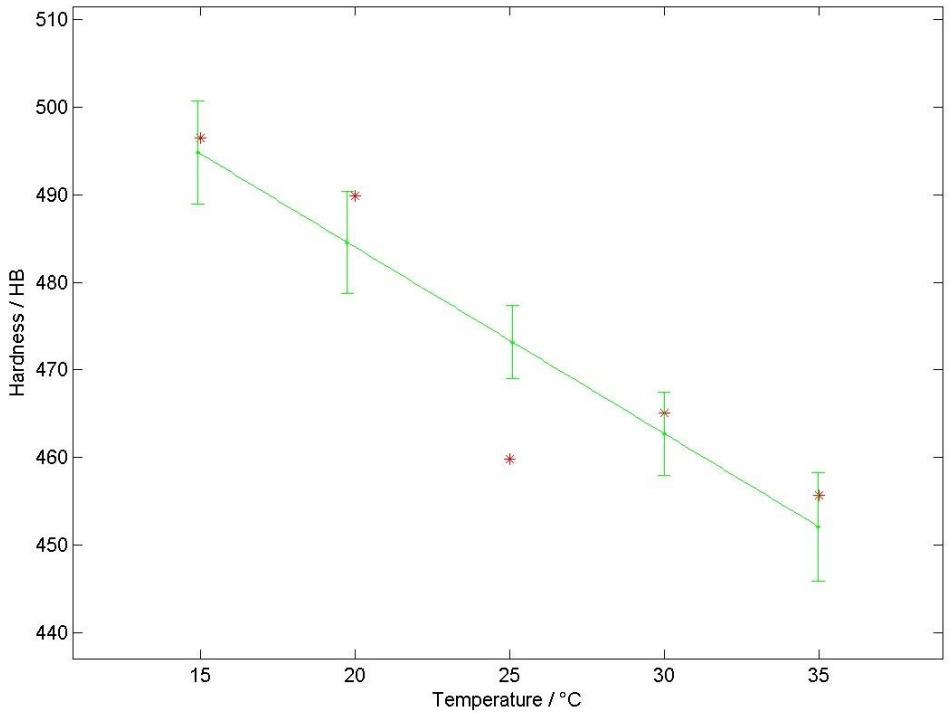

Medium Hard						
Temperature / $°C$	Hardness / HWB 2,5/ 62,5	c_T / $HHWB$ 2,5 /62,5 $°C^{-1}$	$u(c_T)$ / $HHWB$ 2,5 /62,5 $°C^{-1}$	H_0 / $HHWB$ 2,5 /62,5	$u(H_0)$ / HWB 2,5 /62,5	p-value
15	666	0,02	0,32	664,2	8,199	56,86%
20	660					
25	664					
30	672					
35	661					

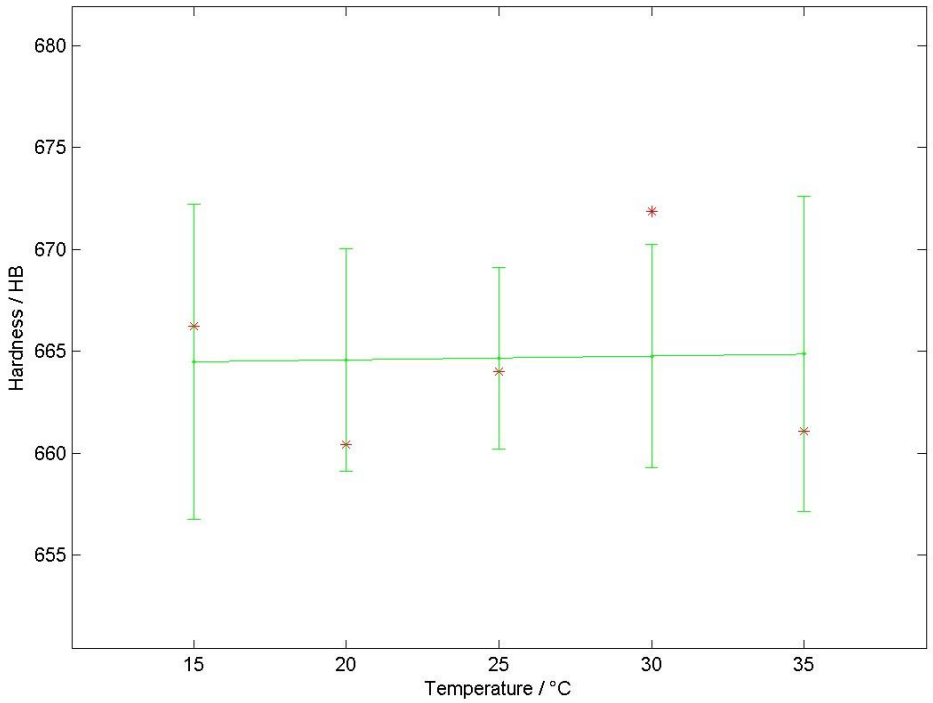

$Hard$						
Temperature / $°C$	Hardness / HWB 2,5/ 62,5	c_T / $HHWB$ 2,5 /62,5 $°C^{-1}$	$u(c_T)$ / $HHWB$ 2,5 /62,5 $°C^{-1}$	H_0 / $HHWB$ 2,5 /62,5	$u(H_0)$ / HWB 2,5 /62,5	p-value
15	809	-0,43	0,38	815,1	9,93	5,60%
20	805					
25	804					
30	805					
35	798					

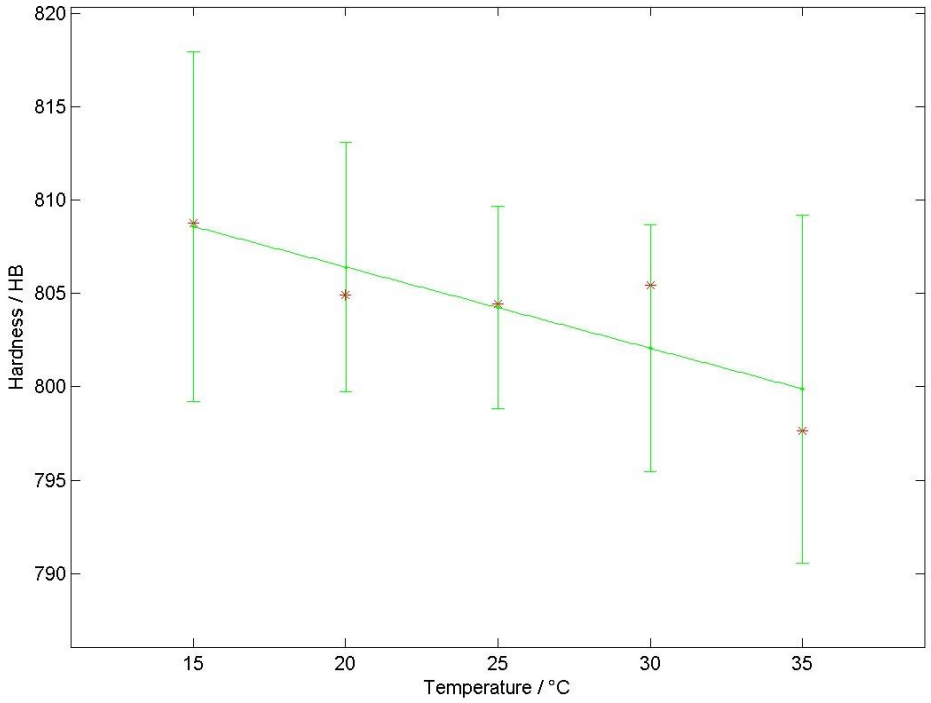

HBW 2,5/31,25

$Soft$						
Temperature / $°C$	Hardness / HWB 2,5/ 31.25	c_T / HWB 2,5 /31.25 $°C^{-1}$	$u(c_T)$ / HWB 2,5 /31.25 $°C^{-1}$	H_0 / HWB 2,5 /31.25	$u(H_0)$ / HWB 2,5 /31.25	p-value
15	177	-0,91	0,09	190,2	2,22	99,48%
20	176					
25	163					
30	160					
35	163					

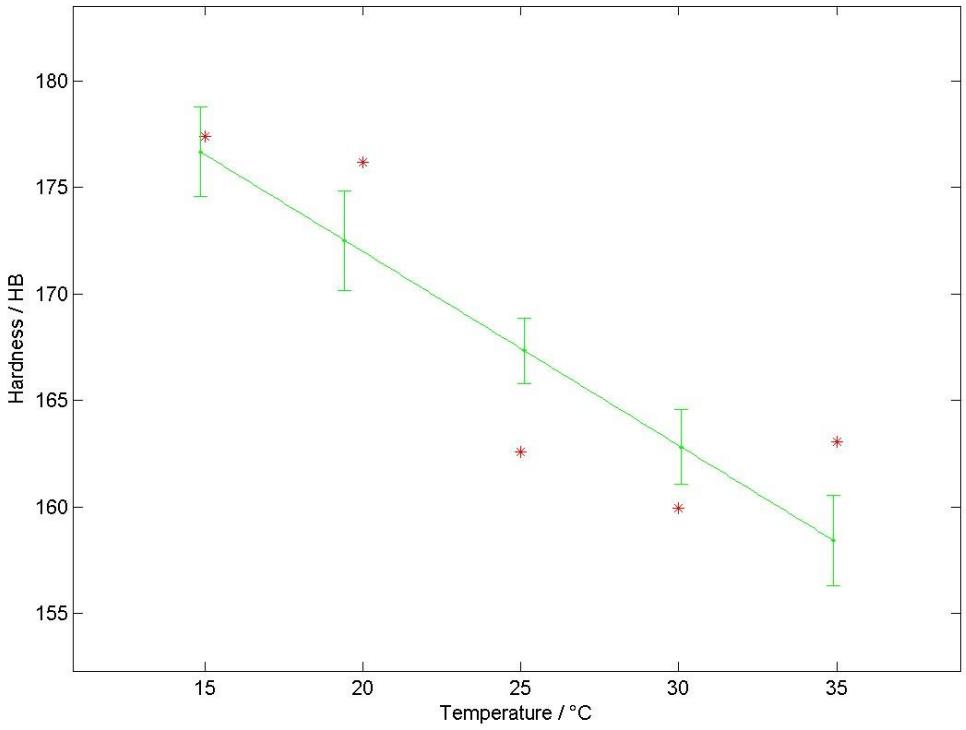

$Medium\ Soft$						
Temperature / $°C$	Hardness / HWB 2,5/ 31.25	c_T / HWB 2,5 /31.25 $°C^{-1}$	$u(c_T)$ / HWB 2,5 /31.25 $°C^{-1}$	H_0 / HWB 2,5 /31.25	$u(H_0)$ / HWB 2,5 /31.25	p-value
15	451	-1,09	0,04	462,62	-1,12	99,55%
20	449					
25	420					
30	423					
35	436					

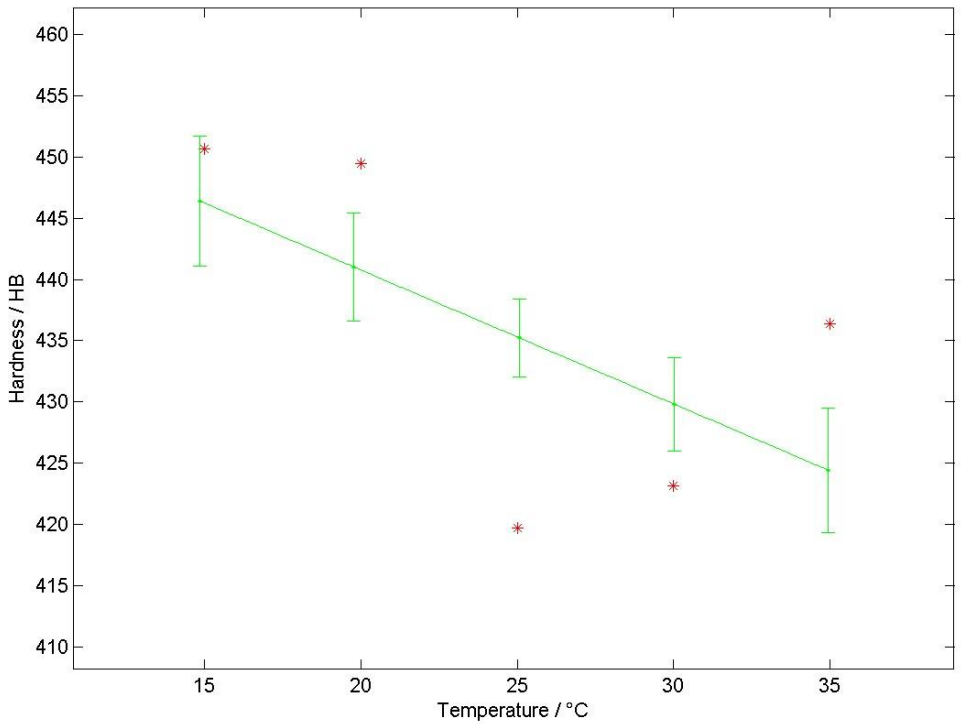

Medium Hard						
Temperature / $°C$	Hardness / HWB 2,5/ 31.25	c_T / HWB 2,5 /31.25 $°C^{-1}$	$u(c_T)$ / HWB 2,5 /31.25 $°C^{-1}$	H_0 / HWB 2,5 /31.25	$u(H_0)$ / HWB 2,5 /31.25	p-value
15	604	-0,46	0,28	604,24	7,43	80,61%
20	586					
25	594					
30	593					
35	588					

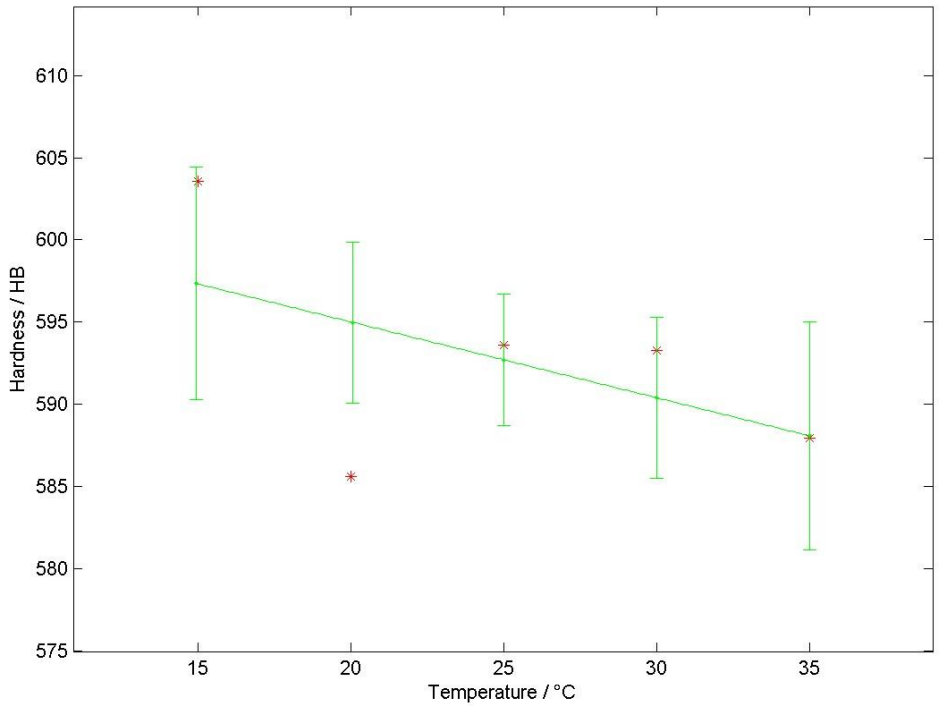

$Hard$						
Temperature / $°C$	Hardness / HWB 2,5/ 31.25	c_T / HWB 2,5 /31.25 $°C^{-1}$	$u(c_T)$ / HWB 2,5 /31.25 $°C^{-1}$	H_0 / HWB 2,5 /31.25	$u(H_0)$ / HWB 2,5 /31.25	p-value
15	768	-2,46	0,37	779,4	9,64	99,75%
20	705					
25	702					
30	721					
35	697					

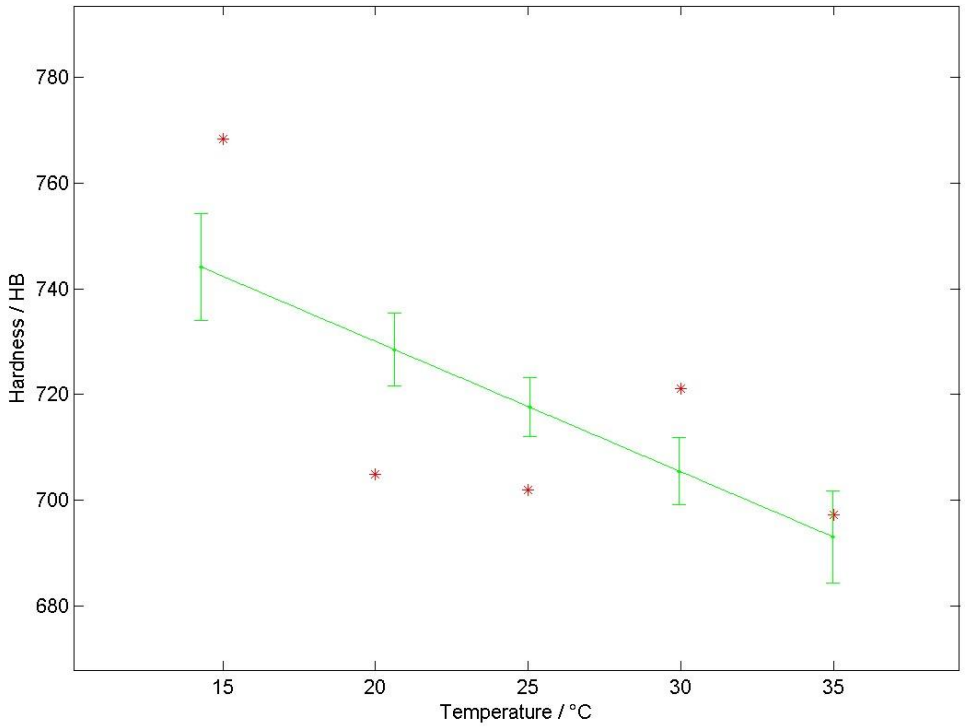

HV 30

$Soft$						
Temperature / $°C$	Hardness / $HV\ 30$	c_T / $HV\ 30\ °C^{-1}$	$u(c_T)$ / $HV\ 30\ °C^{-1}$	H_0 / $HV\ 30$	$u(H_0)$ / $HV\ 30$	p-value
15	182	0,09	0,09	181,1	2,240	50,13%
20	182					
25	184					
30	185					
35	183					

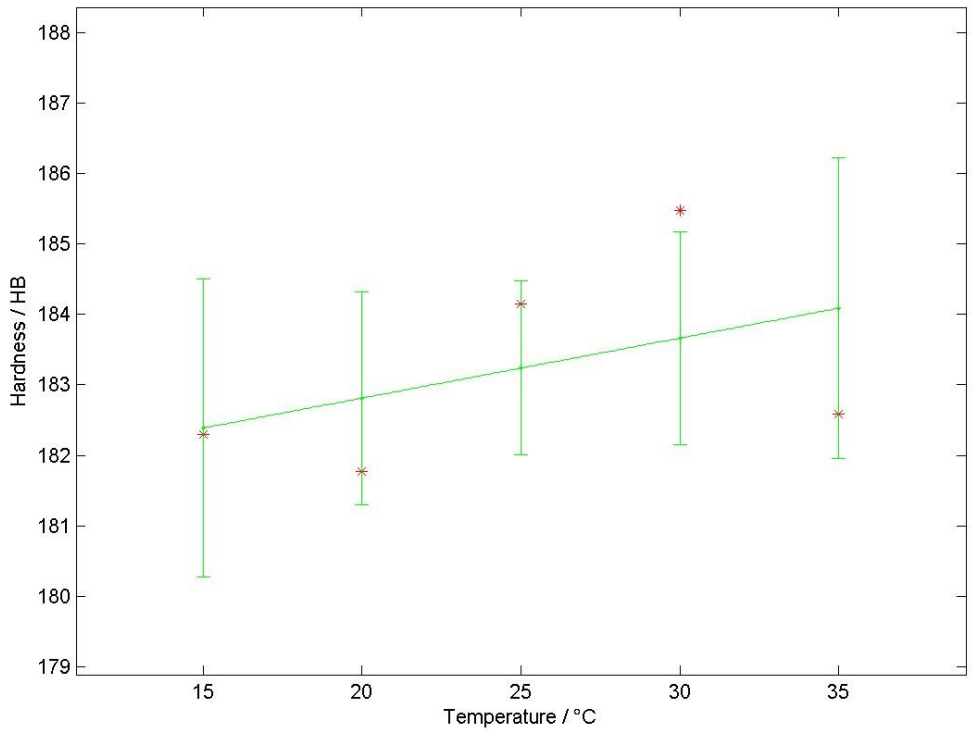

$Medium\ Soft$						
Temperature / $°C$	Hardness / $HV\ 30$	c_T / $HV\ 30\ °C^{-1}$	$u(c_T)$ / $HV\ 30\ °C^{-1}$	H_0 / $HV\ 30$	$u(H_0)$ / $HV\ 30$	p-value
15	513	-0,13	0,24	516,3	6,320	53,18%
20	510					
25	518					
30	516					
35	508					

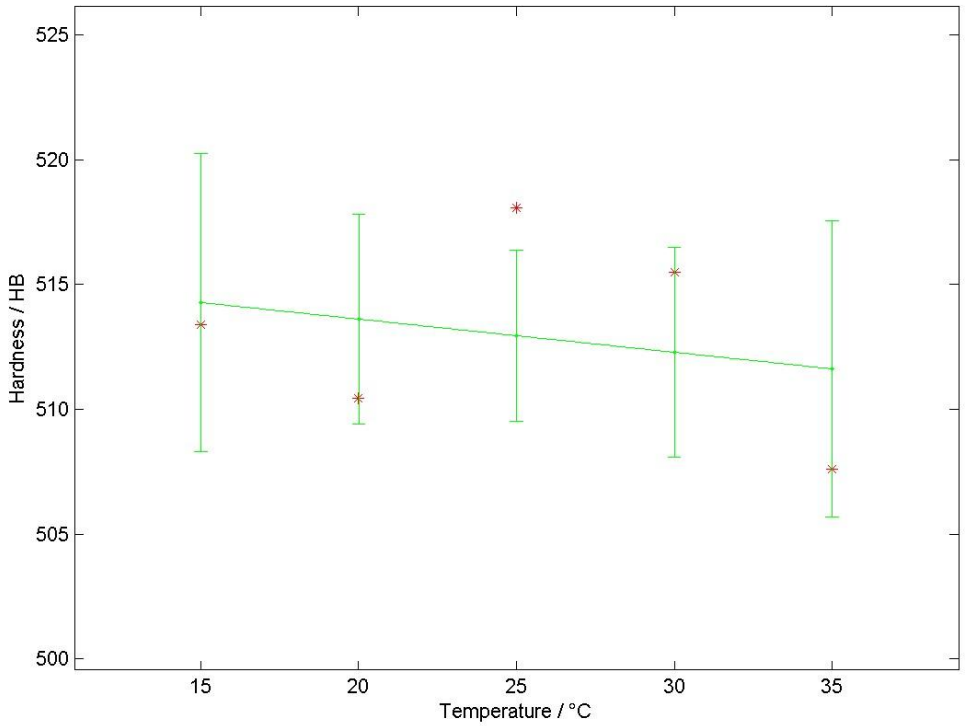

Medium Hard						
Temperature / °C	Hardness / HV 30	c_T / HV 30 °C^{-1}	$u(c_T)$ / HV 30 °C^{-1}	H_0 / HV 30	$u(H_0)$ / HV 30	p-value
15	692	-0,45	0,33	699,1	8,51	1,12%
20	692					
25	686					
30	685					
35	684					

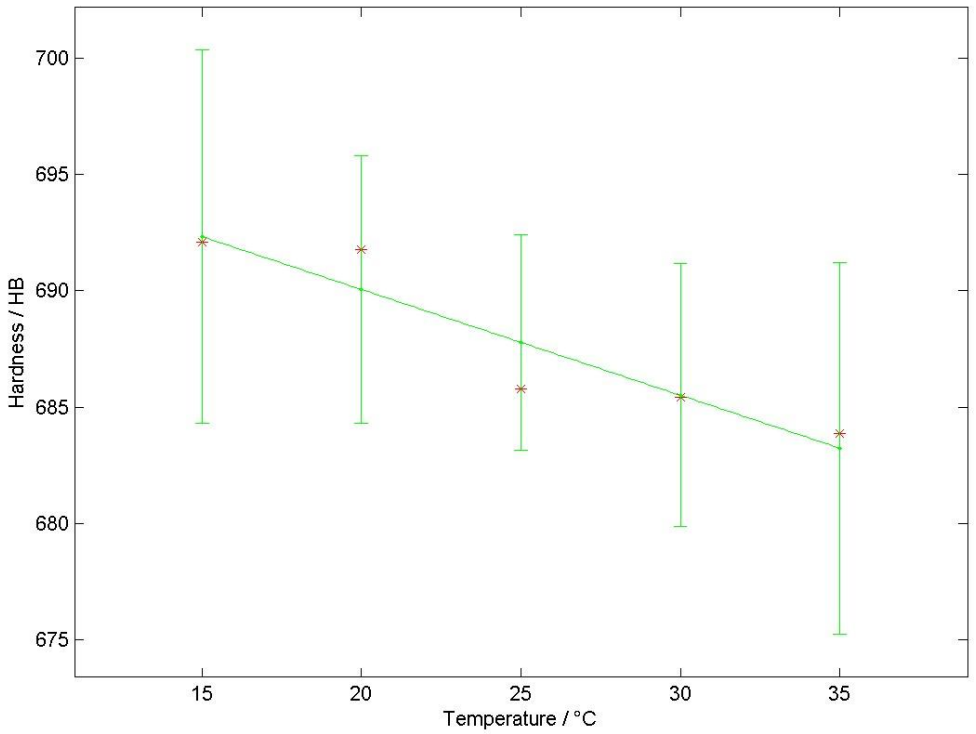

$Hard$						
Temperature / $°C$	Hardness / $HV\ 30$	c_T / $HV\ 30\ °C^{-1}$	$u(c_T)$ / $HV\ 30\ °C^{-1}$	H_0 / $HV\ 30$	$u(H_0)$ / $HV\ 30$	p-value
15	897	-0,56	0,42	904,1	11,01	11,29%
20	896					
25	884					
30	888					
35	887					

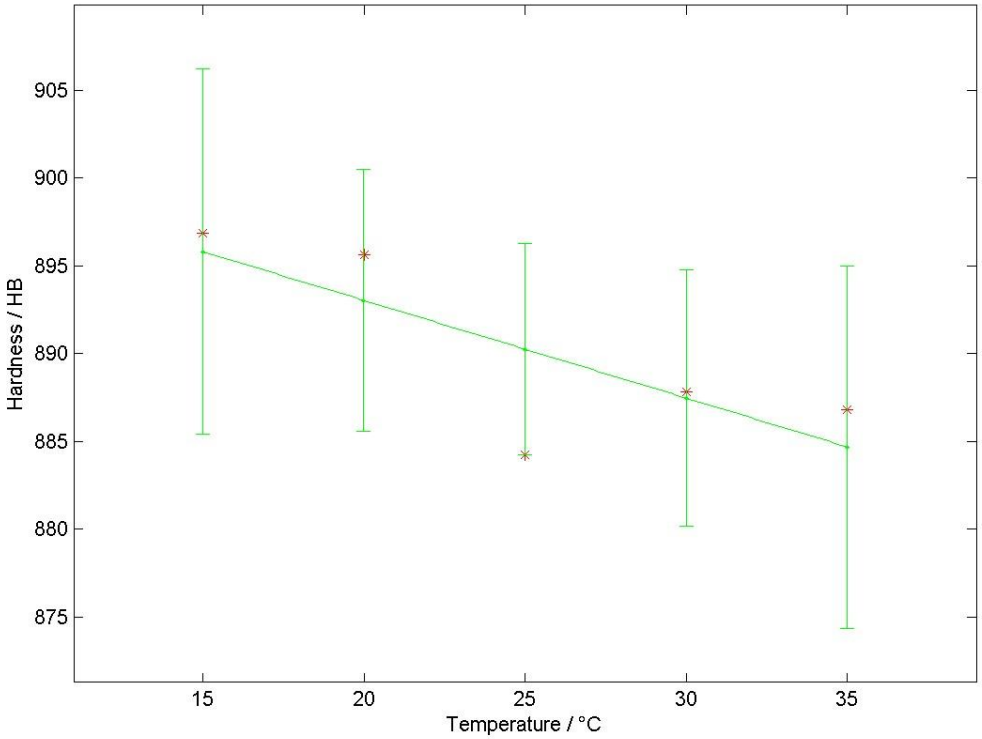

HV 1

$Soft$						
Temperature / $°C$	Hardness / $HV1$	c_T / $HV\ 1\ °C^{-1}$	$u(c_T)$ / $HV\ 1\ °C^{-1}$	H_0 / $HV\ 1$	$u(H_0)$ / $HV\ 1$	p-value
15	194	-0,34	0,09	196,7	2,36	82,15%
20	192					
25	181					
30	188					
35	187					

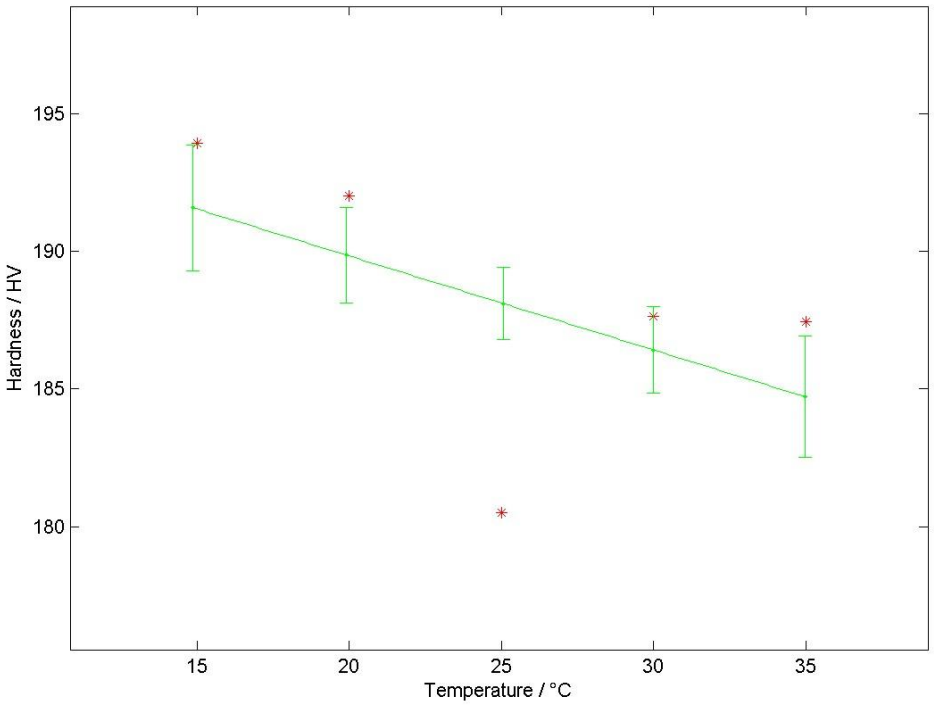

Medium Soft						
Temperature / $°C$	Hardness / $HV1$	c_T / $HV\ 1\ °C^{-1}$	$u(c_T)$ / $HV\ 1\ °C^{-1}$	H_0 / $HV\ 1$	$u(H_0)$ / $HV\ 1$	p-value
15	520	-0,38	0,25	527,4	6,41	12,33%
20	517					
25	524					
30	518					
35	510					

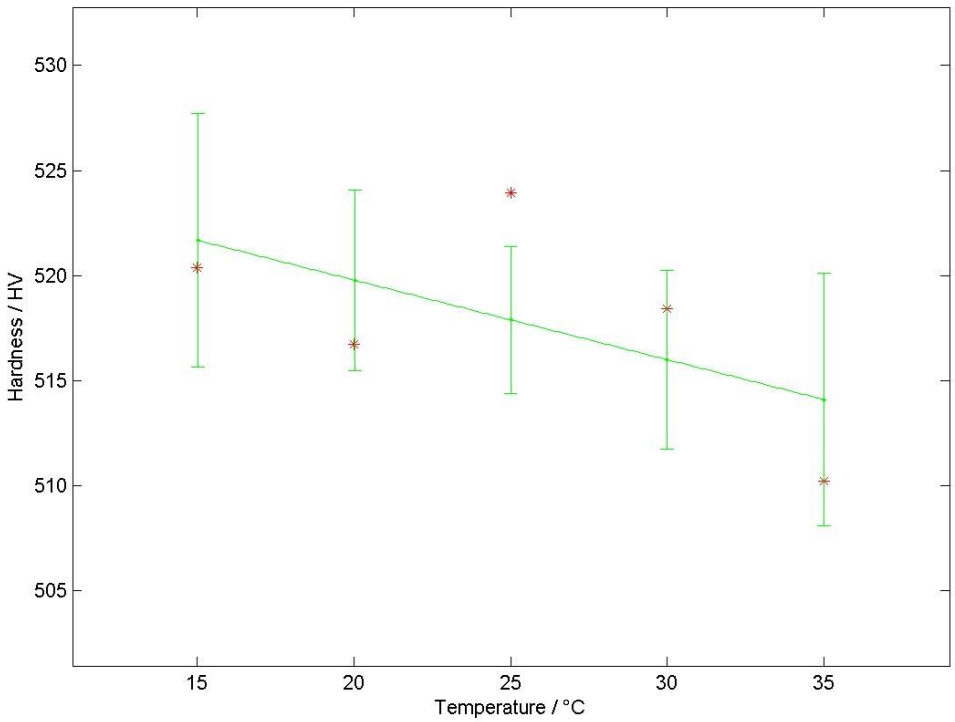

Medium Hard						
Temperature / °C	Hardness / $HV1$	c_T / $HV\ 1\ °C^{-1}$	$u(c_T)$ / $HV\ 1\ °C^{-1}$	H_0 / $HV\ 1$	$u(H_0)$ / $HV\ 1$	p-value
15	698	0,13	0,33	702,7	8,67	73,70%
20	699					
25	723					
30	720					
35	691					

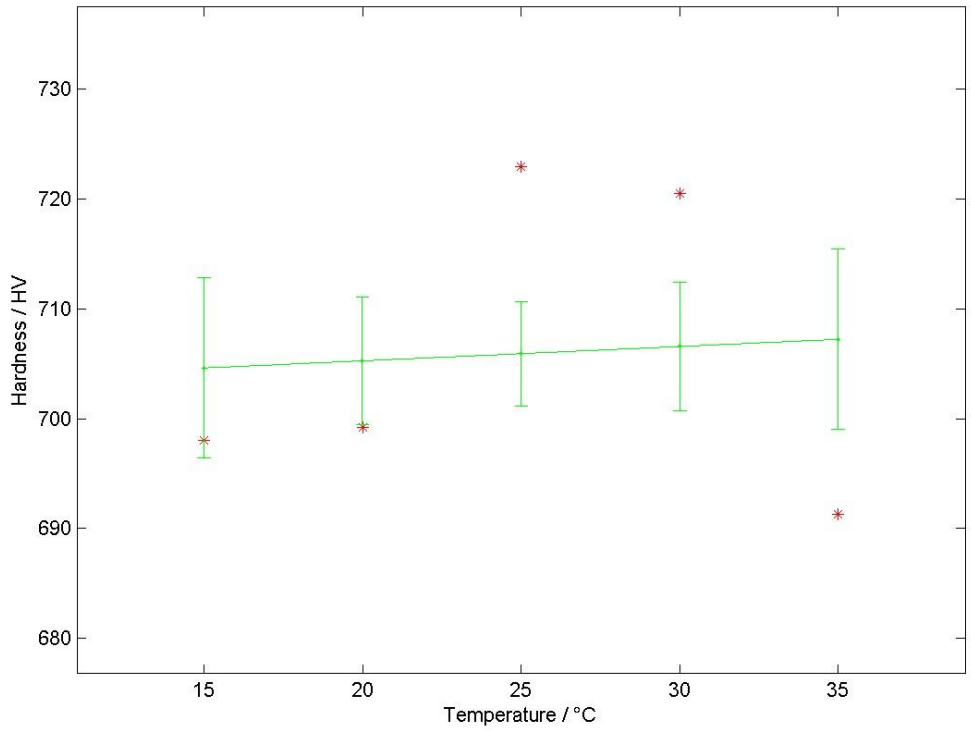

$Hard$						
Temperature / $°C$	Hardness / $HV1$	c_T / $HV\ 1\ °C^{-1}$	$u(c_T)$ / $HV\ 1\ °C^{-1}$	H_0 / $HV\ 1$	$u(H_0)$ / $HV\ 1$	p-value
15	949	1,72	1,72	1,72	1,72	1,72
20	948					
25	933					
30	947					
35	994					

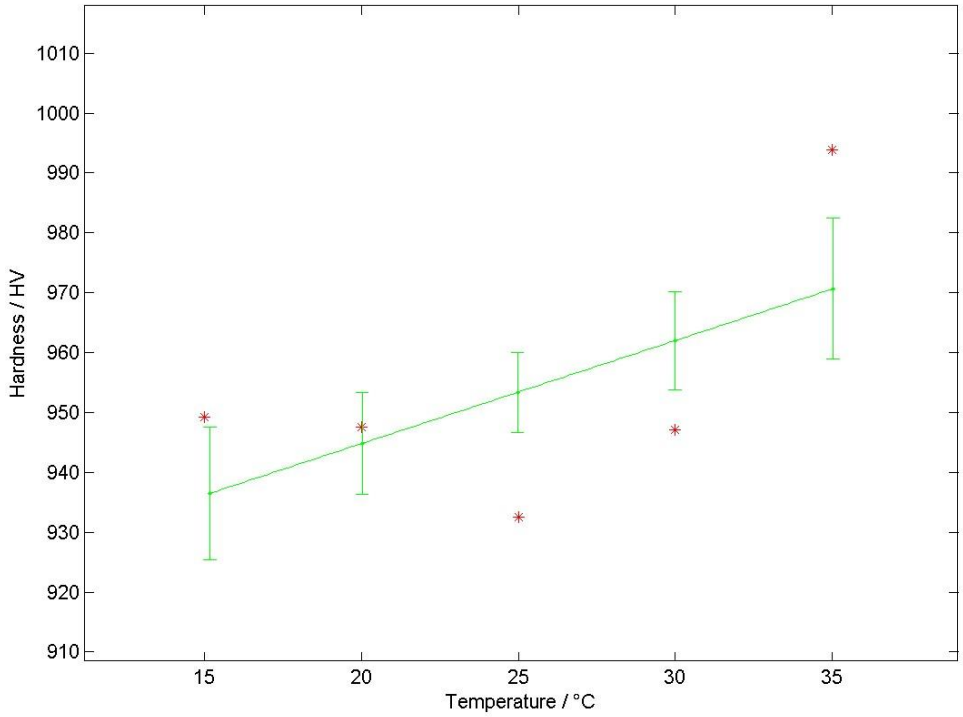

HV 0,2

$Soft$						
Temperature / °C	Hardness / HV 0,2	c_T / HV 0,2 °C^{-1}	$u(c_T)$ / HV 0,2 °C^{-1}	H_0 / HV 0,2	$u(H_0)$ / HV 0,2	p-value
15	183	-0,30	0,09	192,4	2,44	92,29%
20	189					
25	189					
30	189					
35	176					

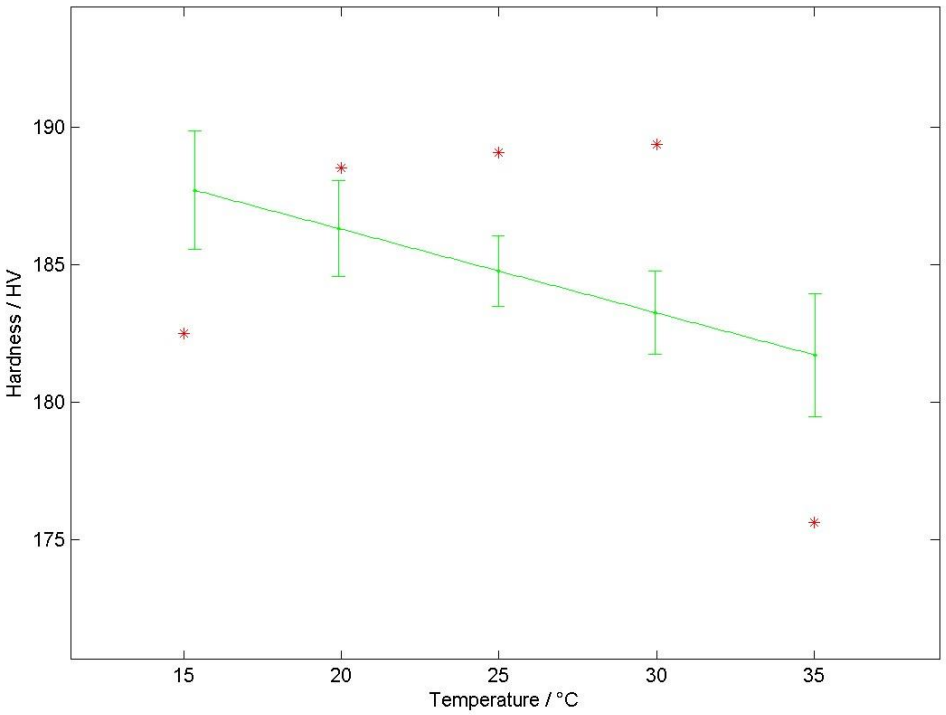

Medium Soft						
Temperature / °C	Hardness / HV 0,2	c_T / HV 0,2 °C^{-1}	$u(c_T)$ / HV 0,2 °C^{-1}	H_0 / HV 0,2	$u(H_0)$ / HV 0,2	p-value
15	490	-2,35	0,38	562,3	10,9	99,63%
20	545					
25	508					
30	528					
35	458					

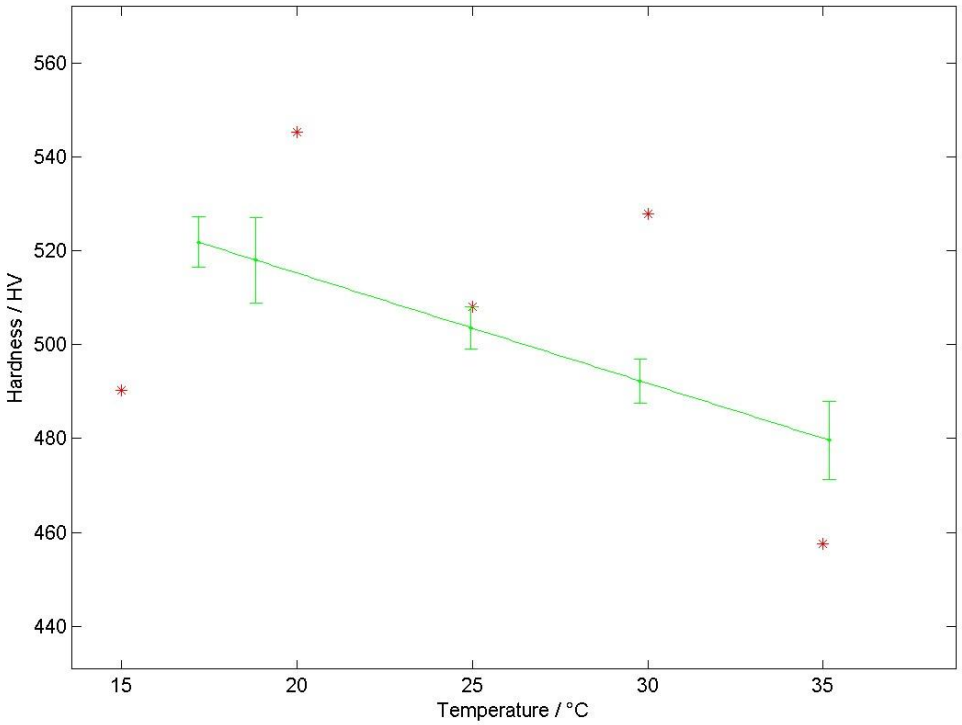

Medium Hard						
Temperature / $°C$	Hardness / $HV\ 0{,}2$	c_T / $HV\ 0{,}2\ °C^{-1}$	$u(c_T)$ / $HV\ 0{,}2\ °C^{-1}$	H_0 / $HV\ 0{,}2$	$u(H_0)$ / $HV\ 0{,}2$	p-value
15	726	-0,51	0,35	739,4	9,03	13,72%
20	738					
25	724					
30	728					
35	718					

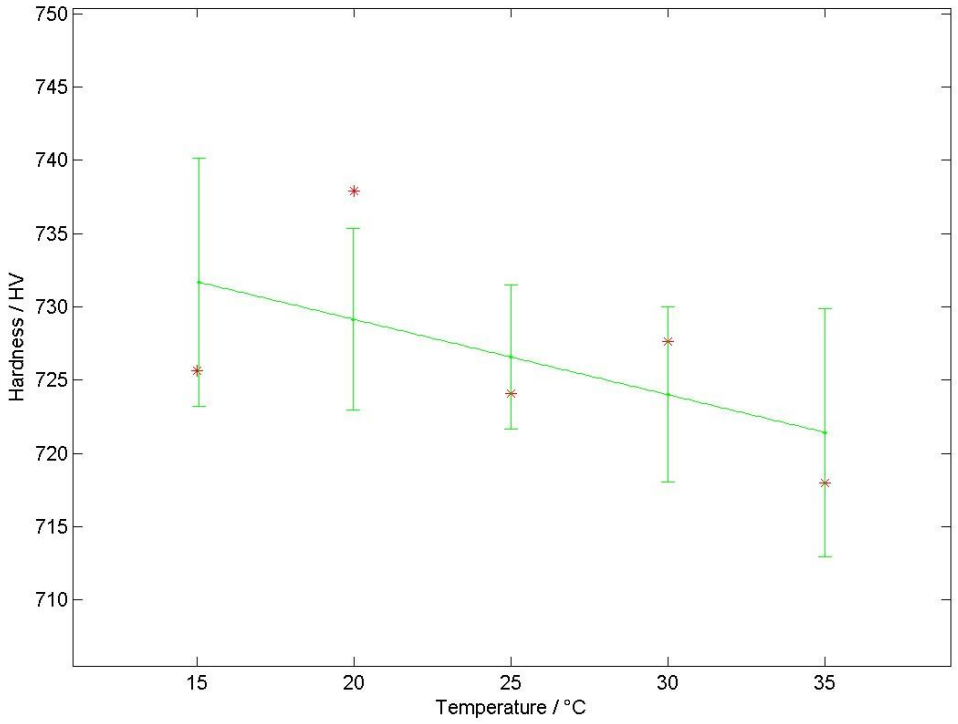

$Hard$						
Temperature / $°C$	Hardness / HV 0,2	c_T / HV 0,2 $°C^{-1}$	$u(c_T)$ / HV 0,2 $°C^{-1}$	H_0 / HV 0,2	$u(H_0)$ / HV 0,2	p-value
15	978	0,09	0,47	982,46	12,13	3,82%
20	990					
25	991					
30	980					
35	985					

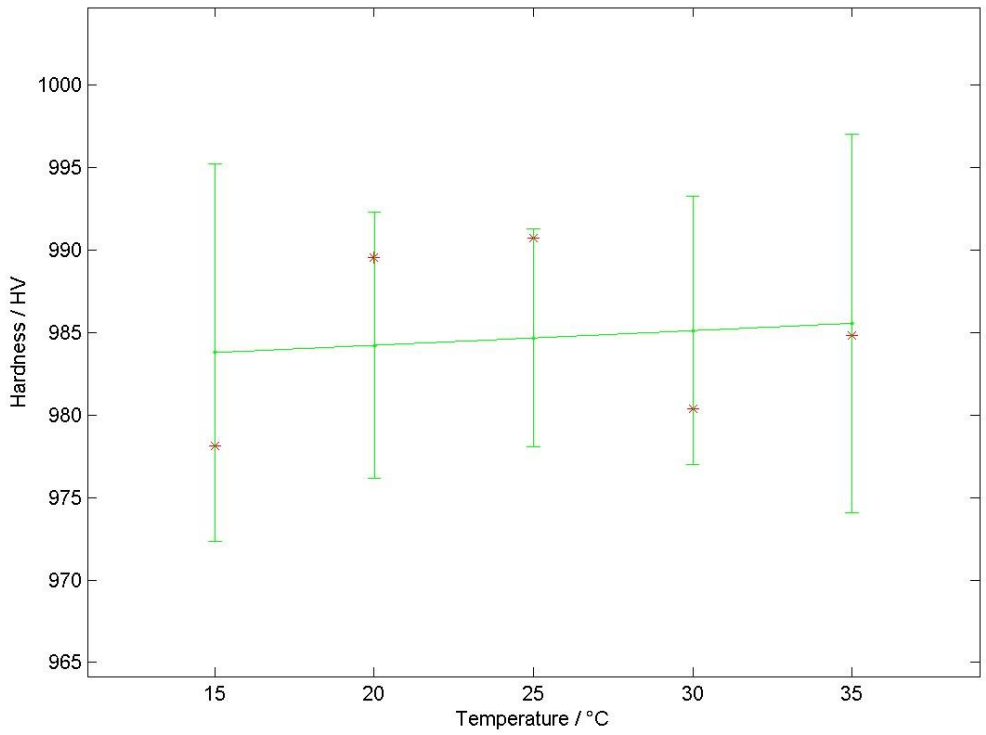

HK 2

$Soft$						
Temperature / $°C$	Hardness / $HK\ 2$	c_T / $HK\ 2\ °C^{-1}$	$u(c_T)$ / $HK\ 2\ °C^{-1}$	H_0 / $HK\ 2$	$u(H_0)$ / $HK\ 2$	p-value
15	207	-0,15	0,10	209,21	2,53	0,58%
20	205					
25	206					
30	206					
35	203					

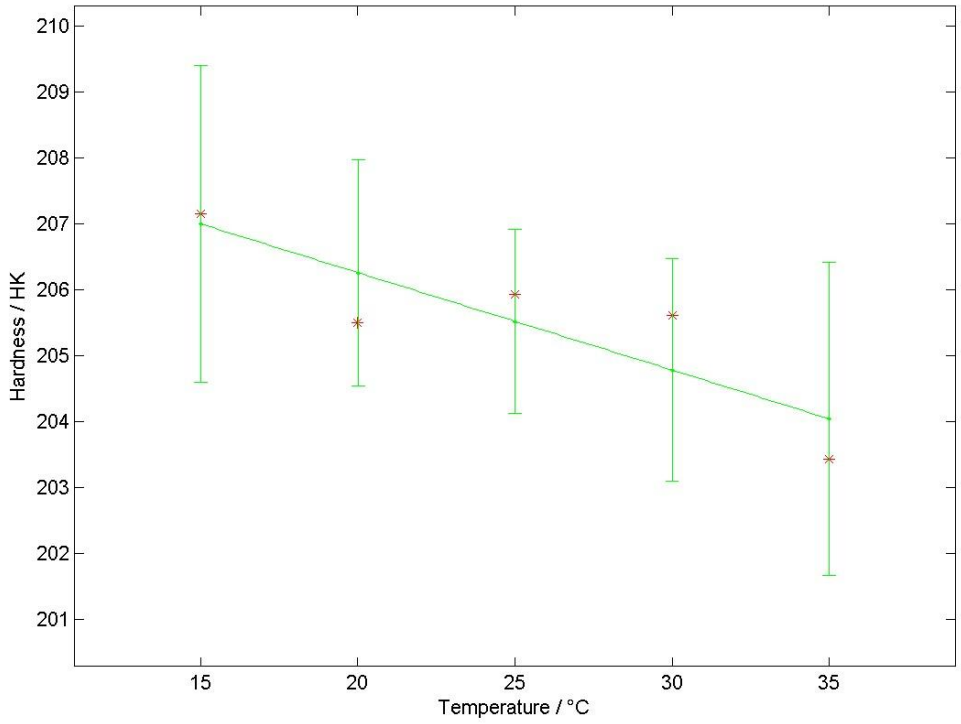

Medium Soft						
Temperature / $°C$	Hardness / $HK\ 2$	c_T / $HK\ 2\ °C^{-1}$	$u(c_T)$ / $HK\ 2\ °C^{-1}$	H_0 / $HK\ 2$	$u(H_0)$ / $HK\ 2$	p-value
15	535	-0,55	0,23	542,8	6,36	32,47%
20	531					
25	525					
30	537					
35	519					

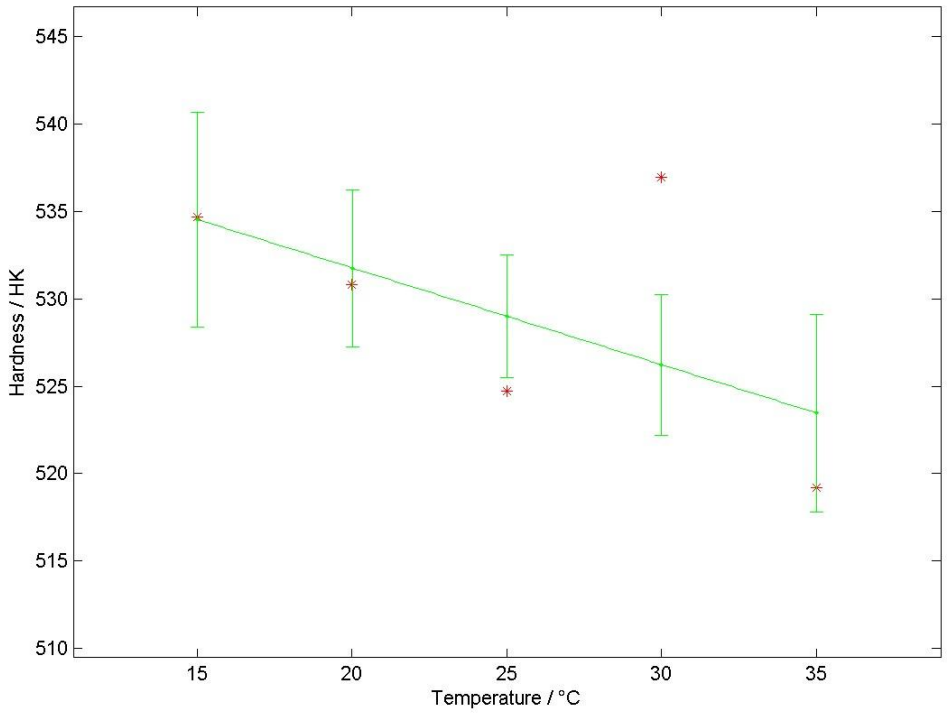

Medium Hard						
Temperature / $°C$	Hardness / $HK\ 2$	c_T / $HK\ 2\ °C^{-1}$	$u(c_T)$ / $HK\ 2\ °C^{-1}$	H_0 / $HK\ 2$	$u(H_0)$ / $HK\ 2$	p-value
15	711	-0,52	0,33	719,4	8,71	10,87%
20	711					
25	701					
30	712					
35	698					

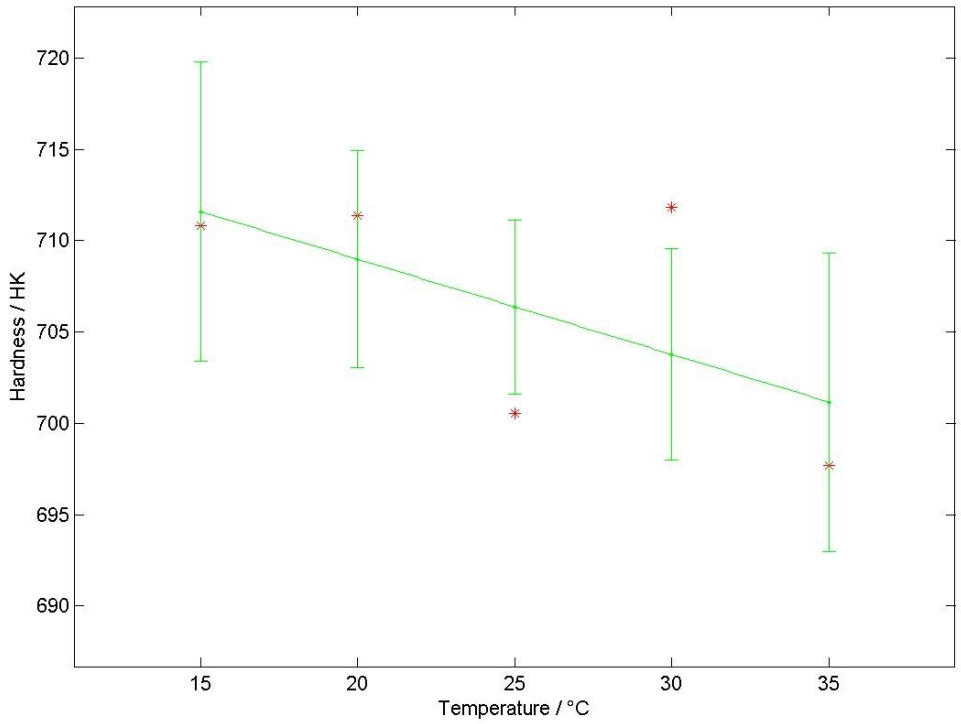

$Hard$						
Temperature / $°C$	Hardness / $HK\ 2$	c_T / $HK\ 2\ °C^{-1}$	$u(c_T)$ / $HK\ 2\ °C^{-1}$	H_0 / $HK\ 2$	$u(H_0)$ / $HK\ 2$	p-value
15	858	-1,08	0,51	907,9	13,13	98,29%
20	946					
25	858					
30	902					
35	853					

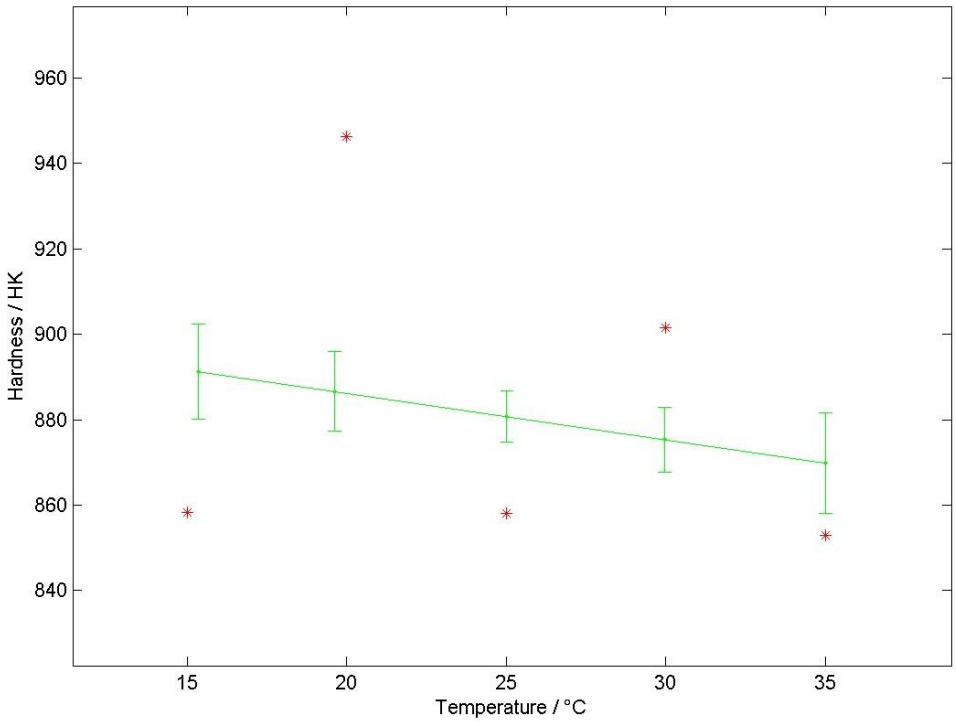

HK 0,2

$Soft$						
Temperature / °C	Hardness HK 0,2	c_T / HK 0,2 °C^{-1}	$u(c_T)$ / HK 0,2 °C^{-1}	H_0 / HK 0,2	$u(H_0)$ / HK 0,2	p-value
15	216	-0,10	0,10	214,8	2,67	43,20 %
20	208					
25	214					
30	212					
35	212					

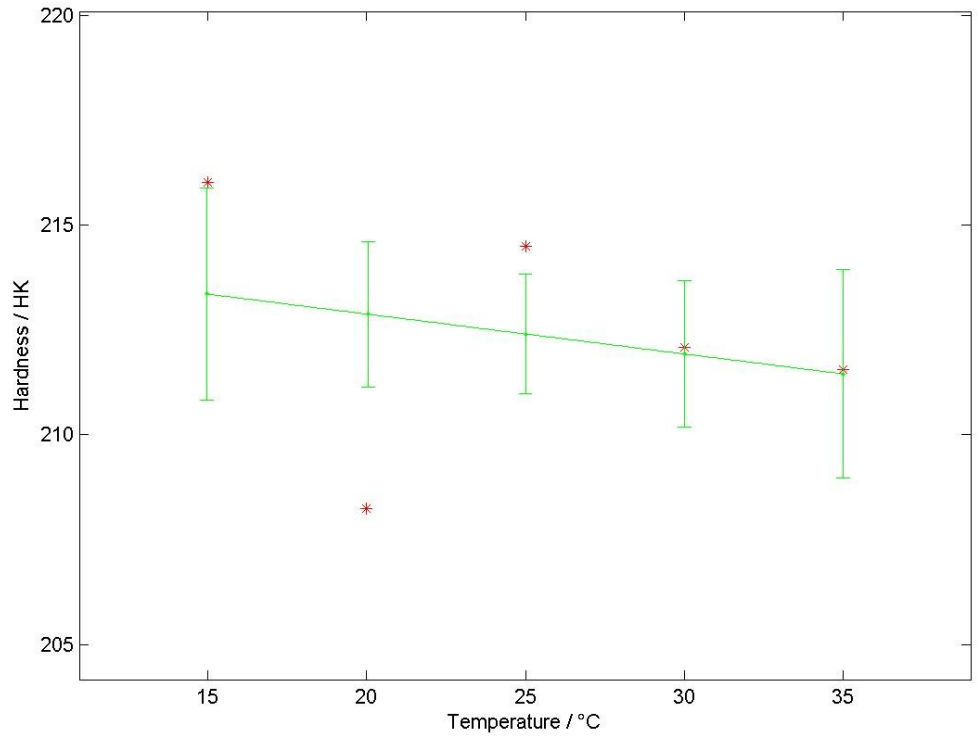

$Medium\ Soft$						
Temperature / $°C$	Hardness / $HK\ 0{,}2$	c_T / $HK\ 0{,}2\ °C^{-1}$	$u(c_T)$ / $HK\ 0{,}2\ °C^{-1}$	H_0 / $HK\ 0{,}2$	$u(H_0)$ / $HK\ 0{,}2$	p-value
15	570	-1,60	0,39	597,4	10,2	41,36%
20	569					
25	576					
30	509					
35	561					

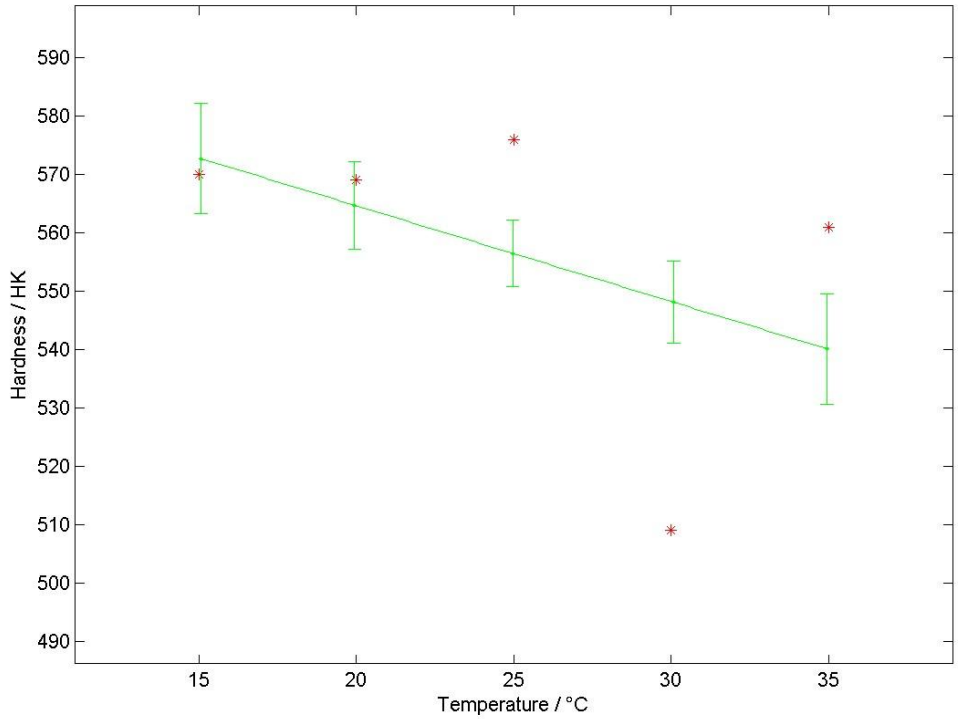

Medium Hard						
Temperature / $°C$	Hardness / $HK\ 0{,}2$	c_T / $HK\ 0{,}2\ °C^{-1}$	$u(c_T)$ / $HK\ 0{,}2\ °C^{-1}$	H_0 / $HK\ 0{,}2$	$u(H_0)$ / $HK\ 0{,}2$	p-value
15	811	-0,44	0,39	810,9	10,02	3,25%
20	791					
25	814					
30	779					
35	806					

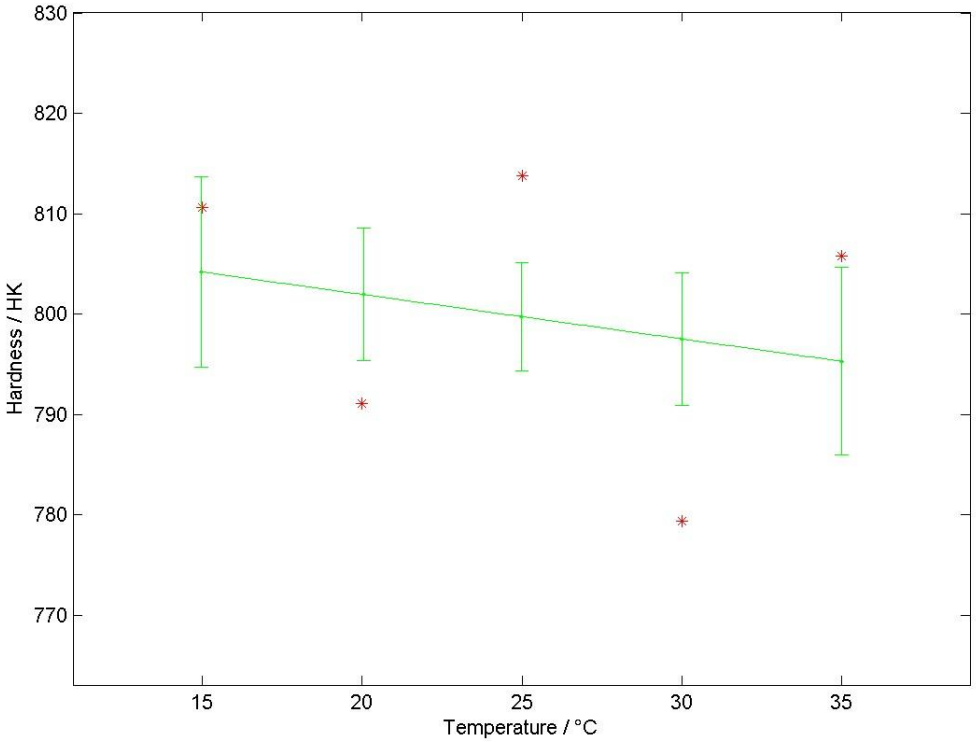

$Hard$						
Temperature / $°C$	Hardness / HK 0,2	c_T / HK 0,2 $°C^{-1}$	$u(c_T)$ / HK 0,2 $°C^{-1}$	H_0 / HK 0,2	$u(H_0)$ / HK 0,2	p-value
15	1080	-3,76	0,50	1104	13,29	9,95%
20	1002					
25	1001					
30	978					
35	995					

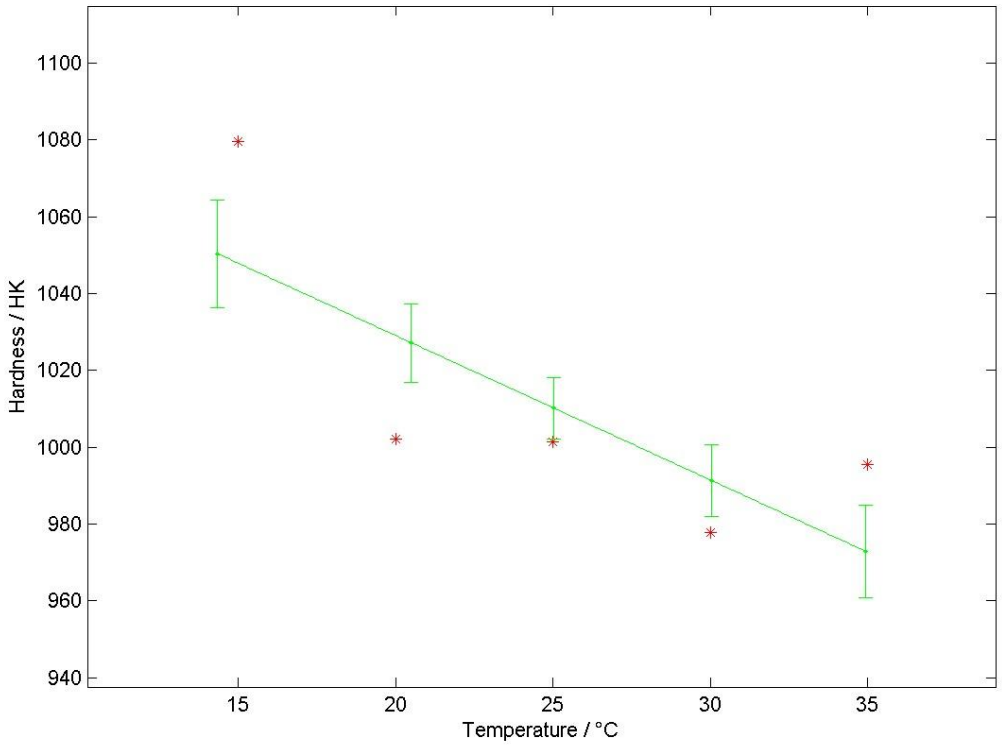

APPENDIX B

Sensitivity Coefficients b / H/°C										
> 0	HBW 2,5/187,5	HBW 2,5/62,5	HBW 2,5/31,25	HV 30	HK 2	HV 1	HV 0,2	HK 0,2	average	st.dv
Soft	-1,20	-0,86	-0,91	0,09	-0,15	-0,34	-0,30	-0,10	-0,47	0,46
Medium Soft	-2,45	-2,13	-1,09	-0,13	-0,55	-0,38	-2,35	-1,60	-1,34	0,93
Medium Hard	0,17	0,02	-0,46	-0,45	-0,52	0,13	-0,51	-0,44	-0,26	0,31
Hard	-0,22	-0,43	-2,46	-0,56	-1,08	1,72	0,09	-3,76	-0,84	1,66
average	-0,93	-0,85	-1,23	-0,26	-0,58	0,28	-0,77	-1,47	-0,73	0,84
st.dv	1,17	0,93	0,86	0,30	0,38	0,99	1,08	1,65	0,47	0,61

Relative Sensitivity Coefficients b/H / 1/°C										
> 0	HBW 2,5/187,5	HBW 2,5/62,5	HBW 2,5/31,25	HV 30	HK 2	HV 1	HV 0,2	HK 0,2	average	st.dv
Soft	0,61%	0,47%	0,54%	0,05%	0,07%	0,18%	0,16%	0,05%	0,27%	0,24%
Medium Soft	0,47%	0,45%	0,25%	0,03%	0,10%	0,07%	0,46%	0,29%	0,27%	0,18%
Medium Hard	0,02%	0,00%	0,08%	0,07%	0,07%	0,02%	0,07%	0,05%	0,05%	0,03%
Hard	0,02%	0,05%	0,34%	0,06%	0,12%	0,18%	0,01%	0,37%	0,15%	0,14%
average	0,28%	0,24%	0,30%	0,05%	0,09%	0,11%	0,18%	0,19%	0,18%	0,15%
st.dv	0,30%	0,25%	0,19%	0,02%	0,02%	0,08%	0,20%	0,17%	0,11%	0,09%

P value										
> 4,64	HBW 2,5/187,5	HBW 2,5/62,5	HBW 2,5/31,25	HV 30	HK 2	HV 1	HV 0,2	HK 0,2	average	st.dv
Soft	98,50%	97,42%	99,48%	50,13%	0,58%	82,15%	17,75%	1,26%	56%	44%
Medium Soft	98,49%	96,60%	99,55%	53,18%	32,47%	12,33%	69,29%	41,36%	63%	33%
Medium Hard	0,04%	56,86%	80,61%	1,12%	10,87%	73,70%	0,20%	3,25%	28%	36%
Hard	73%	5,60%	99,75%	11,29%	98,29%	71,03%	0,04%	9,95%	46%	43%
average	67%	64%	95%	29%	36%	60%	22%	14%	48%	39%
st.dv	47%	43%	9%	27%	44%	32%	33%	19%	15%	5%

Chi Square										
> 4,64	HBW 2,5/187,5	HBW 2,5/62,5	HBW 2,5/31,25	HV 30	HK 2	HV 1	HV 0,2	HK 0,2	average	st.dv
Soft	8,89	6,71	14,44	1,31	0,26	13,70	22,24	4,45	9,00	7,45
Medium Soft	9,06	5,42	16,73	1,42	3,39	1,50	86,85	22,63	18,38	28,69
Medium Hard	0,01	1,14	2,29	0,09	1,39	9,60	1,61	7,46	2,95	3,57
Hard	1,80	0,17	19,40	0,36	44,22	8,80	0,73	13,35	11,10	15,14
average	4,94	3,36	13,22	0,80	12,31	8,40	27,86	11,97	10,36	13,71
st.dv	4,72	3,19	7,56	0,67	21,31	5,08	40,57	8,01	6,37	11,08

Residual Variance / H^2										
	HBW 2,5/187,5	HBW 2,5/62,5	HBW 2,5/31,25	HV 30	HK 2	HV 1	HV 0,2	HK 0,2	average	st.dv
Soft	15,5	10,3	18,2	1,9	0,5	19,4	31,5	8,2	13,2	10,2
Medium Soft	108,6	60,0	131,4	15,9	38,3	17,1	1020,8	599,7	249,0	366,5
Medium Hard	0,3	21,4	34,0	1,9	29,3	204,0	36,4	198,7	65,7	84,8
Hard	64,2	4,7	456,3	12,3	1558,0	343,6	29,7	629,1	387,2	528,5
average	47,1	24,1	160,0	8,0	406,5	146,0	279,6	358,9	178,8	247,5
st.dv	49,2	24,9	203,8	7,2	767,8	158,2	494,1	305,3	171,8	242,1